Human induced pluripotent stem cell models of Rett Syndrome reveal deficits in early cortical development

by

Danielle A. Feldman

B.A. / M.A., Biology with specialization in Biotechnology
Macaulay Honors College at CUNY Hunter College, 2010

SUBMITTED TO THE DEPARTMENT OF BRAIN AND COGNITIVE SCIENCES IN PARTIAL FULFILLMENT OF THE REQUIREMENTS FOR THE DEGREE OF

DOCTOR OF PHILOSOPHY IN NEUROSCIENCE
AT THE
MASSACHUSETTS INSTITUTE OF TECHNOLOGY

AUGUST 2016
[September 2016]

Signature of Author: Signature redacted
Department of Brain and Cognitive Sciences
August 10, 2016

Certified by: Signature redacted
Mriganka Sur
Paul E. and Lilah Newton Professor of Neuroscience
Thesis Supervisor

Accepted by: Signature redacted
Matthew A. Wilson
Sherman Fairchild Professor of Neuroscience and Picower Scholar
Director of Graduate Education for Brain and Cognitive Sciences

Human induced pluripotent stem cell models of Rett Syndrome reveal deficits in early cortical development

by

Danielle A. Feldman

Submitted to the Department of Brain and Cognitive Sciences on August ___, 2016

in Partial Fulfillment of the Requirements of the Degree of

Doctor of Philosophy in Neuroscience

Abstract

Rett Syndrome (RTT) is a pervasive, X-linked neurodevelopmental disorder that predominantly affects girls. The clinical patient features of RTT are most commonly reported to emerge between the ages of 6-18 months and as such, RTT has largely been considered to be a postnatal disorder. The vast majority of cases are caused by sporadic mutations in the gene encoding methyl CpG-binding protein 2 (MeCP2), which is expressed in the brain during prenatal neurogenesis and continuously throughout adulthood. MeCP2 is a pleiotropic gene that functions as a complex, high-level transcriptional modulator. It both regulates and is regulated by coding genes and non-coding RNAs including microRNAs (miRNAs). The effects of MeCP2 are mediated by diverse signaling, transcriptional, and epigenetic mechanisms. Whereas the postnatal effects of MeCP2 have been widely studied, pre-symptomatic stages of RTT have yet to be thoroughly investigated. Recent evidence from our lab among others

suggests a role for MeCP2 during prenatal neurogenesis that may contribute to the neuropathology observed later in life. We sought to characterize the course of neurogenesis in MeCP2-deficient human neurons with the use of induced pluripotent stem cells (iPSCs) derived from RTT patient skin samples. We generated a variety of monolayer and 3D neuronal models and found that RTT phenotypes are present at the earliest stages of brain development including neuroepithelial expansion, neural progenitor migration and differentiation, and later stages of membrane and synaptic physiological development. We established a link between MeCP2 and key microRNAs that are misregulated in RTT and lie upstream of signalling pathways that contribute to aberrant neuronal maturation in the absence of MeCP2. We have uncovered novel roles of MeCP2 in human neurogenesis. Whereas the processes that comprise early neural development were previously considered irrelevant to RTT pathology, the deficits we observed in neuronal differentiation, migration, and maturation are a crucial component to the larger picture of RTT pathogenesis and provide additional insight into the emergence of RTT patient symptoms.

Thesis Supervisor: Mriganka Sur, Ph.D.
Paul E. Newton Professor of Neuroscience
Director, Simons Center for the Social Brain

Acknowledgements

I am eternally grateful to the people who have shaped and guided me throughout my PhD. I've learned that fundamental to every PhD is a staggering amount of perseverance, made possible only with the help and support of some very patient loved ones.

My thesis advisor, Mriganka Sur, is effervescently enthusiastic about science— he absorbs, shapes, and reverberates ideas in such a way as to engage all those around him. I am grateful to have been trained by someone so passionate and I thank him for his guidance, trust, and patience throughout the last five years.

I would also like to thank my thesis committee: Rudolf Jaenisch, Kwanghun Chung, and Paul Feinstein. They are scientists I am lucky to have met; that I have received insights, feedback, and support from them has been a highlight of my time at MIT. Paul Feinstein got me started on this road back at Hunter College, and it feels both serendipitous and perfectly logical that he is a part of the culmination of my work almost a decade later. As my professor back at Hunter, Paul challenged me to think differently and to approach failures boldly. He is a shrewd scientist and a generous mentor without whom I would not be writing this thesis.

The Sur lab is kept running smoothly thanks in large part to a few people with superhuman powers: Travis Emery, Eleana Ricci, and Alexandra Sokhina. In addition to their remarkable abilities to remedy any situation, they also happen to be wonderful people to work alongside and laugh with. Similarly, I've formed long-lasting bonds over countless hours of tissue culture work with Sur lab members Sally Kwok, Bess Rosen, and Stephanie Chou. These women have made the hours shorter, the challenges less daunting, and the successes more vivid. Without them, there would be no thesis to speak of.

I am incredibly lucky to have patient and supportive friends who smile and nod when I arrive late (if at all) because cells needed feeding. Maureen and Giorgio Napoli are my chosen family; they keep me grounded, laughing, and true. I can't imagine my life in Cambridge without them. Laura Lewis and Jakob Voigts are two of the sincerest, most generous friends I've made here. They also happen to be exceptional scientists whom I admire greatly. Rachel Schecter has taught me how to push through and laugh while doing it. She reminds me warmly and often that it'll all be just fine.

Rodrigo Garcia, my wiser and more capable partner, has balanced me at every turn. He challenges me to be better, to be stronger, to be more thoughtful. And in times that I've failed to do so, he's taught me how to move on. I am grateful for his patience, proud of his accomplishments, and lucky to have made this march alongside him.

Finally, I am dedicating this thesis to my parents, Marianne and Ira Feldman, who believe in education and curiosity above all else. My father, perhaps the most beloved teacher in Brooklyn, NY, who sat with me countless childhood nights hunched over math textbooks, who mailed flash drives to Cambridge filled with hundreds of neuroscience PDFs, who downloaded and learned MATLAB when I was certain I couldn't, who kept persuading me to do "just one more year" until that became "just finish it up, kid," deserves a PhD and a very long vacation. My mother, whose warmth and support are infinite and seemingly tireless, has encouraged every avenue I've ever peeked down. She made every costume, attended every play, and ensured something home-baked was sent with every flash drive. Ultimately, she also absorbed every stressor, every failed experiment, and every long night. I owe everything I have ever done and will do to my parents and though they may not realize it, I am even more proud of them than they are of me.

Table of Contents

Chapter I

Developmental Dynamics of Rett Syndrome

(Adapted from Feldman et al. 2016)

Introduction

Rett Syndrome (RTT) has long been considered to be simply a disorder of postnatal development, with phenotypes that manifest only late in development and into adulthood. A variety of recent evidence demonstrates that the phenotypes of Rett Syndrome are present at the earliest stages of brain development, including developmental stages that define neurogenesis, migration, and patterning in addition to stages of synaptic and circuit development and plasticity. These phenotypes arise from the pleotropic effects of MeCP2, which is expressed very early in neuronal progenitors (NPs) and continues to be expressed into adulthood. The effects of MeCP2 are mediated by diverse signaling, transcriptional, and epigenetic mechanisms. Attempts to reverse the effects of Rett Syndrome need to take into account the developmental dynamics and temporal impact of MeCP2 loss.

Rett Syndrome

RTT is a developmental neurological disorder that affects 1 in every 10,000-15,000 live female births in the US (Chahrour and Zoghbi, 2007). The genetic origin of RTT, in ~90% of patients, has been traced to sporadic loss-of-function mutations in the X-linked gene *MECP2* coding for methyl CpG-binding protein 2, mainly localized to methylated pericentric heterochromatin (Amir et al., 1999). Clinical features of the disorder involve marked developmental regression, progressive loss of acquired motor and language skills, the acquisition of stereotyped repetitive hand movements, muscle hypotonia, autonomic dysfunctions, and severe cognitive impairment. Due to an overlap of symptoms (e.g., speech and motor abnormalities; social interaction deficits),

RTT was formerly classified as an autism spectrum disorder (ASD). It has since been classified as a separate disorder and was removed from the DSM-V in 2013.

MeCP2 is an epigenetic modulator of gene expression. It acts as both a transcriptional activator and repressor (Chahrour et al., 2008; Li et al., 2013), in addition to regulating gene expression post-transcriptionally via microRNA (miRNA)-processing machinery (Cheng et al., 2014) and in an activity-dependent manner to regulate synaptic activity (Qiu et al., 2012). The binding interaction between MeCP2 and DNA is governed by a variety of genetic and epigenetic factors such as the length of the DNA, nearby sequences, and methylation patterns (Chahrour et al., 2008; Ghosh et al., 2010; Zahir and Brown, 2011). MeCP2 is a known binding partner of 5-methylcytosine (5mC) at CpG dinucleotides throughout the genome, resulting in transcriptional repression in these regions (Guy et al., 2011). However, MeCP2 is also the predominant 5-hydroxymethylcytosine (5hmC)-binding protein in the brain. Enrichment of 5hmC is linked to highly expressed genes (Song et al., 2011; Mellén et al., 2012) in the absence of 5mC, suggesting that in the context of this binding interaction, MeCP2 facilitates transcription (Mellén et al., 2012). Of note, MeCP2 is itself subject to methylation-dependent regulation, disruptions in which have been linked to autism (Nagarajan et al., 2008). Thus, epigenetic modifications can regulate both the expression of MeCP2 and its downstream binding partners.

Alternative splicing of *Mecp2/MECP2* generates two main isoforms that differ exclusively at the N-terminus (Kriaucionis and Bird, 2004; Mnatzakanian et al., 2004):

MeCP2_e1, the predominant isoform in the brain (Kriaucionis and Bird, 2004; Mnatzakanian et al., 2004; Dragich et al., 2007; Kaddoum et al., 2013), and MeCP2_e2, which displays a later expression onset during mouse brain development (Olson et al., 2014). The two isoforms exhibit differential temporal and region-specific differences in their expression profiles in the brain and both contribute to neurological function and gene expression patterns (Cusack et al., 2004; Orlic-Milacic et al., 2014; Yasui et al., 2014). The ratio of splice variants differs in a temporal- and cell type-specific manner, suggesting dynamic regulation of their expression and non-redundant functionality in the distinct stages of neurogenesis and adulthood (Dragich et al., 2007; Liyanage et al., 2013; Olson et al., 2014; Orlic-Milacic et al., 2014). Whereas MeCP2_e1 has been shown to be the isoform most relevant to RTT pathogenesis (Yasui et al., 2014), MeCP2_e2 interacts with forkhead protein FoxG1, which promotes neuronal survival and maturation and in which mutations can also cause RTT (Dastidar et al., 2012). The physiological significance of these two isoforms is not fully understood. Manipulations of independent isoforms in a cell type-specific manner are required in order to reveal their respective contributions to activity-dependent functions of MeCP2.

Early work demonstrated that RTT-like deficits are evident in the context of a brain-specific deletion of MeCP2, pointing to the importance of the CNS in RTT (Chen et al., 2001). Animals in which MeCP2 was deleted exclusively in postmitotic neurons exhibited a decrease in the size of individual neurons of the cortex, demonstrating that MeCP2 deficiency at postnatal stages of development is sufficient to cause disease phenotypes. Whereas this does not rule out a prenatal component of RTT

pathogenesis, it suggests that MeCP2 may have a critical and lasting role in mature neuronal function, which lends insight into avenues for treatment.

Reversal of functional and behavioral deficits in RTT

One of the key discoveries in RTT has been the amelioration of function following reactivation of endogenous *Mecp2* (Guy et al., 2007; Cobb et al., 2010). This striking finding, an important feature not only of RTT but perhaps also of neurodevelopmental disorders in general, suggests that the neurodevelopmental pathology is reversible.

The phenotypic reversibility of advanced neurological phenotypes in both immature and mature adult animals shows that reactivation of the MeCP2 protein even at late stages of the disorder can partially rescue the mutant phenotype (Giacometti et al., 2007; Guy et al., 2007). Systemic delivery of MeCP2 cDNA via AAV9, under control of a fragment of its own promoter (scAAV9/MeCP2), has been shown to significantly rescue behavioral and cellular deficits when administered systemically into female RTT mice (Garg et al., 2013). Proposed as a model for gene therapy, the retroviral-mediated overexpression of the MeCP2_e1 isoform in neural stem cells taken from *Mecp2* heterozygous mice was shown to promote dendritic branching *in vitro* (Rastegar et al., 2009). Perhaps more practically, pharmacological manipulations, such as the treatment of *Mecp2* null mice with recombinant human IGF1 (rhIGF1) or a peptide fragment of IGF1, also resulted in a partial rescue of synaptic defects and cortical excitatory synaptic transmission, in addition to restoring activation of signaling pathway proteins (Tropea et al., 2009; Castro et al., 2014). These studies argue that the brain circuits

involved in neural processing may not functionally decline but rather remain in a labile, immature state; their subsequent activation by the re-introduction of *Mecp2* (Giacometti et al., 2007; Guy et al., 2007) or by pharmacological manipulations to activate downstream signaling pathways (Tropea et al., 2009; Castro et al., 2014) is an important measure to ameliorate the syndrome's consequences.

Timeline of pathogenesis

Traditionally, the dynamic time-course of RTT is thought to involve a period of apparently normal early development followed by profound neurological regression—a defining feature of RTT—and subsequent stabilization or partial recovery. This delayed clinical onset suggests a predominantly postnatal component to RTT, which has been supported by early work demonstrating that a loss of MeCP2 exclusively in postmitotic forebrain neurons recapitulates many aspects of disease (Gemelli et al., 2006). Correspondingly, expressing MeCP2 exclusively in postmitotic neurons of *Mecp2* mutant mice rescued a range of RTT phenotypes (Luikenhuis et al., 2004). These seminal studies, though key to our understanding of RTT pathogenesis, leave open the possibility of earlier effects due to the strong phenotypes examined such as body weight, brain weight, and locomotor behavioral deficits. Cortical development, differentiation, and migration effects that occur during neurogenesis may be evident in subtle phenotypes. Similarly, postnatal restoration of MeCP2 may leave subtle phenotypes uncorrected. In a similar vein, our clinical understanding of the disease initiation and progression and the ways in which *MECP2* impacts distinct phases of neurodevelopment is gradually evolving. In recent years, there has been a gradual shift

in our understanding of atypical regression in RTT patients, with growing evidence of prenatal and early postnatal developmental abnormalities resulting in defects in the establishment and refinement of early neural circuits and, later, cortical plasticity (**Figure 1**).

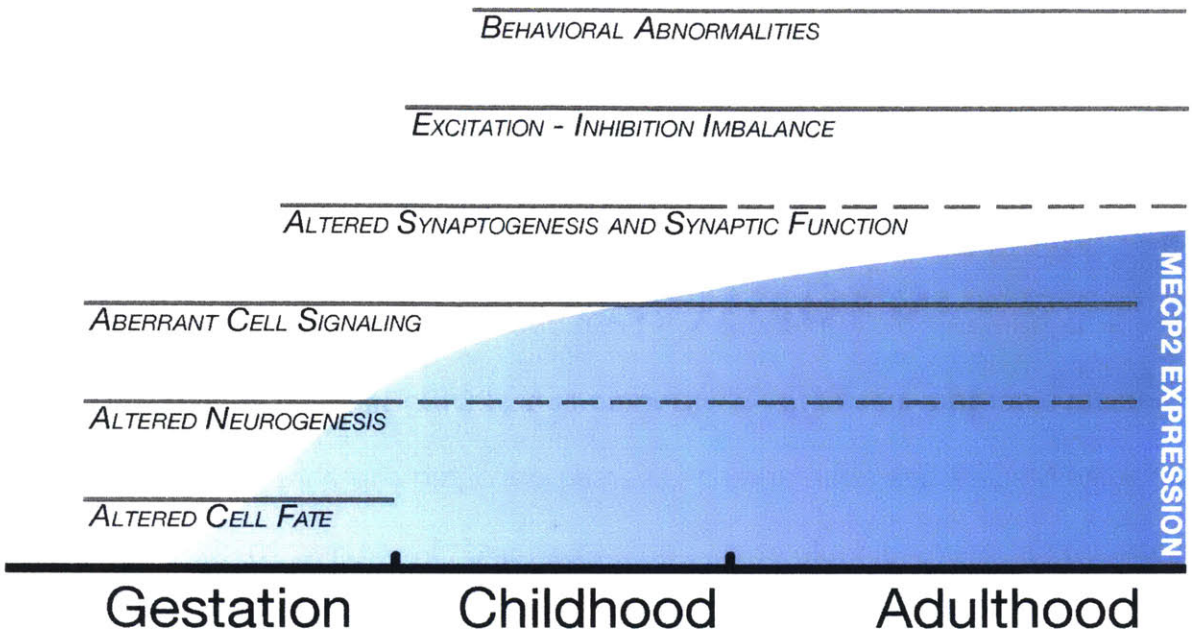

Figure 1. Roles of MeCP2 throughout the lifespan

MeCP2 influences multiple features of brain development and function, at a variety of time points as its expression increases and is maintained. Thus, prenatal and postnatal brain development, as well as adult function, are all potentially affected in Rett Syndrome.

MeCP2 expression affects successive stages of brain development including prenatal neurogenesis, postnatal development of synaptic connections and function, experience-dependent synaptic plasticity, and maintenance of adult neural function including sensory integration (Chahrour and Zoghbi, 2007; Banerjee et al., 2012; Lyst and Bird, 2015). MeCP2 critically maintains synaptic excitation (E) and inhibition (I), which are fundamental to the function of brain circuits and are often disrupted in neurological disorders including RTT (Boggio et al., 2010; Banerjee et al., 2012). Additionally, MeCP2 has a remarkably diverse pool of binding partners and downstream targets (Urdinguio et al., 2008; Ebert and Greenberg, 2013). This functional and binding complexity, in combination with the domain-specific functionality of the MeCP2 protein (Kumar et al., 2008; Adkins and Georgel, 2011), confers a pleiotropic effect across age- and cell-type specific backgrounds (Zahir and Brown, 2011). Accordingly, different mutations in MeCP2 result in a wide range of phenotypic variability and severity in RTT patients (Cuddapah et al., 2014), necessitating context-dependent mechanistic insights into MeCP2 function.

Whereas MeCP2 is known to be a dynamic, pleiotropic regulator of gene expression, several reports suggest that at a fundamental level, RTT is a metabolic disorder that affects both neurons and glia (Saywell et al., 2006; Viola et al., 2007). Global reductions in transcription and translation in human RTT neurons (Li et al., 2013) support this concept. A mitochondrial component has been suggested as the causal metabolic defect in RTT (Kriaucionis et al., 2006); others have demonstrated altered

concentrations of several brain metabolites in MeCP2-deficient male mice at 5-8 weeks of age that suggest deficits in membrane lipid metabolism, osmoregulation, and glutamatergic neurotransmission (Viola et al., 2007). Accordingly, oxidative stress has been suggested as one of the main causes of neuronal dysfunction in RTT (Filosa et al., 2015) and could potentially explain the toxicity of MeCP2-deficient neurons on neighboring WT cells. Whereas metabolic pathways utilized by NPs differ from those in neurons (Candelario et al., 2013), effects of MeCP2 depletion on various metabolic components may differ throughout development and potentially contribute to its pleiotropic effects. Of note, glucose metabolism increases in the cortex at approximately 8-12 months of age, close to the age in which clinical RTT symptoms begin to emerge (Shahbazian et al., 2002a).

Transgenic mouse models that harbor cell-type specific mutations in MeCP2 have shed light on our understanding of RTT pathogenesis in the brain. Expression of MeCP2 under the CamKII or neuron-specific enolase promoter did not prevent the appearance of most RTT phenotypes, suggesting a more complex network of involvement for MeCP2 (Alvarez-Saavedra et al., 2007). Interestingly, mice lacking MeCP2 exclusively in GABAergic neurons recapitulate many RTT features (Chao et al., 2010), and deletion of MeCP2 in the parvalbumin (PV)-expressing subset of GABAergic neurons abolishes experience-dependent critical plasticity in the absence of most RTT phenotypes (He et al., 2014). The restoration of MeCP2 exclusively in astrocytes resulted in a non-cell-autonomous ameliorative effect on neurons *in vivo* (Lioy et al., 2011), whereas RTT microglia were shown to exhibit adverse non-cell-autonomous

effects on WT neurons in vitro (Maezawa and Jin, 2010). In spite of their differing roles and effects on downstream gene regulation (Orlic-Milacic et al., 2014), transgenic expression of either the MeCP2_e1 or MeCP2_e2 splice variant has been shown to prevent the development of a number of RTT phenotypes in a mouse model lacking MeCP2. However, many abnormalities were only partially prevented, negating the notion that both transcripts are capable of acting independently and without fault to fulfill all of the roles of MeCP2 (Kerr et al., 2012). Accordingly, another study demonstrated that a point mutation in the MeCP2_e1 splice variant is sufficient to recapitulate many RTT phenotypes observed in MeCP2 KO mice (Yasui et al., 2014). Whereas the complexity that underlies the roles of MeCP2 will not be resolved with a single mouse model, each contributes a fragment to the larger puzzle that represents MeCP2 functionality.

Similar to loss of function mutations in *MECP2*, the duplication of *MECP2* also results in a progressive neurological disorder that includes stereotypic and repetitive hand or body movements, epilepsy, spasticity, and a severe syndromic form of intellectual disability in male patients (Van Esch, 2011). Recent studies show that the neurological dysfunctions in MECP2 duplication syndrome are reversible in adult symptomatic mice and correction of MeCP2 levels genetically or by using antisense oligonucleotides largely restores molecular, electrophysiological, and behavioral deficits (Sztainberg et al., 2015).

Modeling RTT

Mouse models of RTT generated thus far have provided a wealth of knowledge regarding the pathophysiology of the disorder. However, complex genetic and environmental contexts of human disease are virtually impossible to recreate in an engineered mouse model. It is with the advent of iPSCs that the potential for modeling (and drug screening in) genetically accurate human disease *in vitro* has emerged. As a monogenic developmental disorder, RTT is ideally amenable to this approach. Human iPSCs derived from human dermal fibroblasts (HDFs) are comparable to human embryonic stem (hES) cells with respect to proliferative and differentiating potential, but are not subject to the ethical debate surrounding the use of hES cells. Human iPSCs are most often generated via introduction of retroviral vectors containing transformative factors Oct3/4, Sox2, Klf4, and c-Myc into HDFs. Resulting iPSCs express hES markers and display histone modification status characteristic of hES cells. iPSCs selected by marker *Nanog* (target of Oct3/4 and Sox2) are virtually identical to ES cells regarding global gene expression, DNA methylation, and histone modification (Takahashi et al., 2007).

Recent advances in the differentiation of hPSCs have successfully recapitulated cerebral cortical development *in vitro*. Combining retinoid signaling with dual inhibition of SMAD signaling promotes efficient neural induction and generates, in a manner consistent with development *in vivo*, glutamatergic neurons inclusive of all six cortical layers and glia (Shi et al., 2012a; 2012b). GABAergic interneurons, which emanate and tangentially migrate from the ganglionic eminences *in vivo* (Goulburn et al., 2012), can

be generated from hNPCs via the addition of ventralizing signaling molecule Sonic hedgehog (Shh) or its agonist purmorphamine (Goulburn et al., 2012; Ma et al., 2012; Shi et al., 2012b).

Differentiation protocols designed to recapitulate cortical development *in vitro* are useful in their capacity to expose phenotypes during these critical stages of neurogenesis. In order to build on this potential, recent advances in neuronal differentiation techniques have allowed for the generation of cerebral organoids, or spheroids, which are 3D cellular structures that mimic corticogenesis to generate defined regions of cortical identity *in vitro* (Lancaster et al., 2013; Paşca et al., 2015). It is worth noting that protocols designed to recapitulate neurogenesis are often time-consuming, as the cells mature according to an intrinsic time scale. As such, these protocols are best suited to study differentiating or early neurons. In order to study mature neurons in an expedited time frame, protocols have been developed to speed the transition from iPSC or fibroblast to neuron via viral-mediated (Zhang et al., 2013a) and miRNA-mediated (Kuo and Ying, 2012) methods. The viral-mediated overexpression of Ngn2 in iPSCs (Zhang et al., 2013b) induces a neuronal identity (as defined by gene expression and electrophysiological properties) two weeks post-infection. This rapid induction, albeit poorly suited for studies of early neurogenesis, is highly effective for the study of neuronal activity and has been shown to generate neurons that functionally integrate into the mouse brain.

Amidst the excitement over the multitude of potential applications for the "disease-in-a-dish" approach, it is critical to acknowledge that studying genetic disorders in human cells faces substantially more challenges regarding controls as compared to inbred mouse lines. Comparing patient-derived iPSCs to control iPSCs that share partial or no genetic background poses considerable risks of under- or over-interpreting disease-related phenotypes. Therefore, to provide a solid foundation for investigating disease mechanisms, testing therapy efficacy, and identifying new treatments, the derivation and analysis of hPSCs must be performed in an isogenic context.

Two main approaches exist for the generation of an isogenic iPSC line modeling an X-linked disease. The first exploits the mechanism of XCI throughout the processes of cellular reprogramming and differentiation. Controversy exists as to whether or not hiPSCs reactivate the inactive X-chromosome during the process of reprogramming (Cheung et al., 2012). Specifically, in the generation of RTT hiPSCs, some have reported such a reactivation (Marchetto et al., 2010), whereas others have reported the generation of RTT iPSCs that retain the XCI pattern of the original fibroblast (Ananiev et al., 2011; Cheung et al., 2011; Farra et al., 2012). These inconsistencies are possibly due to tissue culture methodology, as XCI is reportedly influenced by atmospheric oxygen concentration (Lengner et al., 2010). Irrespective of XCI activation during the reprogramming stage, each hiPS cell will express one of two X chromosomes, be it the same as its founding somatic cell or the opposite. By isolating iPS colonies at a single-cell level and independently expanding these populations, one can create a homogeneous clonal population of iPSCs from a patient cell that expresses either the

wild type or mutant allele. These two groups allow for comparison between patient-derived cell lines that differ exclusively at the disease locus. Alternatively, genome editing procedures are capable of generating pairs of isogenic lines that differ exclusively at the disease locus. CRISPR-associated endonuclease (Cas)9 (CRISPR/Cas9) has been used to introduce frame-shifting, insertion/deletion (INDEL) mutations that are targeted to the *Mecp2* locus using specific guide RNAs (gRNAs) via adeno-associated viral (AAV) vectors (Heidenreich and Zhang, 2015). The method has also been used to generate isogenic pairs of human ESCs in which to model RTT *in vitro* (Li et al., 2013).

Membrane phenotypes

MeCP2 is known to regulate the expression of voltage-gated channels in addition to genes relevant to synaptic transmission (Orlic-Milacic et al., 2014). iPSC-derived RTT neurons that harbor a mutation in the *MECP2e1* isoform exhibit dysfunction in action potential generation and decreased voltage-gated Na^+ currents. Additionally, these neurons display dysfunctional synaptic activity, with deficits in both amplitude and frequency of mEPSCs (Djuric et al., 2015). Similarly, RTT patient iPSC-derived neurons have been shown to express reduced levels of voltage-gated sodium channel genes *SCN1A* and *SCN1B* (Kim et al., 2011). iPS-derived neurons from heterozygous *Mecp2*^{308} mice also exhibited deficits in evoked action potentials, glutamatergic synaptic transmission, and aberrancies in sodium channel function (Farra et al., 2012), which aligns well with more recent data demonstrating decreased expression of calcium, sodium, and potassium channels in *Mecp2*-null mice (Bedogni et al., 2015)

and altered resting membrane potential and excitability in mouse ESC-derived *Mecp2*$^{-/y}$ neurons (Barth et al., 2014).

Deficits in early neurogenesis

Early work in mouse models on the function of MeCP2 reported a pattern of expression limited to the neural lineage, with low expression in neuroblasts and a progressive increase during embryonic and postnatal development. Such findings led to the belief that MeCP2 is predominantly involved in the maturation and maintenance of neuronal function, as opposed to early cell fate decisions, and were further supported by a lack of phenotype observed with respect to differentiation in MeCP2-null NPs (Kishi and Macklis, 2004).

Evidence has since demonstrated that, whereas MeCP2 expression increases post-mitotically, both mRNA and protein can be detected throughout the majority of the mouse and human lifespan, including embryonic stages during which neurogenesis occurs (Shahbazian et al., 2002b; Balmer et al., 2003; Han et al., 2013; Liyanage et al., 2013; Bedogni et al., 2015; Kumar and Thakur, 2015). MeCP2 protein expression does indeed increase post-neuronal differentiation, at which point the vast majority of RTT phenotypes have been described. Experiments designed to determine isoform-specific expression have detected MeCP2_e1 protein in the mouse hippocampus as early as E14, whereas MeCP2_e2 was first detected at E18. Samples younger than E14 were not analyzed in this study, and thus these results do not preclude the possibility of expression at earlier embryonic stages. MeCP2_e1 expression increased until it

reached a plateau at P7-P21. MeCP2_e2 expression overlapped with MeCP2_e1 after E18, albeit at a decreased level (Olson et al., 2014). As the gestational period of synaptogenesis overlaps with that of neuronal migration in human development (Tau and Peterson, 2010), it stands to reason that MeCP2, known to regulate synaptic development (Fukuda et al., 2005; Kaufmann et al., 2005; Smrt et al., 2007), and cell guidance and laminar organization in the olfactory system (Degano et al., 2009), may contribute to the processes of cell fate specification and migration in the developing brain, especially the cortex. Accordingly, the landscape of clinical literature has been shifting to suggest an earlier onset of symptoms in RTT patients (Fehr et al., 2010; 2011; Marschik et al., 2013; Neul et al., 2014; Tarquinio et al., 2015).

Cell fate and signaling pathways

Expression of MeCP2 during early neurogenesis suggests a consequent role for the protein during this critical developmental time point. Neurogenic functions of MeCP2 have indeed since been demonstrated in mouse, whereby embryonic NPCs overexpressing MeCP2 exhibited a heightened neural identity *in vitro* (Tsujimura et al., 2009). Conversely, embryonic NPCs extracted from mice lacking MeCP2 exhibited a more proliferative—as opposed to late post-mitotic—identity, and revealed morphological alterations as early as 3 days *in vitro* (DIV) (Bedogni et al., 2015). A human patient-derived induced pluripotent stem cell (iPSC) model of Rett Syndrome expressing a *de novo* frame-shift mutation in exon 4 (c.806delG) illustrated a parallel role for MeCP2 in the promotion of neural identity in which neural stem cells lacking MeCP2 exhibited increased astrocytic differentiation *in vitro* (Andoh-Noda et al., 2015).

Mesenchymal stem cells (MSCs) isolated from a Rett patient harboring a different *de novo* mutation (del_1164-1207) also demonstrated impaired neural differentiation *in vitro*, which resulted in a reduced percentage of NeuN-expressing cells and increased senescence (Squillaro et al., 2012). Roles for MeCP2 in determining neurogenic potential have been reported in *Xenopus* (Stancheva et al., 2003), zebrafish (Coverdale et al., 2004; Gao et al., 2015) and chick (Petazzi et al., 2014) embryos.

Mechanisms underlying the function of MeCP2 with respect to early cell fate decisions are largely unknown. Neurogenic signaling cascades such as the *Notch-Delta* and PI3K-Akt pathways have been demonstrated to coordinate with MeCP2 throughout various time points including neurogenesis. Phosphorylation of MeCP2 at Serine421 (S421)—known to regulate gene transcription and synaptic development in an activity-dependent manner (Zhou et al., 2006)—has since been shown to modulate the balance between proliferation and differentiation in NPCs isolated from the adult mouse hippocampus. Evidence suggests that the *Notch-Delta* signaling pathway, mediated via MeCP2-S421 phosphorylation, may serve as the hub linking MeCP2 to neural cell fate decisions in adult NPCs (Li et al., 2014). Experiments performed in *Xenopus* embryos, in which MeCP2 is expressed and is critical for neurogenesis, have demonstrated that the *Notch-Delta* signaling pathway regulates the patterning of primary neuronal differentiation in conjunction with MeCP2 binding. A complete lack of MeCP2 protein resulted in a decrease in the number of neuronal precursors, whereas expression of a truncated form of MeCP2 often found in Rett Syndrome patients—R168X—resulted in an increase in the number of neuronal precursors relative to WT

embryos (Stancheva et al., 2003). This phenotypic variety observed as a result of varying dosages and mutations of MeCP2 is echoed throughout the experimental and clinical literature (Fehr et al., 2010; 2011; Chao and Zoghbi, 2012; Cuddapah et al., 2014).

The PI3K-Akt signaling pathway is implicated in a wide range of cellular functions including cell cycle and transcriptional regulation (Brazil et al., 2004). The pathway has also been shown to regulate key neurological processes such as synaptic transmission (Wang et al., 2003) and neurodegeneration (Humbert et al., 2002; Chen et al., 2003) and is implicated in a range of neurological diseases and disorders such as spinocerebellar ataxia type 1 (Chen et al., 2003), Huntington's disease (Humbert et al., 2002), amyotrophic lateral sclerosis (ALS) (Kaspar et al., 2003), and RTT (Tropea et al., 2009; Ricciardi et al., 2011; Li et al., 2013; Castro et al., 2014). The majority of studies performed in RTT models, including those listed above, have examined the contribution of the PI3K-Akt pathway to disease effects and rescue in mature neurons. Whereas PI3K-Akt signaling has been shown to promote adult neurogenesis in the context of exercise enrichment (Bruel-Jungerman et al., 2009), traumatic brain injury recovery (Wu et al., 2008), and surgical denervation (Zhang et al., 2014), roles for PI3K-Akt signaling have also been demonstrated throughout embryonic neurogenesis in mouse (Chan et al., 2011), *Xenopus* (Peng et al., 2004), and zebrafish (Cheng et al., 2013). However, the precise roles of PI3K-Akt signaling in embryonic neurogenesis in the context of RTT have yet to be elucidated.

microRNAs and MeCP2

microRNAs (miRNAs) finely regulate genetic networks throughout the course of brain development and, with astounding complexity, act as critical determinants of early neurogenic activities such as cortical patterning and activity development, cellular subtype specification, and neuronal differentiation (Coolen and Bally-Cuif, 2009; Fineberg et al., 2009; Lau and Hudson, 2010). They are themselves subject to upstream epigenetic regulation; many are indeed targets of MeCP2 (Szulwach et al., 2010) or, as in the case of miR-132, act in a feedback loop as both target and regulator to maintain MeCP2 levels (Klein et al., 2007). miR-132 has in turn been shown to promote postnatal neurogenesis and synaptic integration in neurons of the olfactory bulb (Pathania et al., 2012). Another brain-enriched miRNA target of MeCP2, miR-137, has been shown to regulate neuronal maturation and dendritogenesis in the postnatal hippocampus (Smrt et al., 2010) and to modulate proliferation and differentiation in adult neurogenesis (Szulwach et al., 2010). Moreover, miR-137 been shown to negatively regulate neural stem cell proliferation and promote differentiation in embryonic mouse brains (Sun et al., 2011). miR-199a has been demonstrated as a link between MeCP2 and the mTOR pathway (Tsujimura et al., 2015), previously implicated in RTT (Ricciardi et al., 2011). MeCP2 facilitates the post-processing of miR-199a, which positively regulates mTOR signaling. Notably, exogenous miR-199a ameliorated several impairments in RTT neurons and the genetic deletion of miR-199a-2 resulted in decreased mTOR activity in the brain and the recapitulation of several RTT phenotypes (Tsujimura et al., 2015). MeCP2 is known to influence the production of growth factors such as BDNF and IGF1—the latter via a miRNA-mediated pathway downstream of

BDNF (Mellios et al., 2014). Many pathways and loops that determine the process of neurogenesis are maintained by the concerted regulation of miRNAs and MeCP2. As such, they provide insight into potential avenues by which MeCP2—or a lack-there-of—can influence the developing cortex.

Deficits in neuronal migration and cortical patterning

Functions of MeCP2 during early neurogenesis result in immediate and long-term effects on neuronal migration and cortical patterning. Migration begins at gestational week 8 in humans and at E11 in mouse, at which point NPs proliferating within the ventricular zone that lines the cerebral ventricles begin to differentiate to form the cortical laminae (Tau and Peterson, 2010; Kwan et al., 2012). Post-mitotic cells migrate over radial glial scaffolds to form the discrete layers of the cerebral cortex in an inside-first, outside-last temporal pattern. Deep-layer cortical neurons are born first and passed by newly born neurons migrating to upper layers. This process is spatiotemporally governed by a variety of signaling, transcriptional, and epigenetic mechanisms (McConnell, 1995; Corbin et al., 2008; Martynoga et al., 2012). Aberrant regulation of the proliferation and differentiation of neural stem cells results in a range of cortical dysplasias and is associated with many neurological and neuropsychiatric disorders including Alzheimer's disease, schizophrenia, and ASDs (Valiente and Marín, 2010).

Early work demonstrated morphological cortical deficits in 8-week-old MeCP2$^{-/y}$ mice including reduced thickness and increased cell density in neocortical layers; due in part

to the belief that MeCP2 was not expressed early on, these alterations were believed to be a result of reduced cell size and complexity as opposed to deficits in corticogenesis (Kishi and Macklis, 2004). Cerebellar expression profiling performed alongside chromatin immunoprecipitation in MeCP2-deficient mice has since revealed increased expression of *Reln*—encoding the extracellular signaling protein Reelin, known to be essential for proper neuronal lamination (Jordan et al., 2007). Accordingly, recent evidence has demonstrated that mouse NPCs lacking MeCP2 exhibit delayed corticogenesis with respect to migration from the sub-ventricular and ventricular zones into the cortical plate (Bedogni et al., 2015). These findings suggest a need for a thorough evaluation of the role of MeCP2 in cortical migration and lamination, as layering deficits observed at postnatal time points in RTT may result from combinatorial deficits in cortical development and maintenance.

Deficits in synaptic transmission and plasticity during postnatal development

Along with deficits in early neurogenesis and cortical patterning, *MECP2* has been shown to play a key role in synaptic maturation and plasticity. Mutant mouse models have been generated with a global deletion of MeCP2 ($MeCP2^{-/y}$) from all neurons and selectively from specific cellular subtypes including various neuronal subtypes and astrocytes. These models have served as a robust genetic starting point in which to study the common principles underlying synaptic defects and how interplay of these cell types might contribute to the disorder.

Functional defects in synaptic transmission have been investigated in an *Mecp2* global deletion model in which cortical connections were found to have weaker excitatory synaptic transmission and lower levels of basal activity (Dani et al., 2005; Chang et al., 2006; Nelson et al., 2006; Chahrour and Zoghbi, 2007; Chao et al., 2007), reminiscent of an immature circuit. Cellular mechanisms of long-term plasticity, considered the functional basis of learning and memory, have also been found to be impaired in *Mecp2* mutant animals (Amir et al., 1999; Asaka et al., 2006; Lonetti et al., 2010). The majority of these early studies have used brain slice preparations, recording synaptic transmission including miniature synaptic currents and synaptic plasticity deficits. Similar to deficits in excitatory transmission, deletion of *Mecp2* from all forebrain GABAergic interneurons also recapitulates key features of RTT, suggesting that inhibition plays a crucial role in RTT pathophysiology. This includes reduced GABA synthesis, Gad1 and Gad2 levels, reduced miniature inhibitory postsynaptic currents (mIPSCs), and an array of behavioral deficits including EEG hyperexcitability and severe respiratory dysrhythmias (Chahrour et al., 2008; Chao et al., 2010; Li et al., 2013). Anatomical studies have reported enhanced PV+ neuronal puncta and hyperconnected PV+ circuitry in mouse visual cortex, suggesting these microcircuits contribute to enhanced inhibition in MeCP2$^{-/y}$ mice (Durand et al., 2012; Cheng et al., 2014). This altered inhibition mediated by PV+ neurons, which regulates the initiation and termination of the critical period, has been proposed to alter the timing of critical period plasticity in RTT (Qiu et al., 2012; Krishnan et al., 2015). Functional studies, however, have consistently reported decreased inhibitory function including reduced mIPSCs in CA3 pyramidal neurons of MeCP2$^{-/y}$ mice (Chahrour et al., 2008; Ghosh et

al., 2010; Zahir and Brown, 2011; Calfa et al., 2015). Although the density and intrinsic membrane properties of PV+ and somatostatin (SST)+ interneurons were not affected in MeCP2$^{-/y}$ mice, miniature excitatory postsynaptic currents (mEPSCs) were found to be smaller and less frequent in fast-spiking PV+ neurons, suggesting impaired glutamatergic drive specifically onto this interneuron population compared to SST+ neurons (Calfa et al., 2015). Studies in slices have also reported a reduction in mEPSC amplitudes and a deficit in excitatory pathways, in the absence of change in mIPSC amplitude or frequency (Dani et al., 2005; Wood et al., 2009). These results are consistent with the decreased visually-evoked responses found in PV+ interneurons in mouse visual cortex *in vivo* (He et al., 2014). Interestingly, recent studies have highlighted the differential effects of subtype-specific *Mecp2* deletion on GABAergic inhibition regulating non-overlapping neurological symptoms: mice lacking MeCP2 in PV+ neurons showed sensory, motor, memory, and social deficits, whereas those lacking in SOM+ neurons exhibited seizures and stereotypies (Ito-Ishida et al., 2015), further elucidating the complex regulation of inhibition and their disruption in RTT (Banerjee et al., 2012).

Taken together, these features indicate that RTT is a complex disorder that arises from an imbalance of excitation and inhibition and a failure of brain circuitry to attain a mature state (Guy et al., 2011; Banerjee et al., 2012). Many of these defects can have a strong early developmental, even prenatal component (**Figure 1**) when the brain fails to attain 'phenotypic checkpoint' signatures and in turn provides faulty functional feedback that influences gene expression (Ben-Ari and Spitzer, 2010) and network

malfunction (Ben-Ari, 2015). A coherent set of physiological measurements using *in vivo* awake animal models of global and neuronal subtype-specific *Mecp2*-deletion remains necessary to measure and evaluate functional defects in the synaptic balance of excitation and inhibition.

Deficits in adult maintenance and function

The onset of symptoms during early life in RTT patients, in conjunction with findings from mouse models suggesting neurodevelopmental abnormalities in RTT, have raised the question whether *Mecp2* function is necessary for integrative function in the adult brain. To address this, an inducible knockout approach was used to delete *Mecp2* in adult mice (≥ P60) following normal development by crossing floxed *Mecp2* allele mice with mice expressing a tamoxifen-inducible Cre-ER allele (McGraw et al., 2011). This late deletion of *Mecp2* recapitulated key germline knockout phenotypes including abnormal gait, hind-limb clasping, motor abnormalities, impaired nesting ability, and impaired learning and memory, further underscoring the importance of *Mecp2* in adult neurological function (McGraw et al., 2011). Interestingly, this adult deletion recapitulated an epigenetic memory clock, suggesting a mechanism that extends—or is independent—from its early global genetic regulation (Chen et al., 2015).

Similar to behavioral deficits, the physiological response features of adult *Mecp2*-deleted neurons have also been characterized *in vivo. In vivo* genome-editing via CRISPR/Cas9 resulted in ~68% of targeted cells containing INDEL mutations with a >60% reduction in MeCP2 protein levels (Swiech et al., 2015). Stereotactic injection of

AAV-SpCas9 and gRNA targeting *Mecp2* into the superficial layers of mouse primary visual cortex followed by two-photon guided targeted electrophysiological recordings from genome-edited neurons revealed altered integrative visual responses, further emphasizing the maintenance role of *Mecp2* in the adult brain after normal developmental milestones have been achieved.

Thesis Aims

The fluidity with which MeCP2 regulates the genomic landscape renders a uniquely moving target that has proven difficult to fully understand. Amongst many factors to be taken into account when attempting to attribute mechanistic function to MeCP2 (e.g., cell type, mutation and associated functional domain, range of downstream targets), it is crucial to consider the time point in question. Deletion of MeCP2 results in a wide and temporally varied range of phenotypes. A complete picture of the MeCP2 protein includes its roles at various life stages, so as to inform our evolving concept of RTT progression in patients and potential phenotypic reversibility. We have sought to contribute to the growing understanding of the roles of MeCP2 throughout development by generating and characterizing RTT patient-derived neurons during neurogenesis and later in development during the maturation of physiological membrane and synaptic properties. We generated both monolayer and 3D neuronal cultures and demonstrated their utility in reproducing known RTT phenotypes and in revealing novel phenotypes not previously reported in human neurons. We have identified key signatures of RTT at early and late stages of human neurogenesis, including: 1) miRNA-mediated signaling pathway dysfunction, 2) aberrant neurogenesis

and progenitor migration, and 3) aberrant membrane and synaptic development. These features need not act in a mutually exclusive or even independent manner, but rather are likely interconnected pieces of a larger puzzle that comprises the stages of RTT pathophysiology. These components can easily go unnoticed in mouse models of RTT, in which the process of neurogenesis is compressed relative to that in humans. Future studies of RTT should take into account the prenatal component to pathophysiology in order to more fully understand the mechanisms governing patient symptoms and attempts to ameliorate them.

References

Adkins NL, Georgel PT (2011) MeCP2: structure and function. Biochem Cell Biol 89:1–11.

Alvarez-Saavedra M, Sáez MA, Kang D, Zoghbi HY, Young JI (2007) Cell-specific expression of wild-type MeCP2 in mouse models of Rett syndrome yields insight about pathogenesis. Human Molecular Genetics 16:2315–2325.

Amir RE, Van den Veyver IB, Wan M, Tran CQ, Francke U, Zoghbi HY (1999) Rett syndrome is caused by mutations in X-linked MECP2, encoding methyl-CpG-binding protein 2. Nat Genet 23:185–188.

Ananiev G, Williams EC, Li H, Chang Q (2011) Isogenic pairs of wild type and mutant induced pluripotent stem cell (iPSC) lines from Rett syndrome patients as in vitro disease model. PLoS ONE 6:e25255.

Andoh-Noda T, Akamatsu W, Miyake K, Matsumoto T, Yamaguchi R, Sanosaka T, Okada Y, Kobayashi T, Ohyama M, Nakashima K, Kurosawa H, Kubota T, Okano H (2015) Differentiation of multipotent neural stem cells derived from Rett syndrome patients is biased toward the astrocytic lineage. Mol Brain 8:31.

Asaka Y, Jugloff DGM, Zhang L, Eubanks JH, Fitzsimonds RM (2006) Hippocampal synaptic plasticity is impaired in the Mecp2-null mouse model of Rett syndrome. Neurobiol Dis 21:217–227.

Balmer D, Goldstine J, Rao YM, Lasalle JM (2003) Elevated methyl-CpG-binding protein 2 expression is acquired during postnatal human brain development and is correlated with alternative polyadenylation. J Mol Med 81:61–68.

Banerjee A, Castro J, Sur M (2012) Rett syndrome: genes, synapses, circuits, and therapeutics. Front Psychiatry 3:34.

Barth L, Sütterlin R, Nenniger M, Vogt KE (2014) Reduced synaptic activity in neuronal networks derived from embryonic stem cells of murine Rett syndrome model. Front Cell Neurosci 8:79.

Bedogni F, Cobolli Gigli C, Pozzi D, Rossi RL, Scaramuzza L, Rossetti G, Pagani M, Kilstrup-Nielsen C, Matteoli M, Landsberger N (2015) Defects During Mecp2 Null Embryonic Cortex Development Precede the Onset of Overt Neurological Symptoms. Cereb Cortex.

Ben-Ari Y (2015) Is birth a critical period in the pathogenesis of autism spectrum disorders? Nat Rev Neurosci.

Ben-Ari Y, Spitzer NC (2010) Phenotypic checkpoints regulate neuronal development.

Trends in Neurosciences 33:485–492.

Boggio EM, Lonetti G, Plzzorusso T, Giustetto M (2010) Synaptic determinants of rett syndrome. Frontiers in Synaptic Neuroscience 2:28.

Brazil DP, Yang Z-Z, Hemmings BA (2004) Advances in protein kinase B signalling: AKTion on multiple fronts. Trends Biochem Sci 29:233–242.

Bruel-Jungerman E, Veyrac A, Dufour F, Horwood J, Laroche S, Davis S (2009) Inhibition of PI3K-Akt signaling blocks exercise-mediated enhancement of adult neurogenesis and synaptic plasticity in the dentate gyrus. PLoS ONE 4:e7901.

Calfa G, Li W, Rutherford JM, Pozzo-Miller L (2015) Excitation/inhibition imbalance and impaired synaptic inhibition in hippocampal area CA3 of Mecp2 knockout mice. Hippocampus 25:159–168.

Candelario KM, Shuttleworth CW, Cunningham LA (2013) Neural stem/progenitor cells display a low requirement for oxidative metabolism independent of hypoxia inducible factor-1alpha expression. J Neurochem 125:420–429.

Castro J, Garcia RI, Kwok S, Banerjee A, Petravicz J, Woodson J, Mellios N, Tropea D, Sur M (2014) Functional recovery with recombinant human IGF1 treatment in a mouse model of Rett Syndrome. Proc Natl Acad Sci USA 111:9941–9946.

Chahrour M, Jung SY, Shaw C, Zhou X, Wong STC, Qin J, Zoghbi HY (2008) MeCP2, a key contributor to neurological disease, activates and represses transcription. Science 320:1224–1229.

Chahrour M, Zoghbi HY (2007) The story of Rett syndrome: from clinic to neurobiology. Neuron 56:422–437.

Chan CB, Liu X, Pradoldej S, Hao C, An J, Yepes M, Luo HR, Ye K (2011) Phosphoinositide 3-kinase enhancer regulates neuronal dendritogenesis and survival in neocortex. Journal of Neuroscience 31:8083–8092.

Chang Q, Khare G, Dani V, Nelson S, Jaenisch R (2006) The disease progression of Mecp2 mutant mice is affected by the level of BDNF expression. Neuron 49:341–348.

Chao H-T, Chen H, Samaco RC, Xue M, Chahrour M, Yoo J, Neul JL, Gong S, Lu H-C, Heintz N, Ekker M, Rubenstein JLR, Noebels JL, Rosenmund C, Zoghbi HY (2010) Dysfunction in GABA signalling mediates autism-like stereotypies and Rett syndrome phenotypes. Nature 468:263–269.

Chao H-T, Zoghbi HY (2012) MeCP2: only 100% will do. Nat Genet 15:176–177.

Chao H-T, Zoghbi HY, Rosenmund C (2007) MeCP2 controls excitatory synaptic

strength by regulating glutamatergic synapse number. Neuron 56:58–65.

Chen H-K, Fernandez-Funez P, Acevedo SF, Lam YC, Kaytor MD, Fernandez MH, Aitken A, Skoulakis EMC, Orr HT, Botas J, Zoghbi HY (2003) Interaction of Akt-phosphorylated ataxin-1 with 14-3-3 mediates neurodegeneration in spinocerebellar ataxia type 1. Cell 113:457–468.

Chen L, Chen K, Lavery LA, Baker SA, Shaw CA, Li W, Zoghbi HY (2015) MeCP2 binds to non-CG methylated DNA as neurons mature, influencing transcription and the timing of onset for Rett syndrome. Proc Natl Acad Sci USA 112:5509–5514.

Chen RZ, Akbarian S, Tudor M, Jaenisch R (2001) Deficiency of methyl-CpG binding protein-2 in CNS neurons results in a Rett-like phenotype in mice. Nat Genet 27:327–331.

Cheng T-L, Wang Z, Liao Q, Zhu Y, Zhou W-H, Xu W, Qiu Z (2014) MeCP2 suppresses nuclear microRNA processing and dendritic growth by regulating the DGCR8/Drosha complex. Dev Cell 28:547–560.

Cheng Y-C, Hsieh F-Y, Chiang M-C, Scotting PJ, Shih H-Y, Lin S-J, Wu H-L, Lee H-T (2013) Akt1 Mediates Neuronal Differentiation in Zebrafish via a Reciprocal Interaction with Notch Signaling. PLoS ONE 8:e54262.

Cheung AYL, Horvath LM, Carrel L, Ellis J (2012) X-chromosome inactivation in rett syndrome human induced pluripotent stem cells. Front Psychiatry 3:24.

Cheung AYL, Horvath LM, Grafodatskaya D, Pasceri P, Weksberg R, Hotta A, Carrel L, Ellis J (2011) Isolation of MECP2-null Rett Syndrome patient hiPS cells and isogenic controls through X-chromosome inactivation. Human Molecular Genetics.

Cobb S, Guy J, Bird A (2010) Reversibility of functional deficits in experimental models of Rett syndrome. Biochem Soc Trans 38:498–506.

Coolen M, Bally-Cuif L (2009) MicroRNAs in brain development and physiology. Curr Opin Neurobiol 19:461–470.

Corbin JG, Gaiano N, Juliano SL, Poluch S, Stancik E, Haydar TF (2008) Regulation of neural progenitor cell development in the nervous system. J Neurochem 106:2272–2287.

Coverdale LE, Martyniuk CJ, Trudeau VL, Martin CC (2004) Differential expression of the methyl-cytosine binding protein 2 gene in embryonic and adult brain of zebrafish. Brain Res Dev Brain Res 153:281–287.

Cuddapah VA, Pillai RB, Shekar KV, Lane JB, Motil KJ, Skinner SA, Tarquinio DC, Glaze DG, McGwin G, Kaufmann WE, Percy AK, Neul JL, Olsen ML (2014) Methyl-CpG-binding protein 2 (MECP2) mutation type is associated with disease severity

in Rett syndrome. Journal of Medical Genetics 51:152–158.

Cusack SM, Rohn TT, Medeck RJ, Irwin KM, Brown RJ, Mercer LM, Oxford JT (2004) Suppression of MeCP2beta expression inhibits neurite extension in PC12 cells. Exp Cell Res 299:442–453.

Dani VS, Chang Q, Maffei A, Turrigiano GG, Jaenisch R, Nelson SB (2005) Reduced cortical activity due to a shift in the balance between excitation and inhibition in a mouse model of Rett syndrome. Proc Natl Acad Sci USA 102:12560–12565.

Dastidar SG, Bardai FH, Ma C, Price V, Rawat V, Verma P, Narayanan V, D'Mello SR (2012) Isoform-specific toxicity of Mecp2 in postmitotic neurons: suppression of neurotoxicity by FoxG1. Journal of Neuroscience 32:2846–2855.

Degano AL, Pasterkamp RJ, Ronnett GV (2009) MeCP2 deficiency disrupts axonal guidance, fasciculation, and targeting by altering Semaphorin 3F function. Mol Cell Neurosci 42:243–254.

Djuric U, Cheung AYL, Zhang W, Mok RS, Lai W, Piekna A, Hendry JA, Ross PJ, Pasceri P, Kim D-S, Salter MW, Ellis J (2015) MECP2e1 isoform mutation affects the form and function of neurons derived from Rett syndrome patient iPS cells. Neurobiol Dis 76:37–45.

Dragich JM, Kim YH, Arnold AP (2007) Differential distribution of the MeCP2 splice variants in the postnatal mouse brain. Journal of Comparative ....

Durand S, Patrizi A, Quast KB, Hachigian L, Pavlyuk R, Saxena A, Carninci P, Hensch TK, Fagiolini M (2012) NMDA receptor regulation prevents regression of visual cortical function in the absence of Mecp2. Neuron 76:1078–1090.

Ebert DH, Greenberg ME (2013) Activity-dependent neuronal signalling and autism spectrum disorder. Nature 493:327–337.

Farra N, Zhang W-B, Pasceri P, Eubanks JH, Salter MW, Ellis J (2012) Rett syndrome induced pluripotent stem cell-derived neurons reveal novel neurophysiological alterations. Mol Psychiatry.

Fehr S, Bebbington A, Ellaway C, Rowe P, Leonard H, Downs J (2011) Altered attainment of developmental milestones influences the age of diagnosis of rett syndrome. J Child Neurol 26:980–987.

Fehr S, Downs J, Bebbington A, Leonard H (2010) Atypical presentations and specific genotypes are associated with a delay in diagnosis in females with Rett syndrome. Am J Med Genet A 152A:2535–2542.

Filosa S, Pecorelli A, D'Espositoc M, Valacchi G, Hajek J (2015) Exploring the possible link between MeCP2 and oxidative stress in Rett syndrome. Free Radic Biol Med

88:81–90.

Fineberg SK, Kosik KS, Davidson BL (2009) MicroRNAs potentiate neural development. Neuron 64:303–309.

Fukuda T, Itoh M, Ichikawa T, Washiyama K, Goto Y-I (2005) Delayed maturation of neuronal architecture and synaptogenesis in cerebral cortex of Mecp2-deficient mice. J Neuropathol Exp Neurol 64:537–544.

Gao H, Bu Y, Wu Q, Wang X, Chang N, Lei L, Chen S, Liu D, Zhu X, Hu K, Xiong J-W (2015) Mecp2 regulates neural cell differentiation by suppressing the Id1 to Her2 axis in zebrafish. J Cell Sci 128:2340–2350.

Garg SK, Lioy DT, Cheval H, McGann JC, Bissonnette JM, Murtha MJ, Foust KD, Kaspar BK, Bird A, Mandel G (2013) Systemic delivery of MeCP2 rescues behavioral and cellular deficits in female mouse models of Rett syndrome. Journal of Neuroscience 33:13612–13620.

Gemelli T, Berton O, Nelson ED, Perrotti LI, Jaenisch R, Monteggia LM (2006) Postnatal loss of methyl-CpG binding protein 2 in the forebrain is sufficient to mediate behavioral aspects of Rett syndrome in mice. Biol Psychiatry 59:468–476.

Ghosh RP, Horowitz-Scherer RA, Nikitina T, Shlyakhtenko LS, Woodcock CL (2010) MeCP2 binds cooperatively to its substrate and competes with histone H1 for chromatin binding sites. Mol Cell Biol 30:4656–4670.

Giacometti E, Luikenhuis S, Beard C, Jaenisch R (2007) Partial rescue of MeCP2 deficiency by postnatal activation of MeCP2. Proc Natl Acad Sci USA 104:1931–1936.

Goulburn AL, Stanley EG, Elefanty AG, Anderson SA (2012) Generating GABAergic cerebral cortical interneurons from mouse and human embryonic stem cells. Stem Cell Res 8:416–426.

Guy J, Cheval H, Selfridge J, Bird A (2011) The role of MeCP2 in the brain. Annu Rev Cell Dev Biol 27:631–652.

Guy J, Gan J, Selfridge J, Cobb S, Bird A (2007) Reversal of neurological defects in a mouse model of Rett syndrome. Science 315:1143–1147.

Han K, Gennarino VA, Lee Y, Pang K, Hashimoto-Torii K, Choufani S, Raju CS, Oldham MC, Weksberg R, Rakic P, Liu Z, Zoghbi HY (2013) Human-specific regulation of MeCP2 levels in fetal brains by microRNA miR-483-5p. Genes Dev 27:485–490.

He L-J, Liu N, Cheng T-L, Chen X-J, Li Y-D, Shu Y-S, Qiu Z-L, Zhang X-H (2014) Conditional deletion of Mecp2 in parvalbumin-expressing GABAergic cells results in the absence of critical period plasticity. Nat Commun 5:5036.

Heidenreich M, Zhang F (2015) Applications of CRISPR-Cas systems in neuroscience. Nat Rev Neurosci.

Humbert S, Bryson EA, Cordelières FP, Connors NC, Datta SR, Finkbeiner S, Greenberg ME, Saudou F (2002) The IGF-1/Akt pathway is neuroprotective in Huntington's disease and involves Huntingtin phosphorylation by Akt. Dev Cell 2:831–837.

Ito-Ishida A, Ure K, Chen H, Swann JW, Zoghbi HY (2015) Loss of MeCP2 in Parvalbumin-and Somatostatin-Expressing Neurons in Mice Leads to Distinct Rett Syndrome-like Phenotypes. Neuron 88:651–658.

Jordan C, Li HH, Kwan HC, Francke U (2007) Cerebellar gene expression profiles of mouse models for Rett syndrome reveal novel MeCP2 targets. BMC Med Genet 8:36.

Kaddoum L, Panayotis N, Mazarguil H, Giglia-Mari G, Roux JC, Joly E (2013) Isoform-specific anti-MeCP2 antibodies confirm that expression of the e1 isoform strongly predominates in the brain. F1000Res 2:204.

Kaspar BK, Lladó J, Sherkat N, Rothstein JD, Gage FH (2003) Retrograde viral delivery of IGF-1 prolongs survival in a mouse ALS model. Science 301:839–842.

Kaufmann WE, Johnston MV, Blue ME (2005) MeCP2 expression and function during brain development: implications for Rett syndrome's pathogenesis and clinical evolution. Brain Dev 27 Suppl 1:S77–S87.

Kerr B, Soto C J, Saez M, Abrams A, Walz K, Young JI (2012) Transgenic complementation of MeCP2 deficiency: phenotypic rescue of Mecp2-null mice by isoform-specific transgenes. Eur J Hum Genet 20:69–76.

Kim K-Y, Hysolli E, Park I-H (2011) Neuronal maturation defect in induced pluripotent stem cells from patients with Rett syndrome. Proc Natl Acad Sci USA 108:14169–14174.

Kishi N, Macklis JD (2004) MECP2 is progressively expressed in post-migratory neurons and is involved in neuronal maturation rather than cell fate decisions. Mol Cell Neurosci 27:306–321.

Klein ME, Lioy DT, Ma L, Impey S, Mandel G, Goodman RH (2007) Homeostatic regulation of MeCP2 expression by a CREB-induced microRNA. Nat Neurosci 10:1513–1514.

Kriaucionis S, Bird A (2004) The major form of MeCP2 has a novel N-terminus generated by alternative splicing. Nucleic Acids Res 32:1818–1823.

Kriaucionis S, Paterson A, Curtis J, Guy J, Macleod N, Bird A (2006) Gene expression

analysis exposes mitochondrial abnormalities in a mouse model of Rett syndrome. Mol Cell Biol 26:5033–5042.

Krishnan K, Wang B-S, Lu J, Wang L, Maffei A, Cang J, Huang ZJ (2015) MeCP2 regulates the timing of critical period plasticity that shapes functional connectivity in primary visual cortex. Proc Natl Acad Sci USA 112:E4782–E4791.

Kumar A, Kamboj S, Malone BM, Kudo S, Twiss JL, Czymmek KJ, Lasalle JM, Schanen NC (2008) Analysis of protein domains and Rett syndrome mutations indicate that multiple regions influence chromatin-binding dynamics of the chromatin-associated protein MECP2 in vivo. J Cell Sci 121:1128–1137.

Kumar A, Thakur MK (2015) Epigenetic regulation of presenilin 1 and 2 in the cerebral cortex of mice during development. Dev Neurobiol.

Kuo C-H, Ying S-Y (2012) Advances in microRNA-mediated reprogramming technology. Stem Cells Int 2012:823709–4.

Kwan KY, Sestan N, Anton ES (2012) Transcriptional co-regulation of neuronal migration and laminar identity in the neocortex. Development 139:1535–1546.

Lancaster MA, Renner M, Martin C-A, Wenzel D, Bicknell LS, Hurles ME, Homfray T, Penninger JM, Jackson AP, Knoblich JA (2013) Cerebral organoids model human brain development and microcephaly. Nature 501:373–379.

Lau P, Hudson LD (2010) MicroRNAs in neural cell differentiation. Brain Res 1338:14–19.

Lengner CJ, Gimelbrant AA, Erwin JA, Cheng AW, Guenther MG, Welstead GG, Alagappan R, Frampton GM, Xu P, Muffat J (2010) Derivation of pre-X inactivation human embryonic stem cells under physiological oxygen concentrations. Cell 141:872–883.

Li H, Zhong X, Chau KF, Santistevan NJ, Guo W, Kong G, Li X, Kadakia M, Masliah J, Chi J, Jin P, Zhang J, Zhao X, Chang Q (2014) Cell cycle-linked MeCP2 phosphorylation modulates adult neurogenesis involving the Notch signalling pathway. Nat Commun 5:5601.

Li Y, Wang H, Muffat J, Cheng AW, Orlando DA, Lovén J, Kwok S-M, Feldman DA, Bateup HS, Gao Q, Hockemeyer D, Mitalipova M, Lewis CA, Vander Heiden MG, Sur M, Young RA, Jaenisch R (2013) Global transcriptional and translational repression in human-embryonic-stem-cell-derived Rett syndrome neurons. Cell Stem Cell 13:446–458.

Lioy DT, Garg SK, Monaghan CE, Raber J, Foust KD, Kaspar BK, Hirrlinger PG, Kirchhoff F, Bissonnette JM, Ballas N, Mandel G (2011) A role for glia in the progression of Rett's syndrome. Nature 475:497–500.

Liyanage VRB, Zachariah RM, Rastegar M (2013) Decitabine alters the expression of Mecp2 isoforms via dynamic DNA methylation at the Mecp2 regulatory elements in neural stem cells. Mol Autism 4:46.

Lonetti G, Angelucci A, Morando L, Boggio EM, Giustetto M, PIzzorusso T (2010) Early Environmental Enrichment Moderates the Behavioral and Synaptic Phenotype of MeCP2 Null Mice. Biol Psychiatry 67:657–665.

Luikenhuis S, Giacometti E, Beard CF, Jaenisch R (2004) Expression of MeCP2 in postmitotic neurons rescues Rett syndrome in mice. Proceedings of the National Academy of Sciences 101:6033–6038.

Lyst MJ, Bird A (2015) Rett syndrome: a complex disorder with simple roots. Nat Rev Genet 16:261–275.

Ma L, Hu B, Liu Y, Vermilyea SC, Liu H, Gao L, Sun Y, Zhang X, Zhang S-C (2012) Human embryonic stem cell-derived GABA neurons correct locomotion deficits in quinolinic acid-lesioned mice. Cell Stem Cell 10:455–464.

Maezawa I, Jin L-W (2010) Rett syndrome microglia damage dendrites and synapses by the elevated release of glutamate. Journal of Neuroscience 30:5346–5356.

Marchetto MCN, Carromeu C, Acab A, Yu D, Yeo GW, Mu Y, Chen G, Gage FH, Muotri AR (2010) A model for neural development and treatment of Rett syndrome using human induced pluripotent stem cells. Cell 143:527–539.

Marschik PB, Kaufmann WE, Sigafoos J, Wolin T, Zhang D, Bartl-Pokorny KD, Pini G, Zappella M, Tager-Flusberg H, Einspieler C, Johnston MV (2013) Changing the perspective on early development of Rett syndrome. Res Dev Disabil 34:1236–1239.

Martynoga B, Drechsel D, Guillemot F (2012) Molecular control of neurogenesis: a view from the mammalian cerebral cortex. Cold Spring Harb Perspect Biol 4.

McConnell SK (1995) Strategies for the generation of neuronal diversity in the developing central nervous system. J Neurosci 15:6987–6998.

McGraw CM, Samaco RC, Zoghbi HY (2011) Adult neural function requires MeCP2. Science 333:186.

Mellén M, Ayata P, Dewell S, Kriaucionis S, Heintz N (2012) MeCP2 binds to 5hmC enriched within active genes and accessible chromatin in the nervous system. Cell 151:1417–1430.

Mellios N, Woodson J, Garcia RI, Crawford B, Sharma J, Sheridan SD, Haggarty SJ, Sur M (2014) β2-Adrenergic receptor agonist ameliorates phenotypes and corrects microRNA-mediated IGF1 deficits in a mouse model of Rett syndrome. Proc Natl

Acad Sci USA 111:9947–9952.

Mnatzakanian GN, Lohi H, Munteanu I, Alfred SE, Yamada T, MacLeod PJM, Jones JR, Scherer SW, Schanen NC, Friez MJ, Vincent JB, Minassian BA (2004) A previously unidentified MECP2 open reading frame defines a new protein isoform relevant to Rett syndrome. Nat Genet 36:339–341.

Nagarajan RP, Patzel KA, Martin M, Yasui DH, Swanberg SE, Hertz-Picciotto I, Hansen RL, Van de Water J, Pessah IN, Jiang R, Robinson WP, Lasalle JM (2008) MECP2 promoter methylation and X chromosome inactivation in autism. Autism Res 1:169–178.

Nelson ED, Kavalali ET, Monteggia LM (2006) MeCP2-dependent transcriptional repression regulates excitatory neurotransmission. Curr Biol 16:710–716.

Neul JL, Lane JB, Lee H-S, Geerts S, Barrish JO, Annese F, Baggett LM, Barnes K, Skinner SA, Motil KJ, Glaze DG, Kaufmann WE, Percy AK (2014) Developmental delay in Rett syndrome: data from the natural history study. J Neurodev Disord 6:20.

Olson CO, Zachariah RM, Ezeonwuka CD, Liyanage VRB, Rastegar M (2014) Brain region-specific expression of MeCP2 isoforms correlates with DNA methylation within Mecp2 regulatory elements. PLoS ONE 9:e90645.

Orlic-Milacic M, Kaufman L, Mikhailov A, Cheung AYL, Mahmood H, Ellis J, Gianakopoulos PJ, Minassian BA, Vincent JB (2014) Over-expression of either MECP2_e1 or MECP2_e2 in neuronally differentiated cells results in different patterns of gene expression. PLoS ONE 9:e91742.

Paşca AM, Sloan SA, Clarke LE, Tian Y, Makinson CD, Huber N, Kim CH, Park J-Y, O'Rourke NA, Nguyen KD, Smith SJ, Huguenard JR, Geschwind DH, Ben A Barres, Paşca SP (2015) Functional cortical neurons and astrocytes from human pluripotent stem cells in 3D culture. Nat Meth 12:671–678.

Pathania M, Torres-Reveron J, Yan L, Kimura T, Lin TV, Gordon V, Teng Z-Q, Zhao X, Fulga TA, Van Vactor D, Bordey A (2012) miR-132 enhances dendritic morphogenesis, spine density, synaptic integration, and survival of newborn olfactory bulb neurons. PLoS ONE 7:e38174.

Peng Y, Jiang B-H, Yang P-H, Cao Z, Shi X, Lin MCM, He M-L, Kung H-F (2004) Phosphatidylinositol 3-kinase signaling is involved in neurogenesis during Xenopus embryonic development. J Biol Chem 279:28509–28514.

Petazzi P, Akizu N, García A, Estarás C, Martínez de Paz A, Rodríguez-Paredes M, Martínez-Balbás MA, Huertas D, Esteller M (2014) An increase in MECP2 dosage impairs neural tube formation. Neurobiol Dis 67:49–56.

Qiu Z, Sylwestrak EL, Lieberman DN, Zhang Y, Liu X-Y, Ghosh A (2012) The Rett Syndrome Protein MeCP2 Regulates Synaptic Scaling. Journal of Neuroscience 32:989–994.

Rastegar M, Hotta A, Pasceri P, Makarem M, Cheung AYL, Elliott S, Park KJ, Adachi M, Jones FS, Clarke ID, Dirks P, Ellis J (2009) MECP2 isoform-specific vectors with regulated expression for Rett syndrome gene therapy. PLoS ONE 4:e6810.

Ricciardi S, Boggio EM, Grosso S, Lonetti G, Forlani G, Stefanelli G, Calcagno E, Morello N, Landsberger N, Biffo S, Pizzorusso T, Giustetto M, Broccoli V (2011) Reduced AKT/mTOR signaling and protein synthesis dysregulation in a Rett syndrome animal model. Human Molecular Genetics 20:1182–1196.

Saywell V, Viola A, Confort-Gouny S, Le Fur Y, Villard L, Cozzone PJ (2006) Brain magnetic resonance study of Mecp2 deletion effects on anatomy and metabolism. Biochem Biophys Res Commun 340:776–783.

Shahbazian MD, Antalffy B, Armstrong DL, Zoghbi HY (2002a) Insight into Rett syndrome: MeCP2 levels display tissue- and cell-specific differences and correlate with neuronal maturation. Human Molecular Genetics 11:115–124.

Shahbazian MD, Sun Y, Zoghbi HY (2002b) Balanced X chromosome inactivation patterns in the Rett syndrome brain. Am J Med Genet 111:164–168.

Shi Y, Kirwan P, Livesey FJ (2012a) Directed differentiation of human pluripotent stem cells to cerebral cortex neurons and neural networks. Nat Protoc 7:1836–1846.

Shi Y, Kirwan P, Smith J, Robinson HPC, Livesey FJ (2012b) Human cerebral cortex development from pluripotent stem cells to functional excitatory synapses. Nat Neurosci 15:477–486.

Smrt RD, Eaves-Egenes J, Barkho BZ, Santistevan NJ, Zhao C, Aimone JB, Gage FH, Zhao X (2007) Mecp2 deficiency leads to delayed maturation and altered gene expression in hippocampal neurons. Neurobiol Dis 27:77–89.

Smrt RD, Szulwach KE, Pfeiffer RL, Li X, Guo W, Pathania M, Teng Z-Q, Luo Y, Peng J, Bordey A, Jin P, Zhao X (2010) MicroRNA miR-137 regulates neuronal maturation by targeting ubiquitin ligase mind bomb-1. Stem Cells 28:1060–1070.

Song C-X, Szulwach KE, Fu Y, Dai Q, Yi C, Li X, Li Y, Chen C-H, Zhang W, Jian X, Wang J, Zhang L, Looney TJ, Zhang B, Godley LA, Hicks LM, Lahn BT, Jin P, He C (2011) Selective chemical labeling reveals the genome-wide distribution of 5-hydroxymethylcytosine. Nat Biotechnol 29:68–72.

Squillaro T, Alessio N, Cipollaro M, Melone MAB, Hayek G, Renieri A, Giordano A, Galderisi U (2012) Reduced expression of MECP2 affects cell commitment and maintenance in neurons by triggering senescence: new perspective for Rett

syndrome. Mol Biol Cell 23:1435–1445.

Stancheva I, Collins AL, Van den Veyver IB, Zoghbi H (2003) A mutant form of MeCP2 protein associated with human Rett syndrome cannot be displaced from methylated DNA by notch in Xenopus embryos. Mol Cell.

Sun G, Ye P, Murai K, Lang M-F, Li S, Zhang H, Li W, Fu C, Yin J, Wang A, Ma X, Shi Y (2011) miR-137 forms a regulatory loop with nuclear receptor TLX and LSD1 in neural stem cells. Nat Commun 2:529.

Swiech L, Heidenreich M, Banerjee A, Habib N, Li Y, Trombetta J, Sur M, Zhang F (2015) In vivo interrogation of gene function in the mammalian brain using CRISPR-Cas9. Nat Biotechnol 33:102–106.

Sztainberg Y, Chen H-M, Swann JW, Hao S, Tang B, Wu Z, Tang J, Wan Y-W, Liu Z, Rigo F, Zoghbi HY (2015) Reversal of phenotypes in MECP2 duplication mice using genetic rescue or antisense oligonucleotides. Nature 528:123–126.

Szulwach KE, Li X, Smrt RD, Li Y, Luo Y, Lin L, Santistevan NJ, Li W, Zhao X, Jin P (2010) Cross talk between microRNA and epigenetic regulation in adult neurogenesis. J Cell Biol 189:127–141.

Takahashi K, Tanabe K, Ohnuki M, Narita M, Ichisaka T, Tomoda K, Yamanaka S (2007) Induction of pluripotent stem cells from adult human fibroblasts by defined factors. Cell 131:861–872.

Tarquinio DC, Hou W, Neul JL, Lane JB, Barnes KV, O'Leary HM, Bruck NM, Kaufmann WE, Motil KJ, Glaze DG, Skinner SA, Annese F, Baggett L, Barrish JO, Geerts SP, Percy AK (2015) Age of diagnosis in Rett syndrome: patterns of recognition among diagnosticians and risk factors for late diagnosis. Pediatr Neurol 52:585–91.e2.

Tau GZ, Peterson BS (2010) Normal development of brain circuits. Neuropsychopharmacology 35:147–168.

Tropea D, Giacometti E, Wilson NR, Beard C, McCurry C, Fu DD, Flannery R, Jaenisch R, Sur M (2009) Partial reversal of Rett Syndrome-like symptoms in MeCP2 mutant mice. Proc Natl Acad Sci USA 106:2029–2034.

Tsujimura K, Abematsu M, Kohyama J, Namihira M, Nakashima K (2009) Neuronal differentiation of neural precursor cells is promoted by the methyl-CpG-binding protein MeCP2. Experimental Neurology 219:104–111.

Tsujimura K, Irie K, Nakashima H, Egashira Y, Fukao Y, Fujiwara M, Itoh M, Uesaka M, Imamura T, Nakahata Y, Yamashita Y, Abe T, Takamori S, Nakashima K (2015) miR-199a Links MeCP2 with mTOR Signaling and Its Dysregulation Leads to Rett Syndrome Phenotypes. Cell Rep 12:1887–1901.

Urdinguio RG, Lopez-Serra L, Lopez-Nieva P, Alaminos M, Diaz-Uriarte R, Fernandez AF, Esteller M (2008) Mecp2-null mice provide new neuronal targets for Rett syndrome. PLoS ONE 3:e3669.

Valiente M, Marín O (2010) Neuronal migration mechanisms in development and disease. Curr Opin Neurobiol.

Van Esch H (2011) MECP2 duplication syndrome. Molecular syndromology.

Viola A, Saywell V, Villard L, Cozzone PJ, Lutz NW (2007) Metabolic fingerprints of altered brain growth, osmoregulation and neurotransmission in a Rett syndrome model. PLoS ONE 2:e157.

Wang Q, Liu L, Pei L, Ju W, Ahmadian G, Lu J, Wang Y, Liu F, Wang YT (2003) Control of synaptic strength, a novel function of Akt. Neuron 38:915–928.

Wood L, Gray NW, Zhou Z, Greenberg ME, Shepherd GMG (2009) Synaptic circuit abnormalities of motor-frontal layer 2/3 pyramidal neurons in an RNA interference model of methyl-CpG-binding protein 2 deficiency. Journal of Neuroscience 29:12440–12448.

Wu H, Lu D, Jiang H, Xiong Y, Qu C, Li B, Mahmood A, Zhou D, Chopp M (2008) Increase in phosphorylation of Akt and its downstream signaling targets and suppression of apoptosis by simvastatin after traumatic brain injury. J Neurosurg 109:691–698.

Yasui DH, Gonzales ML, Aflatooni JO, Crary FK, Hu DJ, Gavino BJ, Golub MS, Vincent JB, Carolyn Schanen N, Olson CO, Rastegar M, Lasalle JM (2014) Mice with an isoform-ablating Mecp2 exon 1 mutation recapitulate the neurologic deficits of Rett syndrome. Human Molecular Genetics 23:2447–2458.

Zahir FR, Brown CJ (2011) Epigenetic impacts on neurodevelopment: pathophysiological mechanisms and genetic modes of action. Pediatr Res 69:92R–100R.

Zhang X, Zhang L, Cheng X, Guo Y, Sun X, Chen G, Li H, Li P, Lu X, Tian M, Qin J, Zhou H, Jin G (2014) IGF-1 promotes Brn-4 expression and neuronal differentiation of neural stem cells via the PI3K/Akt pathway. PLoS ONE 9:e113801.

Zhang Y, Pak C, Han Y, Ahlenius H, Zhang Z, Chanda S, Marro S, Patzke C, Acuna C, Covy J, Xu W, Yang N, Danko T, Chen L, Wernig M, Südhof TC (2013) Rapid single-step induction of functional neurons from human pluripotent stem cells. Neuron 78:785–798.

Zhou Z, Hong EJ, Cohen S, Zhao W-N, Ho H-YH, Schmidt L, Chen WG, Lin Y, Savner E, Griffith EC, Hu L, Steen JAJ, Weitz CJ, Greenberg ME (2006) Brain-Specific Phosphorylation of MeCP2 Regulates Activity-Dependent Bdnf Transcription,

Dendritic Growth, and Spine Maturation. Neuron 52:255–269.

Chapter II

Generation and characterization of human iPSC-derived neuronal models

Abstract

Rett Syndrome (RTT) is a neurodevelopmental disorder caused primarily by mutations in the X-linked gene encoding Methyl CpG binding protein 2 (MeCP2). MeCP2 is a pleiotropic and complex regulator of downstream gene expression; in its absence, a variety of neuronal phenotypes arise including membrane and synaptic deficits, morphological alterations, and delayed maturation. Whereas the roles of MeCP2 in circuit function and development have been extensively studied in mouse models, its functions during neurogenesis, particularly in the context of human development, have been largely overlooked. Here we report the generation of a variety of induced pluripotent stem cell-derived neuronal models in which to study RTT pathogenesis throughout the timeline of early human development. Neural progenitors (NPs) and immature neurons can be used to reveal key molecular signatures that arise in pre-symptomatic stages of RTT (see: **Chapter 3**) and can be tracked in the context of 3D corticogenesis (see: **Chapter 4**). Physiological phenotypes of RTT can be studied in the context of Ngn2-mediated neuronal differentiation, which generates robustly active neurons in a rapid time frame without the intermediate stages of neurogenesis. Ngn2-derived RTT neurons recapitulate the physiological deficits reported in established RTT models and have demonstrated the capacity to serve as a robust model in which to further explore in-depth electrophysiological mechanisms underlying RTT.

Introduction

Rett Syndrome (RTT) is an X-linked neurodevelopmental disorder that predominantly affects girls. Symptoms typically emerge between the ages of 6 to 18 months, at which point developmental stagnation and subsequent regression occur. In the vast majority of cases, RTT is caused by mutations in the gene encoding Methyl CpG binding protein 2 (MeCP2) (Chahrour and Zoghbi, 2007). *MECP2* is a complex regulator of downstream gene expression (Chahrour et al., 2008), leading to wide-ranging phenotypes in its absence such as aberrant transcription (Li et al., 2013), downstream signaling pathway misregulation (Ricciardi et al., 2011; Castro et al., 2014), synaptic and circuit dysfunction (Boggio et al., 2010; Banerjee et al., 2012), and behavioral abnormalities (Shahbazian et al., 2002; Schaevitz et al., 2010; 2013).

Because RTT has predominantly been considered a postnatal disorder (Feldman et al., 2016), it has largely been studied in the context of juvenile and adult mouse models (Calfa et al., 2011; Banerjee et al., 2012). These models, while useful for identifying mechanisms underlying symptomatic (often male) animals, do not serve to accurately recapitulate the subtle phenotypes or early molecular signatures that could easily go unnoticed in pre-symptomatic female RTT patients (Kerr, 1995; Neul et al., 2014). To this end, we sought to develop a range of induced pluripotent stem cell (iPSC)-derived human neuronal RTT models in which to study various stages of RTT from early neurogenesis to circuit development *in vitro* in a genetically accurate context.

Results

Generation of wild type and mutant iPSC lines

We reprogrammed fibroblasts from two RTT patients (**Table 1**). RTT patient 1 ("RTT-MT1") harbors a missense mutation in the Methyl CpG binding domain (R106W) (**Figure 1A, 1B**: **right panel**). Because *MECP2* is located on the X chromosome, we were also able to generate an isogenic patient-derived line that differed exclusively at the X chromosome by clonally expanding iPSCs that expressed either the mutant or wild type allele. Of note, it has been demonstrated that reprogramming of iPSCs from female RTT patients can result in iPSC clones that stably express either *MECP2* allele (Cheung et al., 2011). We repetitively examined the allele-specific transcription of *MECP2* in these iPSC clones and their differentiated NP / neuron samples and detected the expression of only monoallelic RTT patient-derived iPSCs that retained either the inactive mutant or WT *MECP2* gene during neuronal induction, thus allowing for the development of isogenic iPSCs from RTT patient 2 ("RTT-WT2" and "RTT-MT2") (**Figure 1B**: **right panel**), which harbors a nonsense mutation in the transcription repressor domain of *MECP2* (**Figure 1A**). Additionally, we generated a RTT / WT pair of lines via shRNA-mediated knockdown of *MECP2* ("shControl" and "shMeCP2"). The shRNA construct reduced the expression of *MECP2* by more than 50% in both NPs and neurons (**Figure 1C**). We also employed two healthy wild type lines ("WT1" and "WT2") to serve as additional controls for RTT-MT1 and RTT-MT2, respectively.

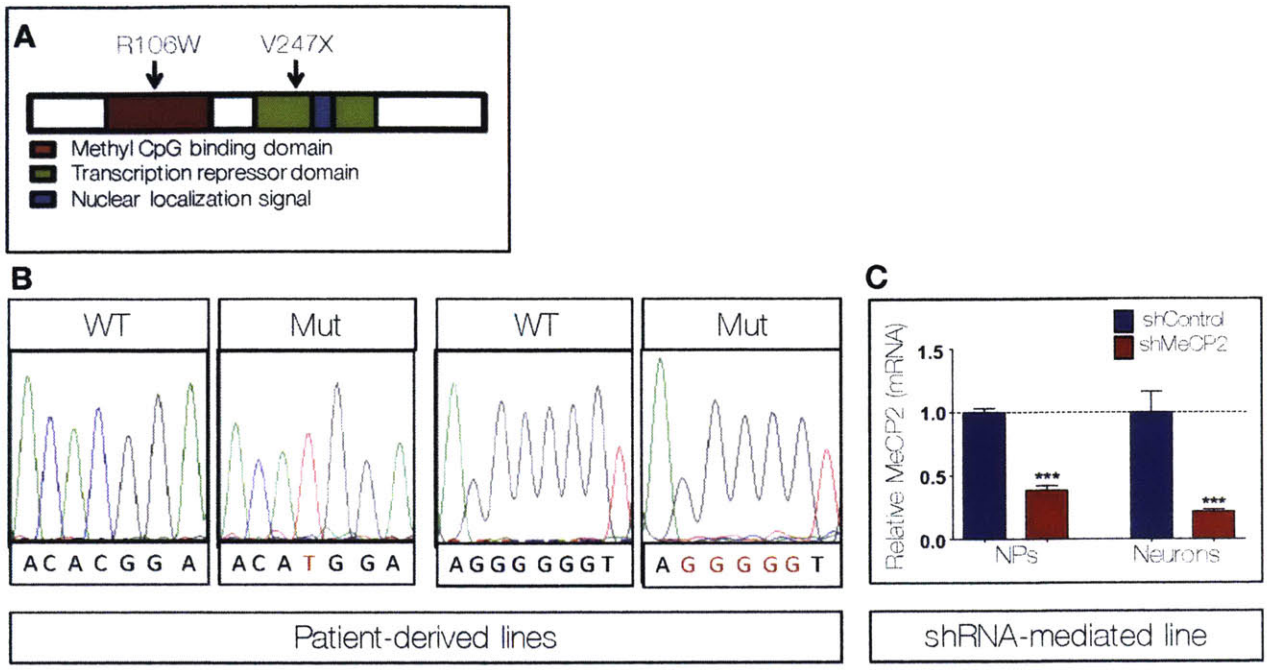

Figure 1: Generation of RTT lines

(A) MECP2 gene depicting the functional domains (*red*, methyl CpG binding domain; *green*, transcription repressor domain; *blue*, nuclear localization signal). Arrows and amino acid changes represent the mutations found in RTT patient 1 (R106W) and RTT patient 2 (V247X), respectively. *(B)* RTT patient 1 (*left*) harbors a missense mutation (C>T) in the methyl CpG binding domain. RTT patient 2 (right) harbors a nonsense mutation (705delG), resulting in a premature stop codon. The mutations are shown in red. *(C)* Mean ± SEM relative to control MECP2 mRNA levels (normalized to 18S rRNA) in MeCP2 shRNA (*red bar, shMECP2*) and shRNA control (*blue bar, shControl*) expressing NPs and differentiated neurons. *(***p < 0.001 student's t-test).*

Line name	Source	Mutation	Sex	Isogenic pair	Neuronal differentiation protocol(s) employed
WT1	Coriell: 8330-8	None	Male	None	FACS sorted NPCs
WT2	Coriell: GM23279A	None	Female	None	Dual SMAD inhibition Cerebral organoids
RTT-MT1	Coriell: 11273	missense mutation, 316C>T	Female	None	FACS sorted NPCs
RTT-MT2	Coriell: 07982	frameshift mutation; 705delG	Female	RTT-WT2	Dual SMAD inhibition Cerebral organoids
RTT-WT2	Coriell: 07982	None expressed	Female	RTT-MT2	Dual SMAD inhibition Cerebral organoids
shControl	Coriell: 08330	None	Male	shMeCP2	FACS sorted NPCs
shMeCP2	Coriell: 08330	shRNA-mediated kncokdown	Male	shControl	FACS sorted NPCs

Table 1: RTT lines used to generate iPSC-derived neurons

Generation of monolayer neuronal models

We generated iPSC-derived neurons using three 2D neuronal differentiation protocols and two 3D neuronal differentiation protocols (**Figure 2**). The former include: 1) magnetic activated cell sorting (MACS) and fluorescence activated cell sorting (FACS) (Sheridan et al., 2011), 2) dual-SMAD inhibition (Shi et al., 2012a; 2012b), and 3) lentiviral-mediated *Neurogenin-2* (Ngn2) overexpression (Zhang et al., 2013a). Sorting-based differentiation and dual-SMAD inhibition protocols generate neural progenitors (NPs) that mature slowly and recapitulate key aspects of neurogenesis with respect to morphology, marker expression, and cortical layer development (Chambers et al., 2009; Mariani et al., 2012; Shi et al., 2012b). As these protocols are thus ideally suited to study early neuronal development, we used both methods to generate NPs in which to study aberrantly regulated miRNAs and the corresponding signaling pathway dysfunction during this early developmental timepoint (see: **Chapter 3**).

Generation of cerebral organoids

RTT patient iPSCs and WT iPSCs were also used to generate 3D cerebral organoids (**Figure 2**) (Lancaster et al., 2013; Lancaster and Knoblich, 2014), advantageous for the recapitulation of corticogenesis in a 3D context *in vitro*. Cerebral organoids have now been developed using a variety of methods (Paşca et al., 2015) and have been used to model neurogenesis-relevant pathologies such as Zika virus infection (Dang et al., 2016; Garcez et al., 2016) and microcephaly (Lancaster et al., 2013). Cerebral organoids are unique in their generation of progenitor-rich regions akin to ventricular /

subventricular zones (VZ/SVZ) from which differentiating neurons migrate radially and acquire cortical layer identities (Götz and Huttner, 2005a). These structures allow for the analyses of key neurogenesis processes such as VZ/SVZ development, neuronal migration, and human-specific cortical layer formation (Lancaster et al., 2013).

Ngn2 overexpression rapidly generates neurons from RTT patient iPSCs

Most neuronal iPSC differentiation protocols act on a time scale intrinsic to human development and thus tend to generate neurons with a prenatal identity. As such, iPSCs have been more useful for the study of neurodevelopmental disease than neurodegenerative disease (Vera and Studer, 2015). Efforts have been made to speed the aging of cells (e.g., by adding progerin (Miller et al., 2013) or inhibiting autophagy (Ross and Akimov, 2014)) in order to study late-onset diseases. Studies of neurons that are functionally mature—albeit not aged to the point of neurodegeneration—have been more abundant. However, the majority of existing protocols report a low yield of active neurons in a heterogeneous landscape of cells (Hu et al., 2010; Zhang et al., 2013b). The forced expression of pro-neural gene *Ngn2* rapidly generates mature neurons (i.e., electrophysiologically active; expressing synaptic markers) that exhibit reduced heterogeneity intra- and inter- culture dishes (Zhang et al., 2013b; Busskamp et al., 2014; Chavez et al., 2015), making them ideally suited for the characterization of active membrane and synaptic properties. Ngn2-derived neurons are electrically active at two to three weeks post-transduction of iPSCs or NPs. We utilized Ngn2-mediated differentiation to generate RTT neurons with physiological deficits comparable in nature

to those observed in established models of RTT, validating the model for the study of RTT physiology *in vitro* (**Figure 2**).

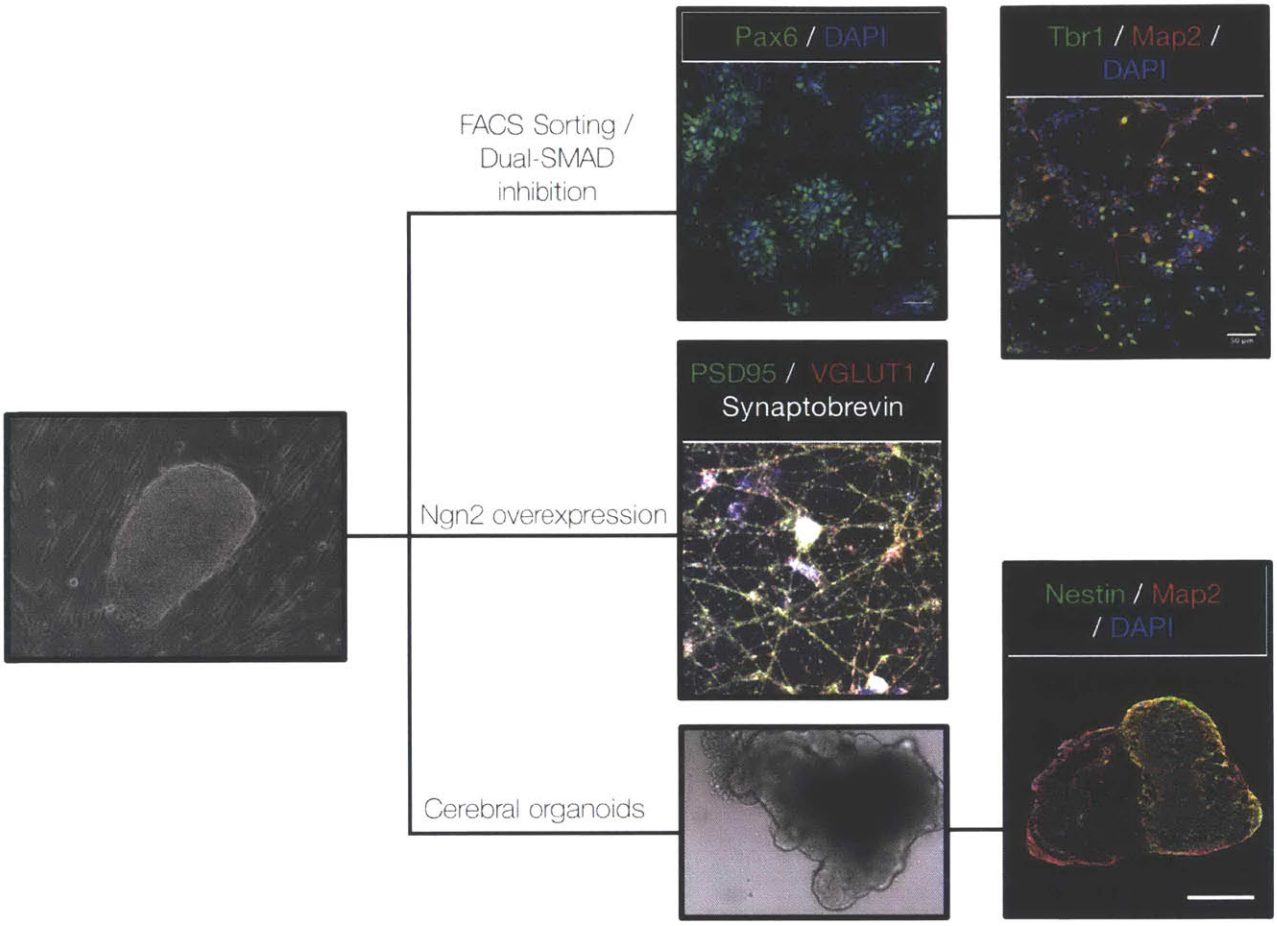

Figure 2: Monolayer and 3D neuronal differentiation protocols

iPSCs (*left*) were differentiated via a total of five monolayer and 3D differentiation protocols. Differentiating iPSCs via sorting-based and dual SMAD inhibition methods generates PAX6-positive NPs (*top, left*) that form excitatory cortical neurons after three weeks in culture (*top, right*), expressing first born cortical layer VI marker Tbr1 (green) and dendritic marker MAP2 (*red*). Ngn2 overexpression (*middle, left*) rapidly induces an excitatory cortical identity; cells express pre- and post- synaptic markers VGLUT1 (*red*), Synaptobrevin (*white*), and PSD-95 (*green*) two weeks post virus transduction. Cerebral organoids develop expanded neuroepithelium evident at 2 weeks in vitro (*bottom, left*). At 5.5 weeks *in vitro* (*bottom, right*), organoids express Nestin-positive progenitor regions (*green*) and dendritic marker MAP2 (*red*) (*bottom, right*). *Scale bar = 500 μM.*

Characterization of iPSCs and NPs

iPSCs were generated via retroviral-mediated transduction of the four reprogramming factors (OCT4, SOX2, KLF4, and c-MYC) as previously described (Yamanaka, 2007). iPSCs were characterized to ensure normal karyotype (**Figure 3A**), tri-germ lineage differentiation potential (**Figure 3B**), and immunocytochemical staining to reveal marker expression typical of pluripotent stem cells (**Figure 3C**). NPs were characterized as well for proper karyotype and marker expression profiles (**Figure 3D**).

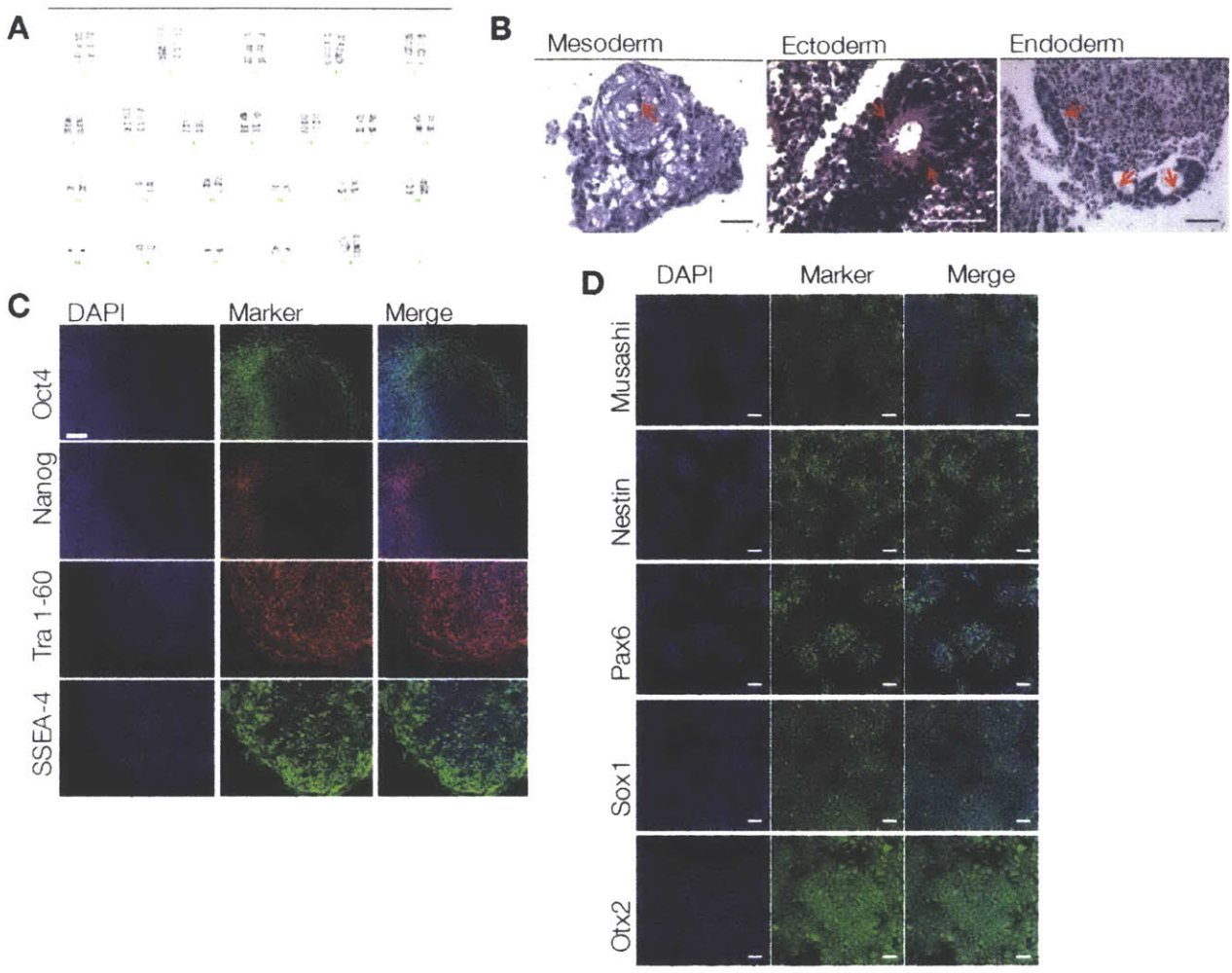

Figure 3: Quality control of patient-derived iPSCs and NPs.

(A) Examples of analysis of germ layer differentiation in iPSC-derived embryoid bodies. Images of hematoxylin and eosin-stained histological sections of iPSC-derived embryoid bodies are shown. Trilineage potential is demonstrated by the presence of medoderm (connective tissue), ectoderm (neuroepithelium), and endoderm (gut epithelium) germ layers. Arrows indicate the corresponding tissue. (*Scale bars = 50 μM.) (B)* Karyotype analysis example for patient-derived iPSCs. *(C)* Example from immunostaining of pluripotency markers OCT4, NANOG, Tra 1-60, and SSEA-4 for patient-derived iPSCs. *Scale bar = 100 μM. (D)* Immunostained examples of NP markers Musashi, Nestin, PAX6, SOX1, and OTX2. (*Scale bar = 100 μM.)*

Ngn2-derived neurons rapidly develop synaptic structures and electrophysiological activity

iPSCs overexpressing Ngn2 express punctate synaptic markers two weeks post-virus transduction (**Figure 4A-C**), suggesting rapid synapse formation in the absence of typical stages of neurogenesis. These neurons are capable of firing action potentials (**Figure 4D**), and exhibit TTX-sensitive sodium currents (**Figure 4E**) in addition to spontaneous synaptic activity that is pharmacologically blocked in the presence of AMPA and NMDA receptor antagonists DNQX and AP-V, respectively (**Figure 4F**).

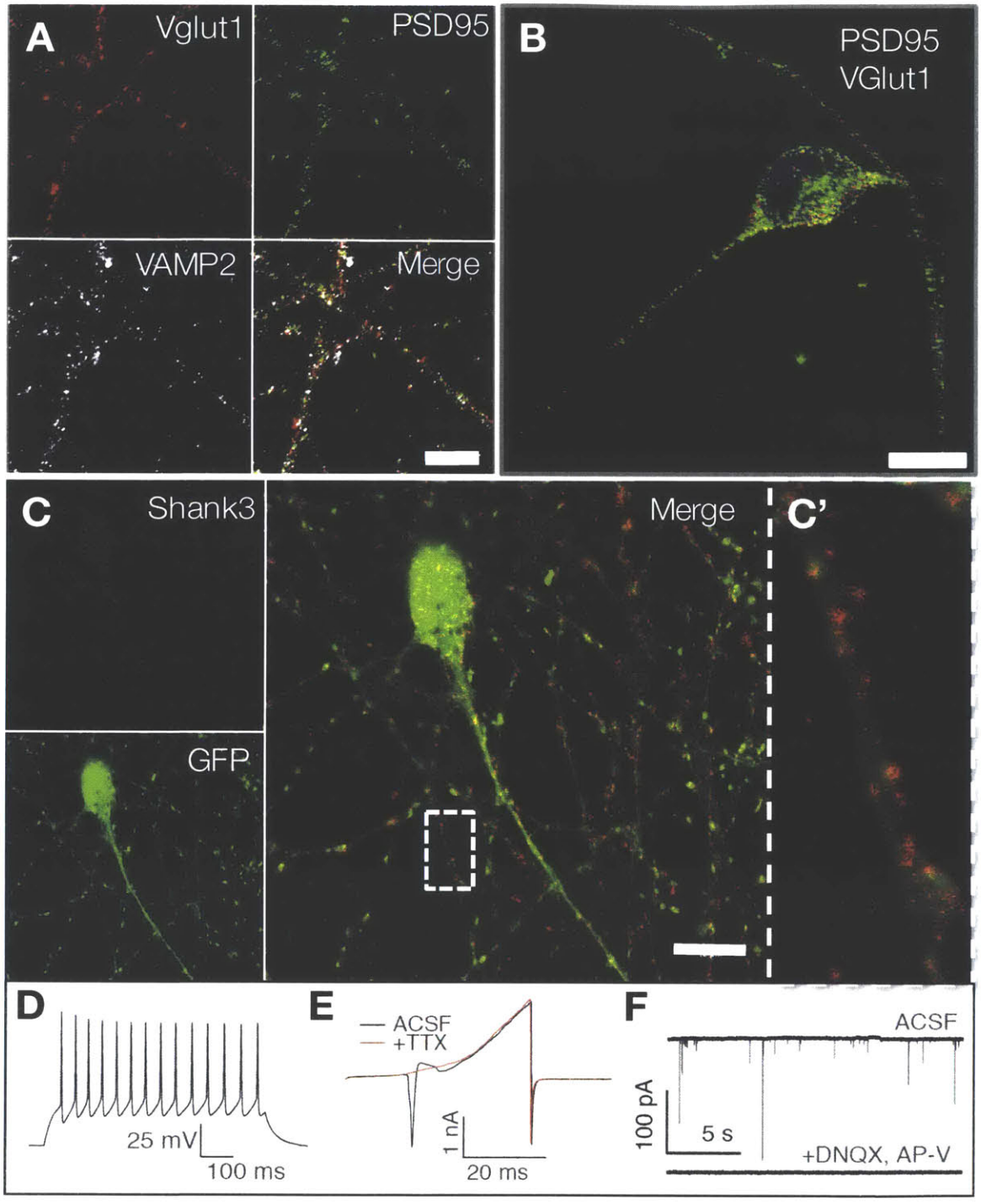

Figure 4: Ngn2-derived neurons develop synapses at two weeks post-induction.

(A-B) Ngn2-derived excitatory cortical neurons express pre-synaptic markers VGLUT1 and VAMP2 in addition to post-synaptic marker PSD95. *(C)* GFP(+) neurons (*green*) express post-synaptic scaffolding protein Shank3 (*red; Scale bar = 10 μM.*) *(D)* Action potentials evoked by a single current pulse injection in a whole-cell patched iPSC-derived neuron. *(E)* Ramp depolarization of a whole-cell

patched iPSC-derived neuron reveals voltage-gated sodium currents (*black trace*) sensitive to TTX (*red trace*). *(F)* Synaptic currents recorded in an iPSC-derived neuron are glutamatergic, as shown by blockage by AMPA and NMDA receptor antagonists DNQX and AP-V, respectively.

RTT NPs and neurons recapitulate morphological deficits including reduced nucleus area

Microcephaly is common to RTT, often presenting in patients by the second year of life (Chahrour and Zoghbi, 2007) and in mice at eight weeks of age (Chen et al., 2001). Several fundamental factors have been attributed to this phenotype, including reduced soma and nucleus size (Chen et al., 2001; Marchetto et al., 2010; Li et al., 2013) and reduced dendritic arborization (Zhou et al., 2006; Kishi and Macklis, 2010; Marchetto et al., 2010; Li et al., 2013). Underlying reduced soma and nucleus size are metabolic deficits in RTT (Ruvinsky et al., 2005; Ricciardi et al., 2012; Li et al., 2013) including a global reduction of transcription and translation in human RTT neurons (Li et al., 2013). We assayed nuclear size in our monolayer RTT neurons at varying stages of neuronal development— NPs (**Figure 5A, B**), immature neurons, (**Figure 5C, D**) and electrophysiologically active neurons (**Figure 5E, F**)— and found that RTT patient-derived neurons exhibited reduced nuclear size at all three developmental stages. These findings have two implications: 1) these neuronal differentiation protocols are capable of revealing RTT phenotypes at various neurodevelopmental stages and 2) the phenotype of reduced nuclear area in RTT cells is not exclusive to postnatal development. The latter is particularly interesting given work that demonstrates no difference in either total RNA levels or gene expression at the NP stage (Li et al., 2013). After two weeks of differentiation, however, human RTT neurons reportedly exhibit a median 25 percent reduction in gene expression (Li et al., 2013). As such, it is possible that the NPs in our study and those described previously (Li et al., 2013) are not precisely matched in terms of developmental age, and that gene expression changes

have indeed taken place in the cells described within, thus leading to their decreased nucleus size. Despite the established non-cell autonomous effects of MeCP2 deficiency, particularly as they relate to cellular metabolism and size, we were able to determine a reduction in the nucleus size of Ngn2-derived RTT-MT2 neurons versus RTT-WT2 cells in a co-culture condition (**Figure 5E, F**). We did not compare this Ngn2-derived co-culture population to cells grown under mutant-only or WT-only conditions, but would expect a difference between WT neurons co-cultured with MeCP2-deficient neurons and those grown in a homogenously WT environment due to the toxic effect of MeCP2 deficiency on neighboring cells.

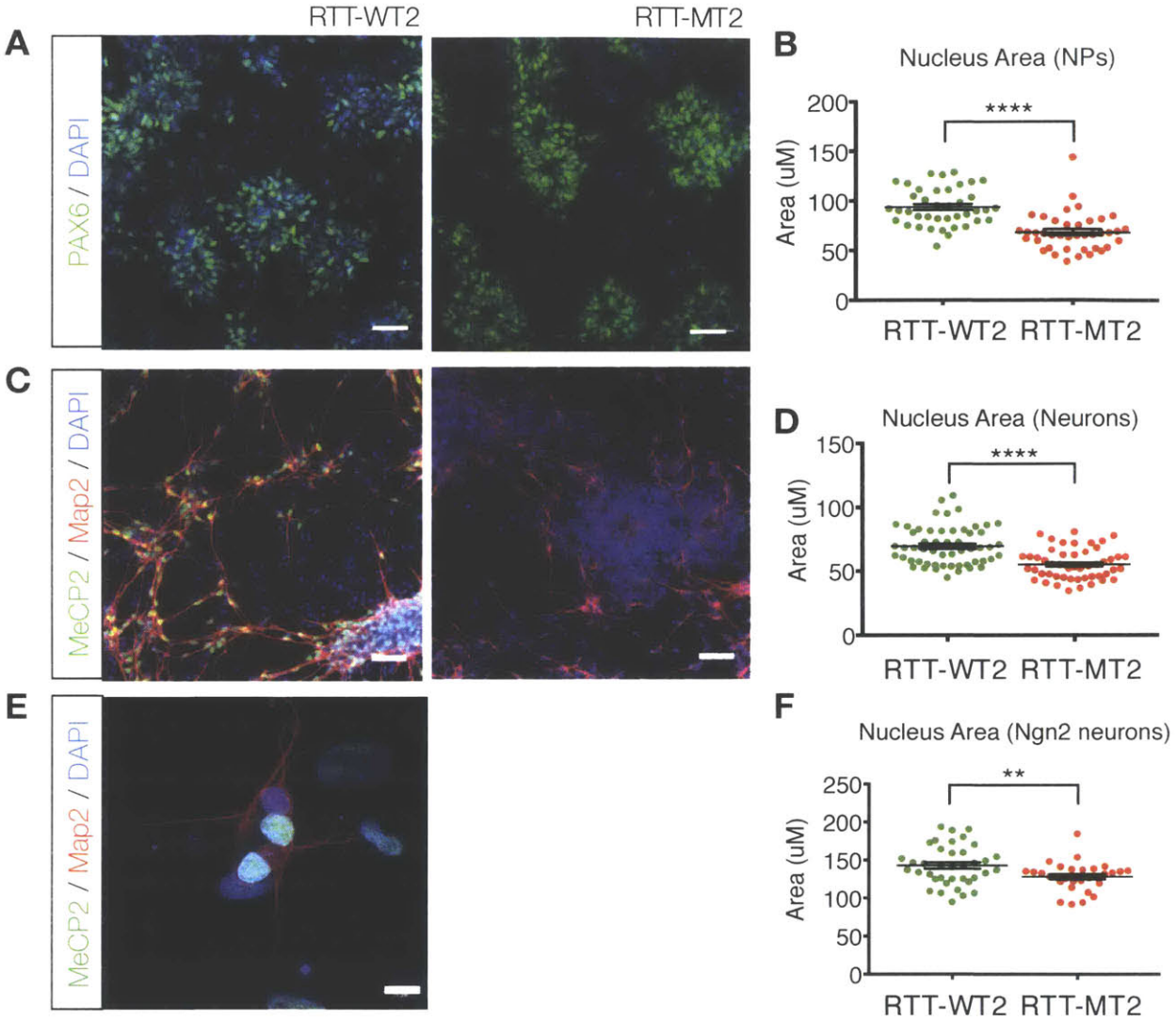

Figure 5: RTT neurons express reduced nucleus size throughout neuronal development.

(A) Nucleus size quantified in RTT patient 2 NPs expressing progenitor marker PAX6 (*green*): RTT-MT2 NPs exhibit significantly smaller nuclei as compared to RTT-WT2 NPs, as quantified in *(B)*. *(C)* Neurons expressing dendritic marker MAP2 (*red*) and MeCP2 (*green*) in RTT-WT2 (lacking in RTT-MT2): RTT-MT2 neurons exhibit decreased nucleus area, as quantified in *(D)*. *(E)* Ngn2-derived RTT-WT2 neurons (MeCP2 (+); *green*) co-cultured with RTT-MT2 neurons (MeCP2 (-); *blue*) stained for dendritic marker MAP2; RTT-MT2 neurons exhibit a significant reduction in nucleus area, quantified in *(F)*. *(All graphs are mean ± SEM. **p < 0.01, ***p < 0.001, ****p < 0.0001 student's t-test).*

Ngn2-derived RTT neurons exhibit physiological deficits including aberrant membrane and synaptic function

RTT neurons are known to exhibit physiological deficits, as reported in mouse (Banerjee et al., 2012), human ESC-derived neurons (Li et al., 2013), and human iPSC-derived neurons (Marchetto et al., 2010). Among the deficits observed are membrane phenotypes such as reduced action potential frequency and amplitude (Farra et al., 2012); synaptic phenotypes including impairments in evoked excitatory neurotransmission (Nelson et al., 2011), GABA transmission (Medrihan et al., 2008), and synaptic scaling (Qiu et al., 2012); and global network deficits such as altered plasticity (Castro et al., 2014; Krishnan et al., 2015), hyperexcitability (Zhang et al., 2008), and a shift in the balance of cortical excitation versus inhibition (Dani et al., 2005). Because Ngn2 is known to positively regulate the neural differentiation of NPs with respect to cell fate, migration, and dendritic morphology (Nieto et al., 2001; Hand et al., 2005; Ge et al., 2006), a question remained as to whether its overexpression in RTT patient-derived iPSCs would mask any potential physiological RTT phenotypes that may arise in the course of a more organic differentiation process. Adding complexity to this issue is the fact that the processes of cell fate determination, NP migration, and dendritic arborization are all known to be altered in the course of MeCP2-deficient neurogenesis (Tsujimura et al., 2009; Andoh-Noda et al., 2015; Bedogni et al., 2015). A potential rescue of early stage neurogenic deficits as a result of Ngn2 overexpression may or may not prevent the emergence of phenotypes later in the course of neuronal maturation. We sought to answer this question by examining whether Ngn2-derived neurons recapitulate the physiological deficits observed in more

commonly established models of RTT. We performed whole cell patch clamp in RTT patient 2 iPS-derived neurons generated via Ngn2 overexpression (**Figure 6A**) grown in wild type human astrocyte-conditioned media. We found that whereas both RTT-WT2 and RTT-MT2 neurons exhibited spontaneous synaptic activity after 2.5 weeks of differentiation, there were significant reductions in both the peak amplitude and frequency of spontaneous excitatory post-synaptic currents (sEPSCs) in RTT-MT2 neurons (**Figure 6B-E**).

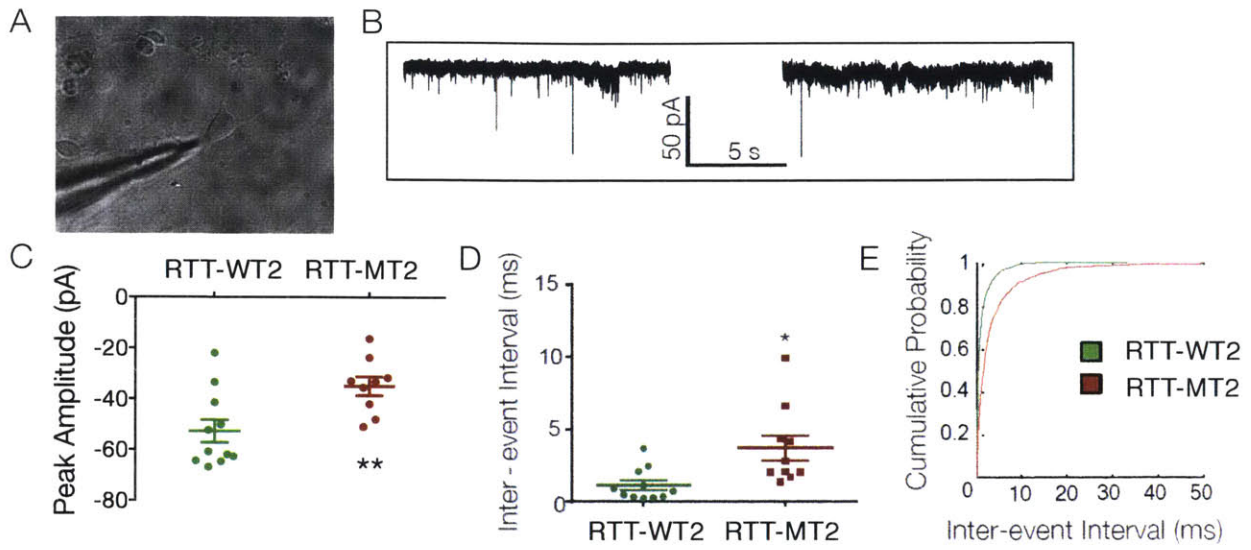

Figure 6: sEPSCs are altered in patient-derived mutant neurons.

(A) Representative DIC image of whole-cell patch clamp of Ngn2-overexpressing neuron. *(B)* Representative raw traces from whole-cell voltage clamp recordings of one WT and one mutant neuron showing spontaneous inward synaptic currents. *(C)* Significant reduction in mean sEPSC peak amplitude in RTT-MT2 neurons relative to isogenic RTT-WT2 neurons. Stars depict statistical significance determined by two-tailed unpaired t-test with Welch's correction ($p = 0.0067$). *(D)* RTT-MT2 neurons exhibit a decreased frequency of sEPSC events, as indicated by a significant shift toward longer inter-event interval. *($p = 0.00047$, Kolmogorov-Smirnov Test).*

We next measured membrane properties in RTT patient 2-derived neurons and found reduced voltage-sensitive sodium currents and unaltered voltage-sensitive potassium currents in RTT-MT2 relative to isogenic RTT-WT2 neurons (**Figure 7B, C**). This reduction in sodium current was partially ameliorated when the neurons were co-cultured with wild type human astrocytes (**Figure 7D, E**), as opposed to being grown in astrocyte-conditioned media (**Figure 7B, C**). These results are not entirely surprising, given the established non-cell autonomous effects of astrocytes with respect to RTT pathology *in vitro* (Ballas et al., 2009; Maezawa et al., 2009). We performed qPCR analyses to determine if altered gene expression underlies the observed deficits in membrane physiology. Voltage-gated sodium channels are essential for the generation and propagation of neuronal action potentials; mutations in genes encoding voltage-gated sodium channels are linked to epilepsy (Estacion et al., 2014), autism (Weiss et al., 2003), and, in particular, RTT (Larsen et al., 2015; Olson et al., 2015). In support of our physiology data, RTT-MT2 neurons exhibit reduced expression of sodium channel voltage-gated subunit genes SCN1A, SCN3A, and SCN8A. This is in accordance with previously reported decreased expression of SCN1A (Kim et al., 2011) and SCN8A (Bedogni et al., 2015) in the context of RTT. We did not detect significant changes in voltage-gated potassium channel function, yet we did find reduced mRNA expression of KCNH2, a potassium channel responsible for repolarizing delayed rectifier currents. Interestingly, KCNH2 dysfunction has been linked to long-QT syndrome (Bellin et al., 2013), described previously in patients with RTT (Ellaway et al., 1999).

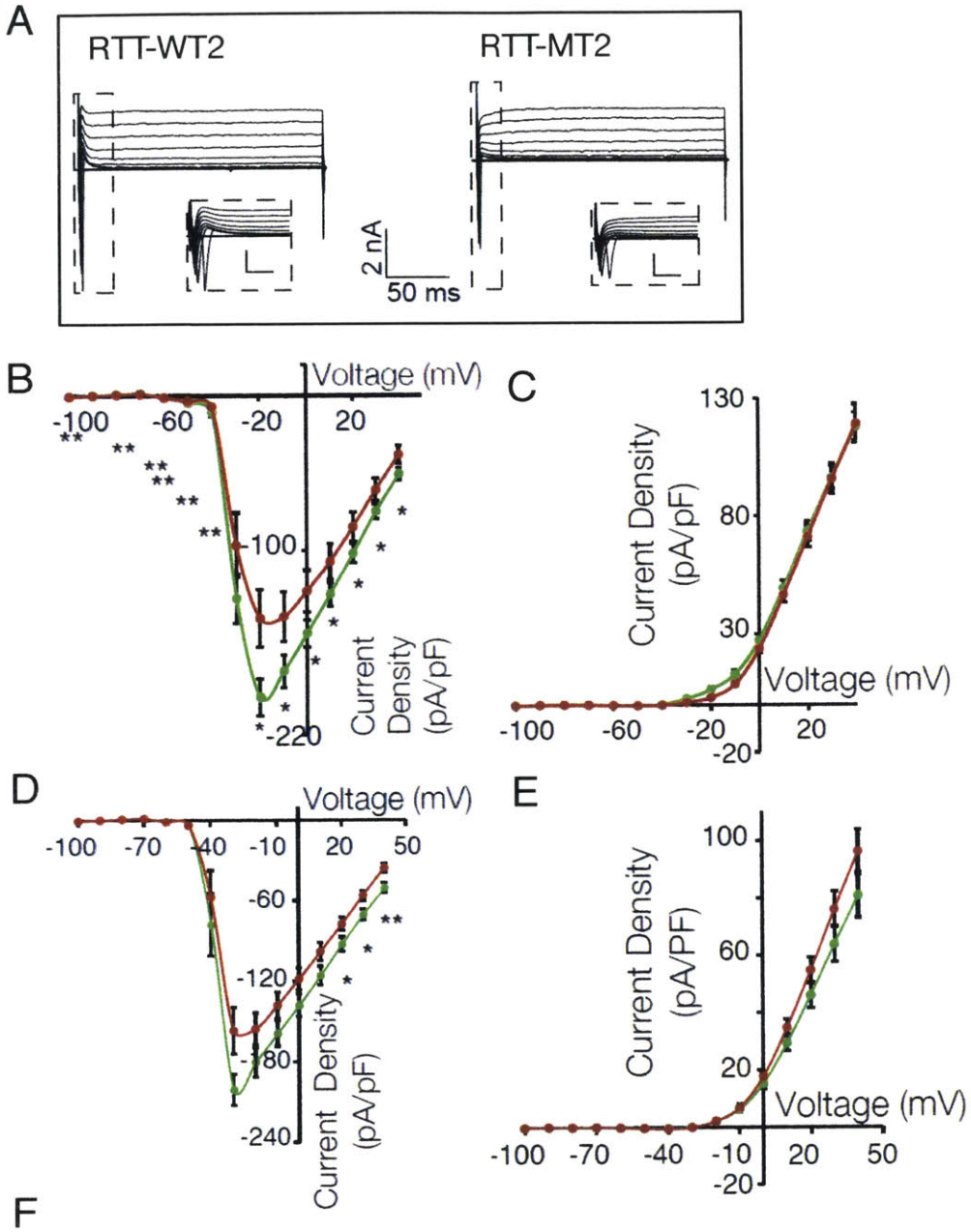
A
RTT-WT2
RTT-MT2
2 nA
50 ms
B
Voltage (mV)
-100
-60
-20
20
-100
-220
Current Density (pA/pF)
C
Current Density (pA/pF)
130
80
30
Voltage (mV)
-100
-60
-20
20
-20
D
Voltage (mV)
-100
-70
-40
-10
20
50
-60
-120
-180
-240
Current Density (pA/pF)
E
Current Density (pA/PF)
100
60
20
Voltage (mV)
-100
-70
-40
-10
20
50
-20
F
Sodium and Potassium Channel Gene Expression
mRNA levels relative to WT
1.5
1.0
0.5
0.0
RTT-WT2
RTT-MT2
**
ns
***
**
**
ns
SCN1A
SCN2A
SCN3A
SCN8A
KCNH2
KCNQ2

Figure 7: Reduced voltage-sensitive currents in RTT iPSC-derived neurons.

(A) Representative trace from whole-cell voltage clamp recordings, showing current responses to voltage steps in one RTT-WT2 (*left*) and one RTT-MT2 (*right*) cell. Insets show depolarization-activated transient inward sodium current. *(B and D)* Mean I-V curve for peak sodium current in RTT-WT2 (*green*, N = 33) and RTT-MT2 (*red*, N = 22) neurons cultured in astrocyte-conditioned media. (C) Steady-state I-V curve from the cells in *(B)* shows no significant changes in putative voltage-sensitive potassium currents. *(D)* Reduced voltage-sensitive sodium current in the same RTT-MT2 line (*red*, N = 23) relative to RTT-WT2 cells (*green*, N = 19), both co-cultured with wild type human astrocytes. *(E)* Steady-state IV curve from the cells in *(D)* demonstrates no significant reduction in putative voltage-gated potassium currents in mutant cells. *(*p < 0.01, **p < 0,001, Kruskall-Wallis Test).*

Discussion

Using a variety of methods to generate RTT lines and NPs / neurons of various ages, we were able to study the course of RTT pathogenesis *in vitro*, controlling for potential artifacts introduced by one particular differentiation method or patient line (Young-Pearse and Morrow, 2016). Whereas many protocols currently exist for the neuronal differentiation of iPSCs *in vitro* (Velasco et al., 2014), it is prudent to avoid a one-size-fits-all approach and tailor the protocol used to the question being asked. For studies of early neuronal development, we have employed both 2D and 3D protocols that recapitulate key aspects of neurogenesis (Sheridan et al., 2011; Shi et al., 2012a; 2012b; Lancaster et al., 2013; Lancaster and Knoblich, 2014).

Concurrently, we employed rapid Ngn2-mediated differentiation to investigate key physiological aspects of neuronal function at later stages of development. Despite the known pro-neural role of Ngn2 (Nieto et al., 2001; Hand et al., 2005; Ge et al., 2006), its overexpression did not prevent the emergence of physiological phenotypes in MeCP2-deficient patient neurons, including impaired synaptic activity and reduced sodium channel function. Additionally, the neurons did not need to progress through established stages of neurogenesis in order to develop physiological profiles that align with established RTT models (Tropea et al., 2009; Farra et al., 2012). This suggests that the manifestation of physiological impairments in RTT may not be dependent upon alterations in neurodevelopment that could feasibly contribute to later stage pathology nor the distinct stages of neuronal migration observed during typical cortical differentiation (i.e., migration, lamination, etc.) (Götz and Huttner, 2005b). Our results

have pointed to a wide range of RTT phenotypes and key molecular signatures that arise in the early stages of neuronal development and those that emerge later in the maturation of membrane and synaptic properties. Whereas these two groups need not be completely mutually exclusive (it is possible that we would observe additional physiological deficits in the context of neurons that did not overexpress Ngn2), each appears to arise in the absence of the other, suggesting an emergence that is at least partially independent in nature.

Methods

Human fibroblast culture

Fibroblasts from two clinically diagnosed RTT female patients (GM07982, and GM11273) and one unrelated, unaffected male (GM08330) were purchased from Coriell Institute for Medical Research. Cells were grown in flasks coated with 0.1% gelatin (EMD Millipore), and grown in fibroblast media composed of 10% heat-inactivated FBS (Gemini Bio-Products), 1% Penicillin/Streptomycin (Invitrogen), 1% non-essential amino acids (Invitrogen) and 88% DMEM (Invitrogen) filtered through a 0.22 μm bottle-top low protein-binding PES filter.

Fibroblast reprogramming and iPSC expansion

Retroviruses were generated by tripartite transient transfection of pIK-MLV (gag.pol), pHDM-G (VSV), and the specific pMIG vectors carrying the hOCT4, hSOX2, hKLF4 or hc-MYC genes) into 293T cells as previously described (Park et al. 2008; Sheridan et al. 2011). Fibroblasts were plated in single wells of 6-well plates (Corning) at 10^5 cells

per well. These cells were then transduced for 24 hours with the four retroviruses with a multiplicity of infection (MOI) of 10 for pMIG-hOCT4-IRES-GFP (Addgene), pMIG-hSOX2-IRES-GFP (Addgene) and pMIG-hKLF4-GFP (Addgene) and MOI of 1 for MCSV-hc-MYC-IRES-GFP (Addgene). After 24 hours, cells were washed with PBS and fresh media was added, and five days later cells were passaged onto 10 cm gelatin-coated dishes with γ-irradiated mouse embryonic fibroblasts (MEFs) (GlobalStem). The next day the media was changed to iPSC media: 20% Knock-out Serum Replacement (KOSR, Invitrogen), 1% penicillin/streptomycin (Invitrogen), 1% non-essential amino acids (Invitrogen), 0.5% L-glutamine (Invitrogen), 100 μM 2-mercaptoethanol (Bio-Rad) and 77.5% DMEM/F-12 (Invitrogen) and 10 ng/mL bFGF (Stemgent) filtered through a 0.22 μm PES filter (EMD Millipore). Dishes had daily media changes until colonies emerged (3 to 6 weeks after transduction). Colonies were first assessed based on morphology, then for silencing of the retroviral vectors (GFP-negative) before being mechanically passaged onto gelatin coated 6-well plates (Corning) with MEFs (GlobalStem) as feeders. Using these methods, multiple clones from each line were chosen for expansion, cryopreservation, and further characterization. In addition to the iPSCs created here, iPSCs from an unaffected female control (WT2) were obtained from Coriell Institute for Medical Research (GM23279).

Reprogrammed colonies were picked into separate wells and subsequently grown as separate clones. The first several passages were grown directly on a feeder layer of MEFs (GlobalStem). For removal of MEFs for downstream RT-PCR and embryoid body formation, iPSCs were grown by indirect co-culture with MEFs (GlobalStem) on

Matrigel-coated (Corning) polyethylene terephthalate (PET) inserts with 1.0 μm pore-size in 6-well plates (Corning) in iPSC media as described (Abraham et al. 2010). iPSC lines were characterized by alkaline phosphatase expression in live cells (Millipore Detection Kit as per vendor instructions) and by immunocytochemical (ICC) analysis of 4% paraformaldehyde (PFA)-fixed undifferentiated colonies. Primary antibodies used for ICC analyses of pluripotent markers: anti-OCT-4 (Santa Cruz), anti-nanog (Abcam), DyLight 488 anti-Tra1-60 (Stemgent) and DyLight 550 anti-SSEA4 (Stemgent). 4G-Band Karyotype analysis was performed on feeder-free iPSC cultures by Cell Line Genetics (http://www.clgenetics.com). Tri-lineage germ layer potency was assessed by embryoid body formation as described previously (Sheridan et al., 2012). Briefly, embryoid bodies (EBs) were formed in ultra-low attachment 6-well plates (Corning) in iPSC media without bFGF and 1% heat-inactivated FBS (Gemini Bio-Products). After 20-28 days, EBs were fixed in 4% PFA followed by embedding in 1% low-melting temperature agarose. These EB containing agarose pellets were further paraffin embedded, sectioned (5 μM), mounted and followed by hematoxylin and eosin staining was performed at the Dana-Farber/Harvard Cancer Center Rodent Histopathology Core Facility.

Generation of RTT lines

To create RTT patient-derived neuronal cultures, fibroblasts from two female RTT patients (GM11273, "RTT-MT1" and GM07982, "RTT-MT2") and one unaffected male control (GM08330, "WT1") were reprogrammed to generate iPSCs using retroviral-mediated transient expression of OCT4, SOX2, cMYC, and KLF4. In addition, we

acquired a healthy control female iPSC line (GM23279, "WT2") generated by the same retroviral-mediated technique (Park et al., 2008; Sheridan et al., 2011). We utilized two complementary methods for promoting neuronal lineage in each of the two RTT patient-derived iPSCs (**Table 1**). For the RTT patient iPSCs that carried a single nucleotide substitution (missense mutation, 316C>T) in the methyl-cytosine-binding domain (MBD) of *MECP2* (RTT-MT1) and the first unaffected control (WT1), we manually picked neural rosettes and used fluorescence-activated cell sorting (FACS) to isolate $CD184^{+}$, $CD271^{-}$ homogeneous NPs. Additionally, we used dual SMAD inhibition (Shi et al. 2012b) to generate NPs from iPSCs of the second unaffected control (WT2) and the second RTT patient (RTT-MT2), the latter harboring a single nucleotide deletion (frameshift 705delG) in the transcriptional repression domain (TRD) that results in premature termination of the MeCP2 transcript.

MeCP2 shRNA construct and stable iPSC-NP line construction

Stable knockdown NP lines targeting human *MECP2* mRNA (clone ID TRCN0000330973 with target sequence 'ACACATCCCTGGACCCTAATG') in NP line 8330-8 (WT1) were made simultaneously with an empty vector control ("PGW"), which does not produce any shRNA. All lentiviral constructs were made at the Broad Institute and all shRNAs were produced as part the RNAi Consortium (TRC) collection. Lentiviruses carry the pLKO.1 plasmid, which contains a single shRNA of interest and the puromycin resistance gene, both of which incorporate into the cell genome upon transfection. To make stable knockdown cell lines, NPs were plated in 6-well plates at a density of 40,000 cells/cm^2 and left overnight. On day 2, cells were washed with PBS,

followed by the addition of 20 μL of viral media (titer =10^8) in 1 mL NP media. This was immediately followed by centrifugation of 6-well plates for 20 minutes at 2200 RPM and returned to incubators at 37 °C, 5% CO_2. Cells were left overnight, followed by a media change and PBS wash on day 3. On day 4, media was replaced with high dose puromycin-NP media (8 μM) and grown alongside un-transfected controls, which die off after three days in NP-puromycin media. After two days in high dose puromycin, cells were maintained in low dose NP-puromycin media (2 μM). After confirmation of knockdown efficiency, cells stored in liquid nitrogen and thawed / expanded as needed.

Generation of neural progenitors (monolayer)

Neural differentiation was initiated from iPSC clones grown under feeder-free conditions to remove MEFs by indirect co-culture with conditioning feeder layers on Matrigel-coated (Corning) 1 μm porosity membrane inserts as described (Abraham et al., 2010). For the first set of RTT patient and control (RTT-MT1 and WT1), neural differentiation was initiated by the formation of embryoid bodies. Briefly, in order to form embryoid bodies, iPSC colonies grown by indirect co-culture were broken up and plated in ultra-low attachment 6-well plates (Corning) in iPSC media supplemented with 20ng/ml bFGF (Stemgent) and 1% heat-inactivated FBS (Gemini Bio-Products) for a minimum of 19 days. NPs were initially isolated by magnetic-activated cell sorting (MACS) using magnetic particles conjugated with antibodies to the polysilated form of neural cell adhesion molecule (PSA-NCAM; Miltenyi Biotech). Isolated cells were expanded in neural expansion medium (70% DMEM (Invitrogen), 30% Ham's F-12

(Mediatech) supplemented with B-27 (Invitrogen), 20 ng/ml each EGF (Sigma) and bFGF (R&D Systems) on poly-ornithine (Sigma)/laminin (Sigma)-coated culture plates. Further purification was performed after initial expansion by fluorescence activated cell sorting (FACS). Sorting was performed at the Massachusetts General Hospital Pathology Flow and Image Core Lab using a Becton-Dickinson 5 Laser Vantage SE DIVA with Sheath Pressure of 20 PSI and 50.2 MHZ drop drive frequency. Cells were stained with CD15 (SSEA1)-FITC and CD184 (CXCR-4)-Cy5-PerCp and CD271 (p75)-Cy5 antibodies per vendor protocol (all from Becton-Dickinson Biosciences). $CD15^{+}$, $CD184^{+}$, $CD271^{-}$ cells were collected and further expanded on poly-ornithine/laminin plates in neural expansion media as described above. After five passages in expansion medium, cells were analyzed for Nestin and SOX1 expression by fixation in 4% PFA followed by primary incubation with rabbit anti-Nestin (Millipore) and mouse anti-SOX1 (Millipore), and subsequent secondary antibody incubation (Alexa Fluor, Molecular Probes) for 1 hour at room temperature). NPs were differentiated via removal of growth factors; neurons were fed every three days until harvest.

For RTT patient 2 and WT2 samples (RTT-MT2, RTT-WT2, and WT2), iPSCs were differentiated into NPs and then neurons as previously described (Shi et al., 2012a). Briefly, iPSCs were cultured on feeder-free matrigel coated wells in mTeSR1 (Stemcell Technologies) until confluent, at which point neural induction media containing 10 μM SB431542 (Tocris Bioscience) and 1 μM dorsomorphin (Stemgent) was used for 8-12 days to generate NPs. These NPs were further expanded in neural maintenance media for 8 days with 10 ng/ml of FGF2 (PeproTech) added upon the appearance of rosettes

(Day ~4). NPs derived from both methods were plated at 100,000 cells/cm^2 for 3 days (NPs) or differentiated for 19 days at 20,000 cells/cm^2 in neural maintenance media (neurons), feeding every 3-5 days until the indicated endpoint time.

Neurogenin-2-mediated differentiation

Lentiviral-mediated overexpression of Ngn2 was used to generate excitatory glutamatergic neurons as previously described (Zhang et al., 2013b). Briefly, iPSCs or NPs were plated as single cells at a density of 2 x 10^5 per cm^2 in Matrigel (Corning)-coated wells (Day 0). iPSCs were plated in mTeSR1 media containing 2 μM thiazovivin (BioVision); NPs were plated in NP media containing ROCK inhibitor (Tocris; Y27632). Lentivirus (M2-rtTA and either Ngn2-GFP fusion construct or Ngn2 and/or GFP single constructs) was added 2 hours post-plating (Day -1). Media was changed the following day (D0) to B27/N2-based neural media plus recombinant human BDNF (10 ng/mL, Peprotech), and recombinant human NT-3 (10 ng/mL, Peprotech). Doxycycline (2 μg/mL, Sigma) was added to induce TetO gene expression and retained in the medium until the end of the experiment. On Day 2, standard culture medium was replaced with wild type human astrocyte-conditioned medium and puromycin (1 μg/mL, Sigma) was added for 48 hours. Cells were passaged on Day 4 using Accutase (Innovative Cell Technologies) and plated at a density of 3 x 10^5 per cm^2. On Day 5, wild type human astrocytes (ScienCell), previously maintained in Astrocyte Medium (ScienCell) and treated with AraC (5 μM, Sigma) were dissociated using TrypLE (Life Technologies) and

plated at a density of 4 x 10^5 onto the Ngn2-derived neurons (to be used for electrophysiology experiments). Neurons were assayed at three weeks post-induction.

Immunocytochemistry

Cells were fixed in 4% PFA and the following primary antibodies were used: mouse α PAX6 (Millipore), rabbit α MeCP2 (Cell Signaling), chicken α Map2 (Encor Biotechnologies), guinea pig α Vglut1 (Synaptic Systems), mouse α PSD95 (Neuromab), rabbit α VAMP2 (Synaptic Systems), mouse α Shank3 (neuromab). Secondary antibodies were AlexaFluor conjugates (Life Technologies). Analysis was performed in ImageJ.

Electrophysiology

Intracellular whole-cell recordings: Borosilicate pipettes (3-5 MΩ, WPI) were pulled using a Sutter P-1000 puller and filled with intracellular solution containing (in mM): 100 K-gluconate, 20 KCl, 0.5 EGTA, 10 NaCl, 10 Na-phosphocreatine, 4 Mg-ATP, 0.3 Na-GTP, and 10 HEPES, pH 7.2-7.3 with 1M KOH. Cells were perfused in a recording solution containing (in mM): 130 NaCl, 10 glucose, 1.25 NaH2PO4, 24 NaCHO3, 3.5 KCl, 2.5 CaCl2, and 1.5 MgCl2. iPSC-derived neurons were grown in plastic-bottom dishes to aid adherence and visualized with a 40x water-immersion lens with infrared DIC optics (Olympus) and detected with a CCD camera (QIMaging). Data acquisition was performed using a Multiclamp 700B amplifier (Axon Instruments) and a Digidata 1440A (Molecular Devices). For each recording, a 5 mV test pulse was applied in

voltage clamp ~10 times to measure input and series resistance. In current clamp, ~10 pulses (500 ms, 40-140 pA at 10 pA increments) were applied to quantify evoked firing rates and cellular excitability. Access resistance, leak, and input resistance was monitored across groups. Spontaneous firing rates were recorded in current clamp using a DC offset to maintain the cell near -60 mV. Spontaneous EPSCs were measured under voltage clamp at -60 mV, sampled at 10 kHz, and low-pass filtered at 1 kHz. Analysis was performed using Clampfit 10.2 software (Molecular Devices), with all events detected according to automated thresholds and blindly verified individually by the experimenter.

RNA extraction and quantification

RNA extraction was performed using the RNeasy Mini Kit (Qiagen). cDNA synthesis for large RNAs was done using SuperScript VILO cDNA Synthesis Kit (Invitrogen) and used as PCR template to examine both allele-specific transcription mRNA and mRNA expression. Taqman gene expression assays were used as previously described (Mellios et al., 2014).

Contributors

Cell culture protocol development and refinement was performed by Danielle Feldman, Sally Kwok, Ph.D., and Steven Sheridan, Ph.D. Cell culture was performed by Danielle Feldman, Sally Kwok, Ph.D., Steven Sheridan, Ph.D., and technical assistants Bess Rosen and Stephanie Chou. PCR experiments were performed by Danielle Feldman and technical assistant Bess Rosen. iPSC characterization and immunocytochemical analysis was performed by Danielle Feldman, Showming Kwok, and Steven Sheridan. Electrophysiology was performed by Vardhan Dani. Ngn2 constructs were supplied by the Wernig lab.

References

Abraham S, Sheridan SD, Laurent LC, Albert K, Stubban C, Ulitsky I, Miller B, Loring JF, Rao RR (2010) Propagation of human embryonic and induced pluripotent stem cells in an indirect co-culture system. Biochem Biophys Res Commun 393:211–216.

Andoh-Noda T, Akamatsu W, Miyake K, Matsumoto T, Yamaguchi R, Sanosaka T, Okada Y, Kobayashi T, Ohyama M, Nakashima K, Kurosawa H, Kubota T, Okano H (2015) Differentiation of multipotent neural stem cells derived from Rett syndrome patients is biased toward the astrocytic lineage. Mol Brain 8:136.

Ballas N, Lioy DT, Grunseich C, Mandel G (2009) Non-cell autonomous influence of MeCP2-deficient glia on neuronal dendritic morphology. Nat Neurosci 12:311–317.

Banerjee A, Castro J, Sur M (2012) Rett syndrome: genes, synapses, circuits, and therapeutics. Front Psychiatry 3:34.

Bedogni F, Cobolli Gigli C, Pozzi D, Rossi RL, Scaramuzza L, Rossetti G, Pagani M, Kilstrup-Nielsen C, Matteoli M, Landsberger N (2015) Defects During Mecp2 Null Embryonic Cortex Development Precede the Onset of Overt Neurological Symptoms. Cereb Cortex.

Bellin M, Casini S, Davis RP, D'Aniello C, Haas J, Oostwaard DW-V, Tertoolen LGJ, Jung CB, Elliott DA, Welling A, Laugwitz K-L, Moretti A, Mummery CL (2013) Isogenic human pluripotent stem cell pairs reveal the role of a KCNH2 mutation in long-QT syndrome. The EMBO Journal 32:3161–3175.

Boggio EM, Lonetti G, Pizzorusso T, Giustetto M (2010) Synaptic determinants of rett syndrome. Frontiers in Synaptic Neuroscience 2:28.

Busskamp V, Lewis NE, Guye P, Ng AHM, Shipman SL, Byrne SM, Sanjana NE, Murn J, Li Y, Li S, Stadler M, Weiss R, Church GM (2014) Rapid neurogenesis through transcriptional activation in human stem cells. Mol Syst Biol 10:760.

Calfa G, Percy AK, Pozzo-Miller L (2011) Experimental models of Rett syndrome based on Mecp2 dysfunction. Exp Biol Med (Maywood) 236:3–19.

Castro J, Garcia RI, Kwok S, Banerjee A, Petravicz J, Woodson J, Mellios N, Tropea D, Sur M (2014) Functional recovery with recombinant human IGF1 treatment in a mouse model of Rett Syndrome. Proc Natl Acad Sci USA 111:9941–9946.

Chahrour M, Jung SY, Shaw C, Zhou X, Wong STC, Qin J, Zoghbi HY (2008) MeCP2, a key contributor to neurological disease, activates and represses transcription. Science 320:1224–1229.

Chahrour M, Zoghbi HY (2007) The story of Rett syndrome: from clinic to neurobiology. Neuron 56:422–437.

Chambers SM, Fasano CA, Papapetrou EP, Tomishima M, Sadelain M, Studer L (2009) Highly efficient neural conversion of human ES and iPS cells by dual inhibition of SMAD signaling. Nat Biotechnol 27:275–280.

Chavez A, Scheiman J, Vora S, Pruitt BW, Tuttle M, Iyer EPR, Lin S, Kiani S, Guzman CD, Wiegand DJ, Ter-Ovanesyan D, Braff JL, Davidsohn N, Housden BE, Perrimon N, Weiss R, Aach J, Collins JJ, Church GM (2015) Highly efficient Cas9-mediated transcriptional programming. Nat Meth 12:326–328.

Chen RZ, Akbarian S, Tudor M, Jaenisch R (2001) Deficiency of methyl-CpG binding protein-2 in CNS neurons results in a Rett-like phenotype in mice. Nat Genet 27:327–331.

Cheung AYL, Horvath LM, Grafodatskaya D, Pasceri P, Weksberg R, Hotta A, Carrel L, Ellis J (2011) Isolation of MECP2-null Rett Syndrome patient hiPS cells and isogenic controls through X-chromosome inactivation. Human Molecular Genetics.

Dang J, Tiwari SK, Lichinchi G, Qin Y, Patil VS, Eroshkin AM, Rana TM (2016) Zika Virus Depletes Neural Progenitors in Human Cerebral Organoids through Activation of the Innate Immune Receptor TLR3. Cell Stem Cell.

Dani VS, Chang Q, Maffei A, Turrigiano GG, Jaenisch R, Nelson SB (2005) Reduced cortical activity due to a shift in the balance between excitation and inhibition in a mouse model of Rett syndrome. Proc Natl Acad Sci USA 102:12560–12565.

Ellaway CJ, Sholler G, Leonard H, Christodoulou J (1999) Prolonged QT interval in Rett syndrome. Arch Dis Child 80:470–472.

Estacion M, O'Brien JE, Conravey A, Hammer MF, Waxman SG, Dib-Hajj SD, Meisler MH (2014) A novel de novo mutation of SCN8A (Nav1.6) with enhanced channel activation in a child with epileptic encephalopathy. Neurobiol Dis 69:117–123.

Farra N, Zhang W-B, Pasceri P, Eubanks JH, Salter MW, Ellis J (2012) Rett syndrome induced pluripotent stem cell-derived neurons reveal novel neurophysiological alterations. Mol Psychiatry 17:1261–1271.

Feldman D, Banerjee A, Sur M (2016) Developmental Dynamics of Rett Syndrome. Neural Plasticity 2016:6154080–6154089.

Garcez PP, Loiola EC, Madeiro da Costa R, Higa LM, Trindade P, Delvecchio R, Nascimento JM, Brindeiro R, Tanuri A, Rehen SK (2016) Zika virus impairs growth in human neurospheres and brain organoids. Science 352:816–818.

Ge W, He F, Kim KJ, Blanchi B, Coskun V, Nguyen L, Wu X, Zhao J, Heng JI-T,

Martinowich K, Tao J, Wu H, Castro D, Sobeih MM, Corfas G, Gleeson JG, Greenberg ME, Guillemot F, Sun YE (2006) Coupling of cell migration with neurogenesis by proneural bHLH factors. Proceedings of the National Academy of Sciences 103:1319–1324.

Götz M, Huttner WB (2005) The cell biology of neurogenesis. Nat Rev Mol Cell Biol.

Hand R, Bortone D, Mattar P, Nguyen L, Heng JI-T, Guerrier S, Boutt E, Peters E, Barnes AP, Parras C, Schuurmans C, Guillemot F, Polleux F (2005) Phosphorylation of Neurogenin2 Specifies the Migration Properties and the Dendritic Morphology of Pyramidal Neurons in the Neocortex. Neuron 48:45–62.

Hu B-Y, Weick JP, Yu J, Ma L-X, Zhang X-Q, Thomson JA, Zhang S-C (2010) Neural differentiation of human induced pluripotent stem cells follows developmental principles but with variable potency. Proc Natl Acad Sci USA 107:4335–4340.

Kerr AM (1995) Early clinical signs in the Rett disorder. Neuropediatrics 26:67–71.

Kim K-Y, Hysolli E, Park I-H (2011) Neuronal maturation defect in induced pluripotent stem cells from patients with Rett syndrome. Proc Natl Acad Sci USA 108:14169–14174.

Kishi N, Macklis JD (2010) MeCP2 functions largely cell-autonomously, but also non-cell-autonomously, in neuronal maturation and dendritic arborization of cortical pyramidal neurons. Experimental Neurology 222:51–58.

Krishnan K, Wang B-S, Lu J, Wang L, Maffei A, Cang J, Huang ZJ (2015) MeCP2 regulates the timing of critical period plasticity that shapes functional connectivity in primary visual cortex. Proc Natl Acad Sci USA 112:E4782–E4791.

Lancaster MA, Knoblich JA (2014) Generation of cerebral organoids from human pluripotent stem cells. Nat Protoc 9:2329–2340.

Lancaster MA, Renner M, Martin C-A, Wenzel D, Bicknell LS, Hurles ME, Homfray T, Penninger JM, Jackson AP, Knoblich JA (2013) Cerebral organoids model human brain development and microcephaly. Nature 501:373–379.

Larsen J et al. (2015) The phenotypic spectrum of SCN8A encephalopathy. Neurology 84:480–489.

Li Y, Wang H, Muffat J, Cheng AW, Orlando DA, Lovén J, Kwok S-M, Feldman DA, Bateup HS, Gao Q, Hockemeyer D, Mitalipova M, Lewis CA, Vander Heiden MG, Sur M, Young RA, Jaenisch R (2013) Global transcriptional and translational repression in human-embryonic-stem-cell-derived Rett syndrome neurons. Cell Stem Cell 13:446–458.

Maezawa I, Swanberg S, Harvey D, Lasalle JM, Jin L-W (2009) Rett syndrome

astrocytes are abnormal and spread MeCP2 deficiency through gap junctions. Journal of Neuroscience 29:5051–5061.

Marchetto MCN, Carromeu C, Acab A, Yu D, Yeo GW, Mu Y, Chen G, Gage FH, Muotri AR (2010) A model for neural development and treatment of Rett syndrome using human induced pluripotent stem cells. Cell 143:527–539.

Mariani J, Simonini MV, Palejev D, Tomasini L, Coppola G, Szekely AM, Horvath TL, Vaccarino FM (2012) Modeling human cortical development in vitro using induced pluripotent stem cells. Proc Natl Acad Sci USA.

Medrihan L, Tantalaki E, Aramuni G, Sargsyan V, Dudanova I, Missler M, Zhang W (2008) Early defects of GABAergic synapses in the brain stem of a MeCP2 mouse model of Rett syndrome. J Neurophysiol 99:112–121.

Mellios N, Woodson J, Garcia RI, Crawford B, Sharma J, Sheridan SD, Haggarty SJ, Sur M (2014) β2-Adrenergic receptor agonist ameliorates phenotypes and corrects microRNA-mediated IGF1 deficits in a mouse model of Rett syndrome. Proc Natl Acad Sci USA 111:9947–9952.

Miller JD, Ganat YM, Kishinevsky S, Bowman RL, Liu B, Tu EY, Mandal PK, Vera E, Shim J-W, Kriks S, Taldone T, Fusaki N, Tomishima MJ, Krainc D, Milner TA, Rossi DJ, Studer L (2013) Human iPSC-Based Modeling of Late-Onset Disease via Progerin-Induced Aging. Cell Stem Cell 13:691–705.

Nelson ED, Bal M, Kavalali ET, Monteggia LM (2011) Selective impact of MeCP2 and associated histone deacetylases on the dynamics of evoked excitatory neurotransmission. J Neurophysiol 106:193–201.

Neul JL, Lane JB, Lee H-S, Geerts S, Barrish JO, Annese F, Baggett LM, Barnes K, Skinner SA, Motil KJ, Glaze DG, Kaufmann WE, Percy AK (2014) Developmental delay in Rett syndrome: data from the natural history study. J Neurodev Disord 6:20.

Nieto M, Schuurmans C, Britz O, Guillemot F (2001) Neural bHLH genes control the neuronal versus glial fate decision in cortical progenitors. Neuron 29:401–413.

Olson HE, Tambunan D, LaCoursiere C, Goldenberg M, Pinsky R, Martin E, Ho E, Khwaja O, Kaufmann WE, Poduri A (2015) Mutations in epilepsy and intellectual disability genes in patients with features of Rett syndrome. Am J Med Genet A 167:2017–2025.

Park I-H, Arora N, Huo H, Maherali N, Ahfeldt T, Shimamura A, Lensch MW, Cowan C, Hochedlinger K, Daley GQ (2008) Disease-specific induced pluripotent stem cells. Cell 134:877–886.

Paşca AM, Sloan SA, Clarke LE, Tian Y, Makinson CD, Huber N, Kim CH, Park J-Y,

O'Rourke NA, Nguyen KD, Smith SJ, Huguenard JR, Geschwind DH, Ben A Barres, Paşca SP (2015) Functional cortical neurons and astrocytes from human pluripotent stem cells in 3D culture. Nat Meth 12:671–678.

Qiu Z, Sylwestrak EL, Lieberman DN, Zhang Y, Liu X-Y, Ghosh A (2012) The Rett Syndrome Protein MeCP2 Regulates Synaptic Scaling. Journal of Neuroscience 32:989–994.

Ricciardi S, Boggio EM, Grosso S, Lonetti G, Forlani G, Stefanelli G, Calcagno E, Morello N, Landsberger N, Biffo S, Pizzorusso T, Giustetto M, Broccoli V (2011) Reduced AKT/mTOR signaling and protein synthesis dysregulation in a Rett syndrome animal model. Human Molecular Genetics 20:1182–1196.

Ricciardi S, Ungaro F, Hambrock M, Rademacher N, Stefanelli G, Brambilla D, Sessa A, Magagnotti C, Bachi A, Giarda E, Verpelli C, Kilstrup-Nielsen C, Sala C, Kalscheuer VM, Broccoli V (2012) CDKL5 ensures excitatory synapse stability by reinforcing NGL-1-PSD95 interaction in the postsynaptic compartment and is impaired in patient iPSC-derived neurons. Nat Cell Biol 14:911–923.

Ross CA, Akimov SS (2014) Human-induced pluripotent stem cells: potential for neurodegenerative diseases. Human Molecular Genetics 23:R17–R26.

Ruvinsky I, Sharon N, Lerer T, Cohen H, Stolovich-Rain M, Nir T, Dor Y, Zisman P, Meyuhas O (2005) Ribosomal protein S6 phosphorylation is a determinant of cell size and glucose homeostasis. Genes Dev 19:2199–2211.

Schaevitz LR, Gómez NB, Zhen DP, Berger-Sweeney JE (2013) MeCP2 R168X male and female mutant mice exhibit Rett-like behavioral deficits. Genes, Brain and Behavior 12:732–740.

Schaevitz LR, Moriuchi JM, Nag N, Mellot TJ, Berger-Sweeney J (2010) Cognitive and social functions and growth factors in a mouse model of Rett syndrome. Physiol Behav 100:255–263.

Shahbazian MD, Sun Y, Zoghbi HY (2002) Balanced X chromosome inactivation patterns in the Rett syndrome brain. Am J Med Genet 111:164–168.

Sheridan SD, Surampudi V, Rao RR (2012) Analysis of Embryoid Bodies Derived from Human Induced Pluripotent Stem Cells as a Means to Assess Pluripotency. Stem Cells Int 2012:1–9.

Sheridan SD, Theriault KM, Reis SA, Zhou F, Madison JM, Daheron L, Loring JF, Haggarty SJ (2011) Epigenetic characterization of the FMR1 gene and aberrant neurodevelopment in human induced pluripotent stem cell models of fragile X syndrome. Cookson MR, ed. PLoS ONE 6:e26203.

Shi Y, Kirwan P, Livesey FJ (2012a) Directed differentiation of human pluripotent stem

cells to cerebral cortex neurons and neural networks. Nat Protoc 7:1836–1846.

Shi Y, Kirwan P, Smith J, Robinson HPC, Livesey FJ (2012b) Human cerebral cortex development from pluripotent stem cells to functional excitatory synapses. Nat Neurosci 15:477–486.

Tropea D, Giacometti E, Wilson NR, Beard C, McCurry C, Fu DD, Flannery R, Jaenisch R, Sur M (2009) Partial reversal of Rett Syndrome-like symptoms in MeCP2 mutant mice. Proc Natl Acad Sci USA 106:2029–2034.

Tsujimura K, Abematsu M, Kohyama J, Namihira M, Nakashima K (2009) Neuronal differentiation of neural precursor cells is promoted by the methyl-CpG-binding protein MeCP2. Experimental Neurology 219:104–111.

Velasco I, Salazar P, Giorgetti A, Ramos Mejía V, Castaño J, Romero Moya D, Menendez P (2014) Concise Review: Generation of Neurons From Somatic Cells of Healthy Individuals and Neurological Patients Through Induced Pluripotency or Direct Conversion. Stem Cells 32:2811–2817.

Vera E, Studer L (2015) When rejuvenation is a problem: challenges of modeling late-onset neurodegenerative disease. Development 142:3085–3089.

Weiss LA, Escayg A, Kearney JA, Trudeau M, MacDonald BT, Mori M, Reichert J, Buxbaum JD, Meisler MH (2003) Sodium channels SCN1A, SCN2A and SCN3A in familial autism. Mol Psychiatry 8:186–194.

Yamanaka S (2007) Strategies and new developments in the generation of patient-specific pluripotent stem cells. Cell Stem Cell 1:39–49.

Young-Pearse TL, Morrow EM (2016) Modeling developmental neuropsychiatric disorders with iPSC technology: challenges and opportunities. Curr Opin Neurobiol 36:66–73.

Zhang L, He J, Jugloff DGM, Eubanks JH (2008) The MeCP2-null mouse hippocampus displays altered basal inhibitory rhythms and is prone to hyperexcitability. Hippocampus 18:294–309.

Zhang Y, Pak C, Han Y, Ahlenius H, Zhang Z, Chanda S, Marro S, Patzke C, Acuna C, Covy J, Xu W, Yang N, Danko T, Chen L, Wernig M, Südhof TC (2013a) Rapid single-step induction of functional neurons from human pluripotent stem cells. Neuron 78:785–798.

Zhou Z, Hong EJ, Cohen S, Zhao W-N, Ho H-YH, Schmidt L, Chen WG, Lin Y, Savner E, Griffith EC, Hu L, Steen JAJ, Weitz CJ, Greenberg ME (2006) Brain-Specific Phosphorylation of MeCP2 Regulates Activity-Dependent Bdnf Transcription, Dendritic Growth, and Spine Maturation. Neuron 52:255–269.

Chapter III

MeCP2-regulated miRNAs control early human neurogenesis through differential effects on ERK and AKT signaling.

Abstract

Rett Syndrome (RTT) is an X-linked neurodevelopmental disorder caused primarily by mutations in the Methyl-CpG-binding protein 2 (*MECP2*) gene, which encodes a multifunctional epigenetic regulator with known links to a wide spectrum of neuropsychiatric disorders. Whereas postnatal functions of MeCP2 have been thoroughly investigated, the role of MECP2 in prenatal brain development remains poorly understood. We characterized the effects on human and mouse neurogenesis and neuronal differentiation brought about by MeCP2 deficiency using human induced pluripotent stem cell (iPSC)-derived neuronal culture models. We generated human neural progenitors (NPs) and neurons using both RTT patient lines and shRNA-mediated knockdown of *MECP2.* Given the well-established importance of miRNAs in neurogenesis, we sought to identify novel MeCP2-regulated miRNAs enriched during early human neuronal development. Focusing on the most dysregulated miRNAs, we found miR-199 and miR-214 to be robustly increased in all examined RTT models and to differentially regulate extracellular signal-regulated kinases (ERK1/2) and protein kinase B (PKB/AKT) signaling. Inhibiting miR-199 or miR-214 expression in iPSC-derived neural progenitors (NPs) deficient in MeCP2 restored AKT and ERK activation, respectively, and ameliorated the downstream gene expression-based alterations in neuronal differentiation. Taken together, our data support a novel miRNA-mediated pathway downstream of MeCP2 that influences neurogenesis via interactions with central molecular hubs linked to autism spectrum disorders (ASDs).

Introduction

Rett syndrome (RTT) is a pervasive neurodevelopmental disorder with early onset that is predominantly caused by mutations that disrupt the function of the X-linked gene *MECP2* (Amir et al., 1999). MeCP2 is known to influence the expression of a wide pool of downstream targets, among which are miRNAs. Governing this miRNA regulation are interactions between MeCP2 and nuclear miRNA transcription and processing machineries (Szulwach et al., 2010; Urdinguio et al., 2010; Wu et al., 2010; Cheng et al., 2014a). RTT is a leading cause of intellectual disability in females, resulting in critical disturbances in motor coordination, seizures, autism-like behavior, and respiratory and cardiac abnormalities (Neul and Zoghbi, 2004; Neul et al., 2010). Although initial observations had suggested that female RTT patients appear relatively normal at birth and during very early stages of development, increasing evidence suggests early developmental delays in female RTT patients (Kerr, 1995; Leonard and Bower, 1998; Einspieler et al., 2005; Neul et al., 2014). Males born with the mutant *MECP2* allele display severe neurological deficits from birth, characteristic of a prenatal pathogenesis (Schanen and Francke, 1998; Trappe et al., 2001). Existing data on the effectiveness of a subset of postnatal treatment options for RTT mouse models have demonstrated the potential for reversibility of a subset of disease symptoms (Giacometti et al., 2007; Guy et al., 2007; Tropea et al., 2009; Castro et al., 2014; Khwaja et al., 2014; Mellios et al., 2014). However, they have also been interpreted as evidence of an exclusively postnatal pathogenesis of RTT. Due to the above, as well as the evidence of increased postnatal expression of MeCP2, the vast majority of studies on RTT have thus far focused on the role of MECP2 in postnatal brain development

and maturation (Shahbazian et al., 2002; Kishi and Macklis, 2004; Fukuda et al., 2005). However, as MECP2 is also expressed in the prenatal brain (Shahbazian et al., 2002; Bedogni et al., 2015), it remains plausible that it plays a role in embryonic brain development. Indeed, recent reports demonstrate that artificially increasing MeCP2 levels in mouse neural progenitor (NP) cultures and chick embryonic neural tubes can impair neurogenesis and lead to premature neuronal differentiation (Tsujimura et al., 2009; Petazzi et al., 2014). Pivotal studies using iPSC-derived early differentiated neuronal cultures from RTT patients noted reductions in the expression of neuronal markers, dendritic complexity, and neuronal migration (Marchetto et al., 2010; Kim et al., 2011; Farra et al., 2012; Fernandes et al., 2015). On a similar note, measurement of NP and early neuronal marker expression in *Mecp2* KO embryonic brains has suggested a potential imbalance in prenatal brain development (Bedogni et al., 2015). Furthermore, iPSC models of genetically engineered and RTT patient-derived differentiated mature neuronal and glial cultures have demonstrated the presence of structural, physiological, and molecular disease-related phenotypes in differentiated neurons (Marchetto et al., 2010; Kim et al., 2011; Farra et al., 2012; Li et al., 2013; Williams et al., 2014). However, no detailed analyses of early neuronal development alterations and the mechanisms that underlie them have been reported to date in human models of RTT.

microRNAs (miRNAs) are an evolutionarily conserved subtype of small noncoding RNAs enriched in the mammalian brain that interact with the majority of protein-coding genes to inhibit protein translation and mRNA stability (Lewis et al., 2003; Coolen and

Bally-Cuif, 2009; Forero et al., 2010; Krol et al., 2010; Mellios and Sur, 2012). In recent years, numerous reports have made a compelling case for the importance of miRNAs in prenatal and adult neurogenesis, brain maturation, and experience-dependent synaptic plasticity (Kosik, 2006; Krichevsky et al., 2006; Coolen and Bally-Cuif, 2009; Mellios et al., 2011; Mellios and Sur, 2012). Unsurprisingly, given the above, a subset of miRNAs has been shown to be altered in neurodevelopmental and neurological disorders and to contribute to essential molecular networks underlying brain disease pathophysiology (Coolen and Bally-Cuif, 2009; Hébert et al., 2009; Mellios and Sur, 2012).

Employing human patient- and *MECP2* knockdown-derived neuronal culture models, we have uncovered significant alterations in neurogenesis and neuronal differentiation in MeCP2-deficient cells. Due to the substantial evidence linking miRNAs to neurogenesis, we hypothesized that these deficits may occur as a result of MeCP2-regulated miRNAs that modulate critical molecular components of NP proliferation and differentiation. Intriguingly, our findings implicated miR-199 and miR-214, two miRNAs robustly upregulated in RTT patient and MeCP2-deficient NPs and early neurons, as important effectors of early neuronal development via their differential effects on AKT and ERK pathway signaling. Overall, our data describe a novel miRNA-mediated molecular cascade downstream of MeCP2 that utilizes known autism spectrum disorder (ASD) pathways to regulate prenatal brain development.

Results

MECP2 deficiency results in aberrant neuronal differentiation in human iPSC-derived cultures.

In order to determine the effects of MeCP2 deficiency on NPs and early neurons, we generated RTT lines from patients and via a virally-mediated shRNA knockdown approach (**Chapter 2: Figure 1, Table 1**). RTT patient neurons (RTT-MT2) and MeCP2 shRNA knockdown neurons (shMeCP2) both exhibited deficits in maturation relative to controls (RTT-WT2 and shControl, respectively) at early stages of neuronal differentiation (**Figure 1A**). Both MeCP2-deficient lines expressed reduced mRNA levels of neuronal markers DCX and MAP2 relative to respective controls (**Figure 1B, C**). A branching analysis confirmed morphological deficits in shMeCP2 neurons, revealing reduced neurite number and length at early stages of neuronal development (**Figure 1D-F**).

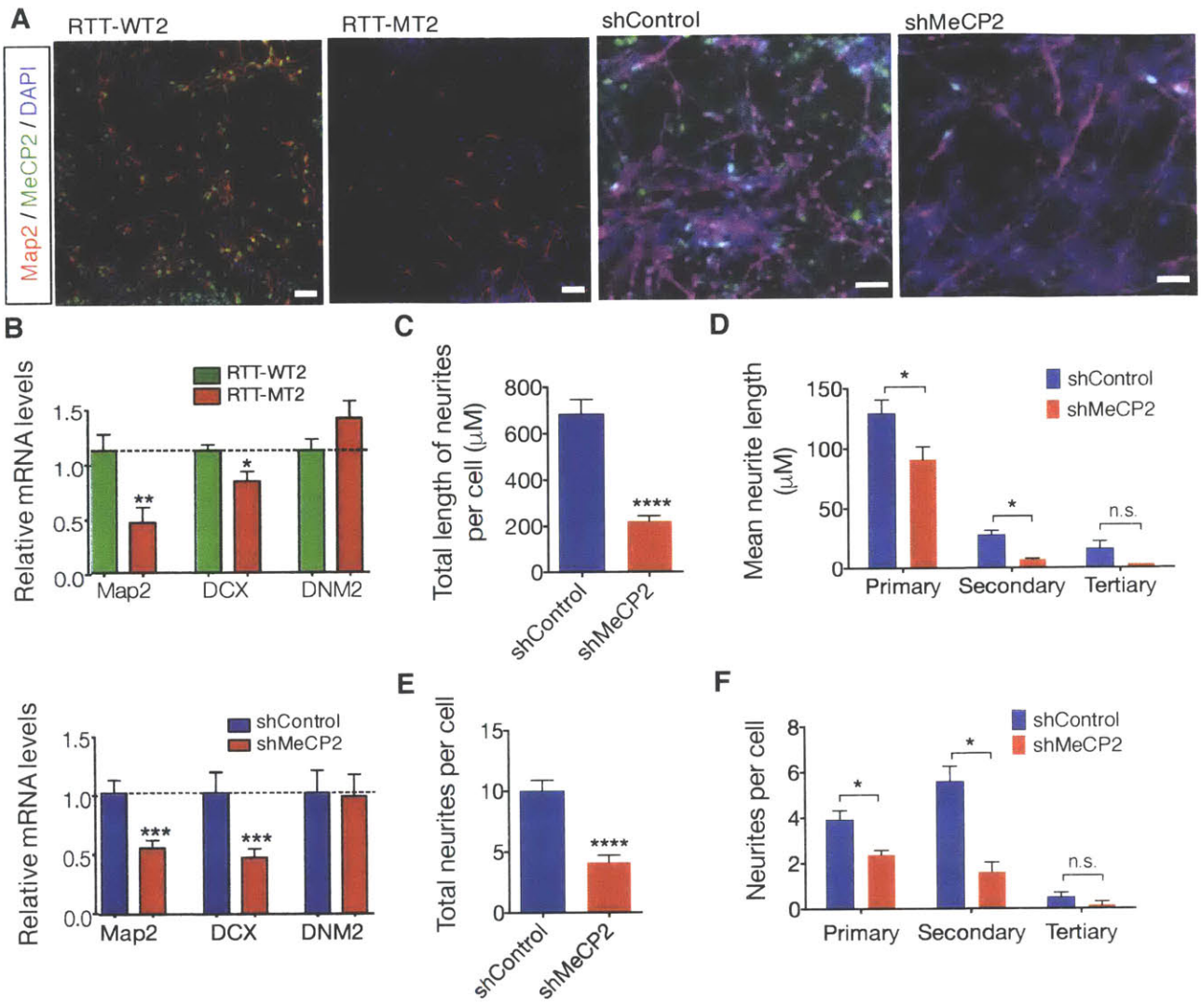

Figure 1: Alterations in neurogenesis and neuronal differentiation in RTT patient-derived and MECP2-deficient neurons.

(A) Immunofluorescence for neuronal marker MAP2 in WT2, RTT-WT2, and RTT-MT2 three-week differentiated neurons. MeCP2 immunostaining using a C-terminus antibody shows no expression in RTT-MT2 neurons. *(Scale bar = 50 μM (left) and 25 μM (right). (B) MAP2* and *DCX* mRNA levels in the RTT patient-derived (*top*) and *MECP2* knockdown (*bottom*) three-week neuronal samples. *DNM2* mRNA is also shown as an example of non-altered mRNA expression. *(Graphs show mean ± SEM. *p < 0.05, **p < 0.01, two-tailed one sample t-test). (C-F)* Branching analysis performed in three-week *MECP2 knockdown* neurons demonstrates a reduction in the total length of neurites per cell *(C)*, the mean neurite length *(D)*, the total

number of neurites per cell *(E)*, and the number of primary and secondary neurites *(F)*. *(Graphs show mean ± SEM. *p < 0.05, ****p < 0.0001, Mann-Whitney test.)*

Given the observed immature morphology in RTT mutant neurons, in addition to evidence linking MeCP2 to neuronal fate determination (Tsujimura et al., 2009; Andoh-Noda et al., 2015), we sought to determine whether the balance of proliferation and differentiation is skewed in RTT mutant NPs. We performed a BrdU assay to measure the percentage of actively dividing cells under the premise that NPs would be labeled more than their post-mitotic neuronal counterparts. Notably, we found significantly higher numbers of BrdU-positive cells in RTT-MT2 cultures at three weeks *in vitro* in comparison to both WT2 and isogenic RTT-WT2 [**Figure 2A, C(top)**], demonstrating an increase in the number of dividing cells in the mutant line. Similar increases in cellular proliferation were observed in shMeCP2 cultures upon assaying BrdU incorporation [**Figure 2B, C(bottom)**]. Taken together, these data suggest that early neuronal differentiation deficits are independent of both the nature of MeCP2 deficiency and the method of neuronal differentiation.

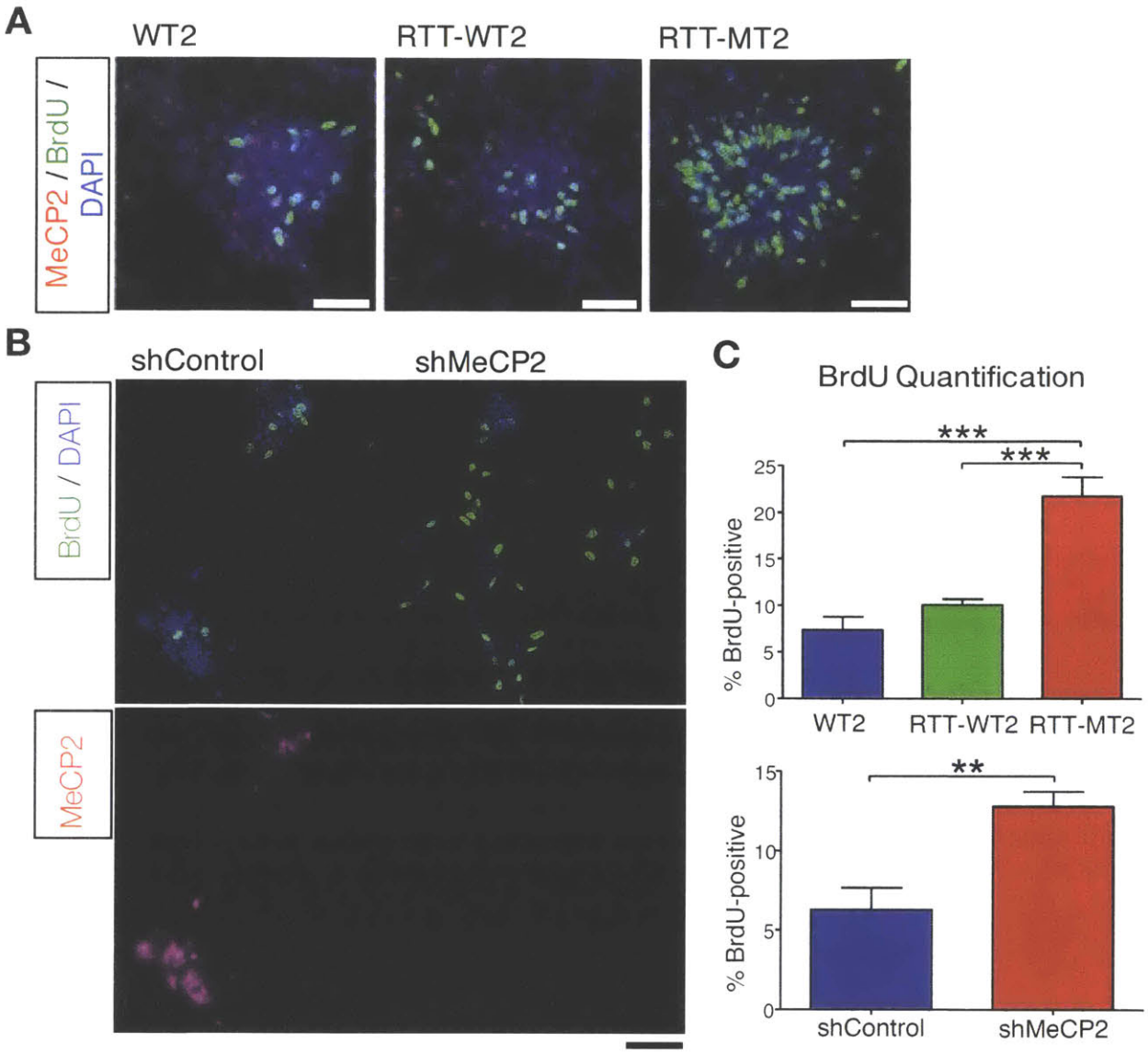

Figure 2: BrdU assay reveals increased proliferation in shMeCP2 neurons

(A-B) Immunostaining for BrdU and MeCP2 in RTT patient line *(A)* and shRNA-mediated knockdown neurons *(B)* at three weeks *in vitro*. (*Red*, MeCP2; *Green*, BrdU) *(C)* Significant increase in the percentage of BrdU-positive cells in RTT patient neurons (*red*) relative to isogenic WT (*green*) and healthy female control (*blue*, *top*) and shRNA knockdown neurons (*red*) relative to shRNA Control neurons (*blue*, *bottom*). *(Graphs show mean ± SEM. **p < 0.01, ***p < 0.001, Student's t-test. Scale bar = 50 μM).*

Deficits in neurogenesis in MeCP2-deficient mouse models

An increase in NP proliferation suggests the potential for impaired migration during neurogenesis. If NPs are unable to exit the cell cycle, a logical hypothesis follows that these cells would be delayed in their migration from the ventricular/sub-ventricular zone (VZ/SVZ) into the cortical plate. To test this hypothesis *in vivo*, we electroporated WT embryonic mouse brains with an *Mecp2* shRNA ("shMeCP2") or control construct ("shControl") together with a GFP construct to visualize the migration of newly-born neurons. Results revealed significant delays in the ability of newly-born shMeCP2 neurons to exit the VZ/SVZ and migrate towards the cortical plate (**Figure 3A, B**), which is in agreement with a recent study (Bedogni et al., 2015). In addition, we found that a significantly increased percentage of MeCP2-deficient neurons remained as PAX6-positive progenitors, suggesting a stunted differentiation process in these cells (**Figure 3B inset**). Given the observed abnormalities in prenatal brain development, we anticipated that newly born *Mecp2* mutant mice should exhibit altered cortical lamination. Indeed, male newborn (P0) *Mecp2*$^{-/y}$ mice were characterized by a modestly reduced cortical thickness (**Figure 3C, D**) indicative of dysfunctional lamination processes and in alignment with our observed deficits in neuronal migration**.** The observed deficits in prenatal brain development in *Mecp2* mice are less severe than those observed in our human neuronal culture models. This is in accordance with the comparatively milder phenotype observed in male *Mecp2* mutant mice vs. male RTT patients and the delayed onset of symptoms in *Mecp2* heterozygous female mice vs. female RTT patients (onset of symptoms at old age in female heterozygous mice vs. early infancy in female RTT patients). This could be due to a variety of factors,

including a temporally and spatially lengthier process of neurogenesis in humans versus mice, and/or varying timelines of expression of key genes that regulate these neurodevelopmental processes.

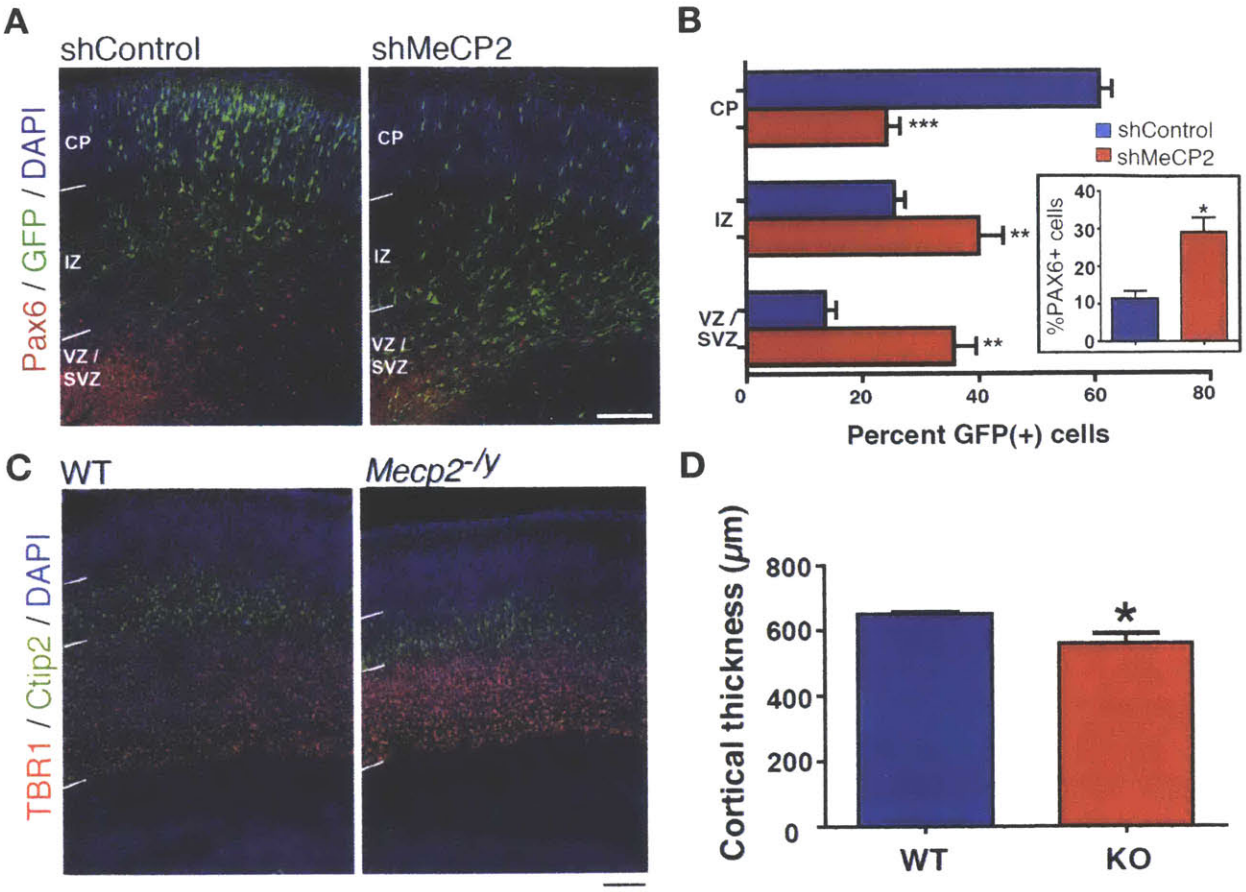

Figure 3: Aberrant neurogenesis following *in vivo* inhibition of mouse and human MeCP2 expression.

(A) Results of *in utero* electroporation of E13 mouse embryos with GFP plasmids together with either a control vector (*left*) or shRNA targeting MeCP2 (*right*). Representative coronal brain sections at E16 were stained with antibodies to GFP (*green*) and PAX6 (*red*) and counterstained with nuclear marker DAPI (*blue*). CP: cortical plate; IZ: intermediate zone; VZ: ventricular zone. *(Scale bar = 100 μm.) (B)* Quantification of the distribution of GFP-positive "GFP(+)" neurons. *(Graphs show mean ± SEM. *p < 0.01, ***p < 0.001; two-tailed Student's t-test).* More than 1,000 GFP(+) neurons from four brains were analyzed in each group. The percentages of PAX6+ GFP+ cells at E16 were quantified (*inset*). *(Graphs show mean ± SEM. *p < 0.05 versus control; two-tailed Student's t-test.) (C)* Representative immunostaining of newborn (P0) WT and *Mecp2*$^{-/y}$ mice with upper (Ctip2) and lower (TBR1) cortical markers. *(Scale bar = 100 μm.) (D)* Quantification of cortical thickness (in μm) in WT and *Mecp2* KO mouse brains. *(Graph shows mean ± SEM. *p < 0.01; two-tailed Student's t-test).*

miRNA dysregulation in MeCP2-knockdown and RTT patient-derived NPs

Given the known role of miRNAs in regulating neurogenesis and neuronal differentiation, we hypothesized that the observed deficits in neuronal differentiation may be related to a misregulation of key miRNAs during this period of development. Thus we performed a screen of miRNA expression in iPSC-derived NPs and immature (~three weeks *in vitro*) neurons in both a non-isogenic pair (RTT-MT1 versus WT1) and an isogenic pair (RTT-MT2 versus RTT-WT2) using NanoString nCounter miRNA analysis— a technique capable of specifically detecting mature miRNAs without any amplification steps (**Figure 4A, 7A, Supplementary Table 1**). Screening results uncovered numerous differentially affected miRNAs that were significantly altered in both proliferative NP and post-mitotic neurodevelopmental stages and in both RTT patient lines (**Supplementary Table 1**). Among them, the most robust changes were in multiple members of the miR-199 and let-7 miRNA families, which were significant after correction for multiple comparisons based on false discovery (FDR) and q-value calculations. However, only the miR-199 family—consisting of miR-199a-5p (produced from both miR-199a-1 and miR-199a-2 precursors), miR-199b-5p, and miR-199a,b-3p (identical 3p sequence showing the highest overall expression and produced from both miR-199a-1,2 and miR-199b—showed a consistent and robust upregulation in both developmental stages and RTT mutant lines. Results from qRT-PCR measuring levels of miR-199a,b-3p (the most highly expressed of the miR-199 family; heretofore referred to as just miR-199) and the co-expressed (together with miR-199a-2) miRNA miR-214 revealed dramatic increases in expression in RTT-MT1 and RTT-MT2 NPs (**Figure 4B**). We validated these results in our shRNA-mediated MeCP2 knockdown NPs, which

also exhibited significantly higher expression of both miR-199 and miR-214. (**Figure 4C**).

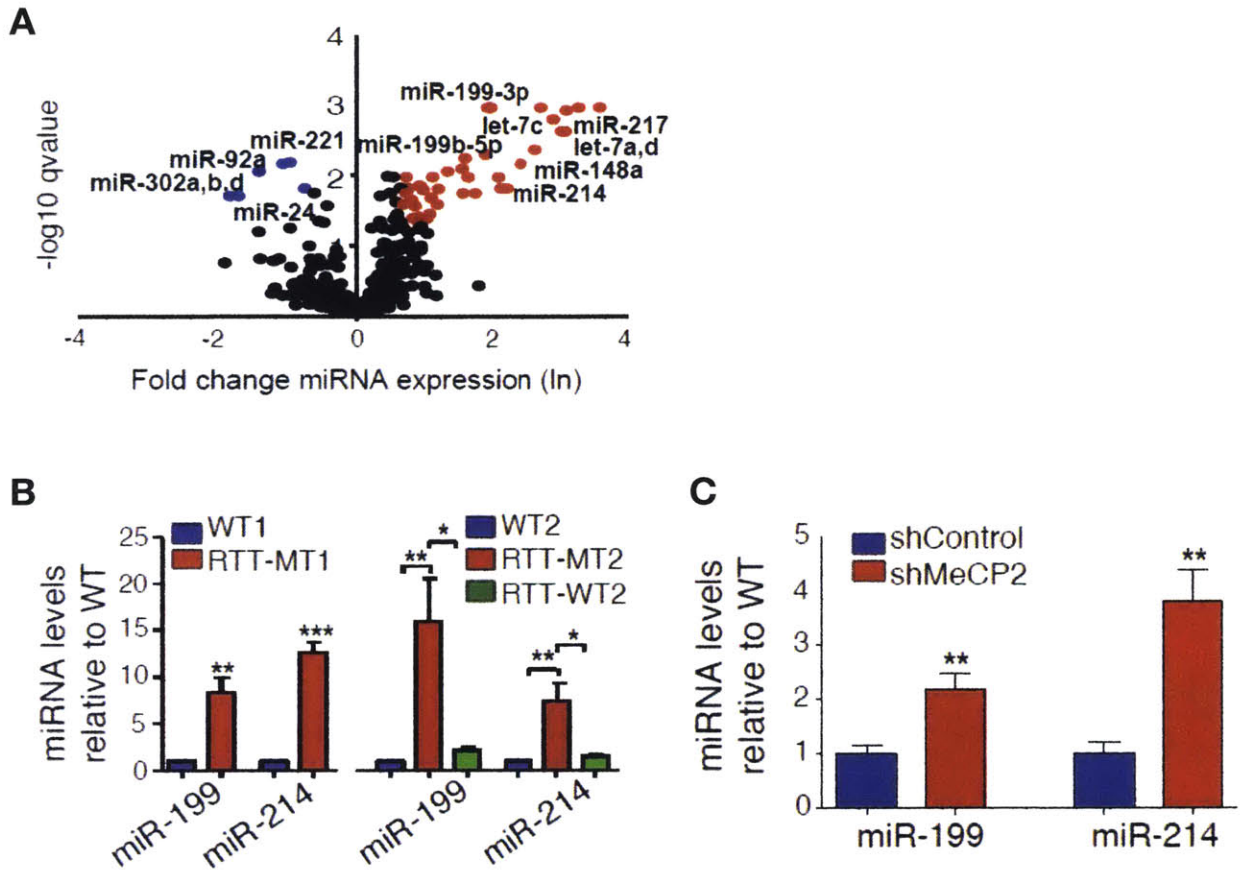

Figure 4: miRNA screen reveals increased miR-199 and miR-214 levels in patient-and shRNA-mediated models of RTT.

(A) Volcano plot showing miRNA fold changes relative to WT1 (x-axes- log transformed) based on NanoString miRNA profiling in RTT-MT1 NPs. Y-axis shows q-value significance. miRNAs with more than 2-fold increase and less than $p < 0.05$ q-values are highlighted in blue (reduced) and red (increased). *(B)* Validation of NanoString miRNA profiling results for upregulated miR-199/214 miRNAs using mature miRNA-specific qRT-PCR in NPs derived from patient-derived mutant (RTT-MT1 and RTT-MT2 – *red bars*) and control (WT1, WT2— *blue bars* and RTT-WT2—*green bars*). *(All values are shown as mean ± SEM relative to WT control ratios. *p < 0.05, **p < 0.01, ***p < 0.001, two-tailed one sample t-test in WT1, RTT-Mut1; ANOVA in WT2, RTT-Mut2, RTT-WT2 with Sidak's multiple comparisons test.) (C)* miR-199 and miR-214 levels in NPs expressing MeCP2 shRNA (shMeCP2 – *red bar*) and control shRNA (shControl – *blue bar*). *(Graphs show mean ± SEM. **p < 0.05, two-tailed one sample t-test).*

Pathway regulation

We hypothesized that miR-199/miR-214 dysregulation could be one mechanism downstream of MeCP2 contributing to the observed alterations in neural development. Toward this end, we related levels of neuronal marker MAP2 in RTT-MT2, WT2, and isogenic RTT-WT2 neurons to expression levels of miR-199 and miR-214. Our results demonstrated a strong inverse correlation between MAP2 versus each of the two affected miRNAs (**Figure 5A-B**).

In order to distinguish between a transcriptional or miRNA processing mechanism underlying the observed increases in miR-199 and miR-214 mature miRNAs in RTT patient-derived cultures, we measured the expression of the primary miRNA precursors (pri-miRNAs) from which mature miR-199 and miR-214 are encoded. Notably, two of the three separate pri-miRNAs that produce identical mature miR-199 sequences (pri-miR-199a at Chr19, pri-miR-199a-2 at Chr1, and pri-miR-199b at Chr9) and the one pri-miRNA responsible for mature miR-214 synthesis (pri-miR-214 at Chr1; adjacent to pri-miR-199a-2) displayed significant reductions (**Figure 5C**). Such a discordance between mature and pri-miRNA expression excludes a transcriptional mechanism and suggests a disturbance in miRNA processing, an effect that has been already attributed to MECP2 (Cheng et al., 2014b).

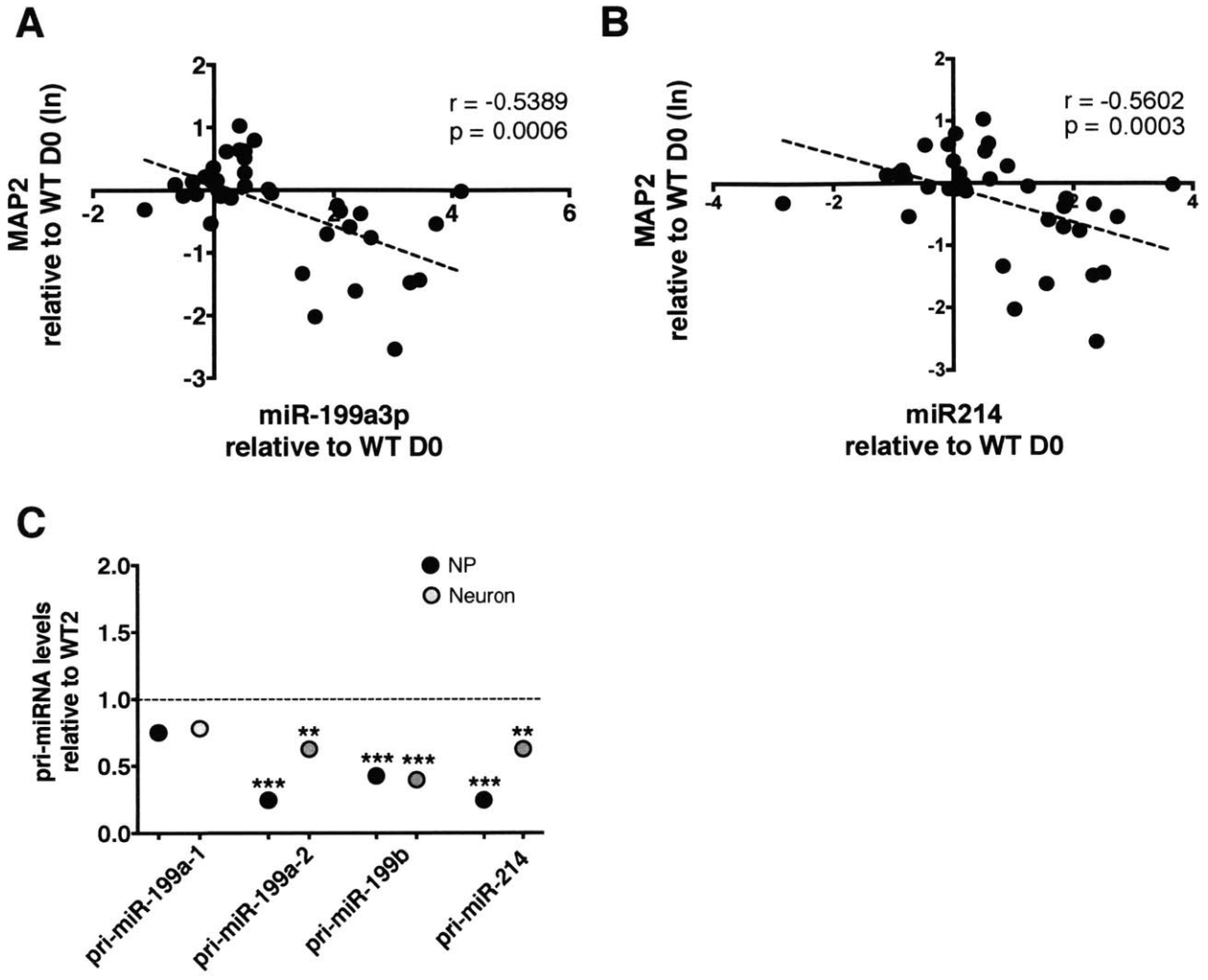

Figure 5: Alterations in miR-199 and miR-214 expression are associated with reduced early neuronal marker expression and are suggestive of altered miRNA processing.

(A-B) Correlations between human MAP2 mRNA and miR-199 *(A)* or miR-214 *(B)* expression in immature neurons (three weeks *in vitro*) shown as relative to WT ratios *(data from WT2, RTT-WT2, and RTT-MT2, are all represented by a black circle)*. *(C)* Precursor miRNA expression in RTT-patient derived neuronal cultures. Primary precursor miRNA (pri-miRNA) expression changes in both NP (*black*) and neuronal (*gray*) RTT-MT2 cultures relative to WT2. *(Graph shows mean ± SEM. *p < 0.05, **p < 0.01, ***p < 0.001, two-tailed one sample t-test).*

Signaling pathways downstream of miR-199 and miR-214 are aberrantly regulated in RTT neural progenitors

To determine the role(s) of miR-199 and miR-214 dysregulation in the observed deficiencies in early human neuronal development, we first performed *in silico* analyses of the predicted targets of significantly altered miR-199 and miR-214 miRNAs by Targetscan using the DAVID bioinformatics database. The scan revealed enrichment in important brain signaling pathways such as MAPK, WNT, Insulin, and mTOR (**Supplementary Table 2**). Aberrant expression of miR-199 and/or miR-214 has been linked to gastric cancer and approximately half of ovarian cancers, supporting a role for these miRNAs in a disease context, particularly as it relates to cellular metabolism and cell cycle (Yang et al., 2008; 2013). Upregulated miR-214 in particular has been linked to de-sensitization of cancerous cells to cancer drug / EGFR inhibitor gefitinib (Wang et al., 2012). Numerous studies have demonstrated that miR-214 targets PTEN, an ASD-related gene known to inhibit the activation of AKT (Yang et al., 2008; Jindra et al., 2010; Li et al., 2011; Wang et al., 2012; Yang et al., 2013; Wang et al., 2014). miR-199a-3p has been shown to be downregulated in several human cancers (Fornari et al., 2010) and has been shown to regulate the MET proto-oncogene in addition to downstream ERK2 signaling (Kim et al., 2008). It has also been shown to influence the doxorubicin sensitivity of human cancer cells *in vitro* via regulation of mTOR and c-Met (Fornari et al., 2010). In addition, one validated target for miR-199a-3p is PAK4, a member of a family of serine/threonine kinases that are critical effector proteins regulated by Rho-family GTPases and capable of activating MAPK signaling (Hou et al., 2011). Previous studies have also suggested that both ERK and AKT are important

for embryonic brain development, yet control different aspects of neurogenesis: ERK promotes neuronal differentiation and AKT induces neuronal progenitor proliferation and survival (Peltier et al., 2007; Samuels et al., 2008; Imamura et al., 2010; Peltier et al., 2011; Pucilowska et al., 2012). Combined, these pathways would predict that in the absence of MeCP2, PAK4 and PTEN would be reduced due to a lack of miR-199 and miR-214, respectively. ERK1/2 would be reduced due to decreased PAK4, and AKT would be increased due to the reduction in negative regulation by PTEN. Both pathways would culminate in aberrant neurogenesis (**Figure 6A**). We measured the protein levels of PTEN, PAK4, as well as phosphorylated-specific (activated) and total AKT and Erk1/2 (pAKT, tAKT and pERK1/2, tERK1/2) using western blotting in NPs derived from RTT patients and MeCP2 knockdown (**Figure 6B**). We found significant reductions in PTEN and PAK4 protein levels in shMECP2 NPs relative to shControl, accompanied by decreased pERK1/2 to tERK1/2 ratios and increased ratios of pAKT to tAKT [**Figure 6B, C (left)**]. Importantly, measurements of ERK, AKT, PAK4, and PTEN were similarly affected in RTT-MT2 [**Figure 6B, C (right)**]. Additionally, we performed a correlation analysis across pathway components and found that, as expected, PTEN and p/t AKT are inversely correlated and PAK4 and p/t ERK 1/2 are positively correlated (**Figure 6D**). Taken together, our results suggest the existence of a consistent molecular network downstream of MECP2-regulated miRNAs miR-199 and miR-214, which is specifically affected during the early stages of neuronal differentiation. Our results thus far have established a consistent upregulation of both miR-199 and miR-214 as a result of MeCP2 mutation or knockdown, which is

accompanied by aberrant early neurogenesis and alterations in downstream pathways known to affect neuronal differentiation in both human and animal models.

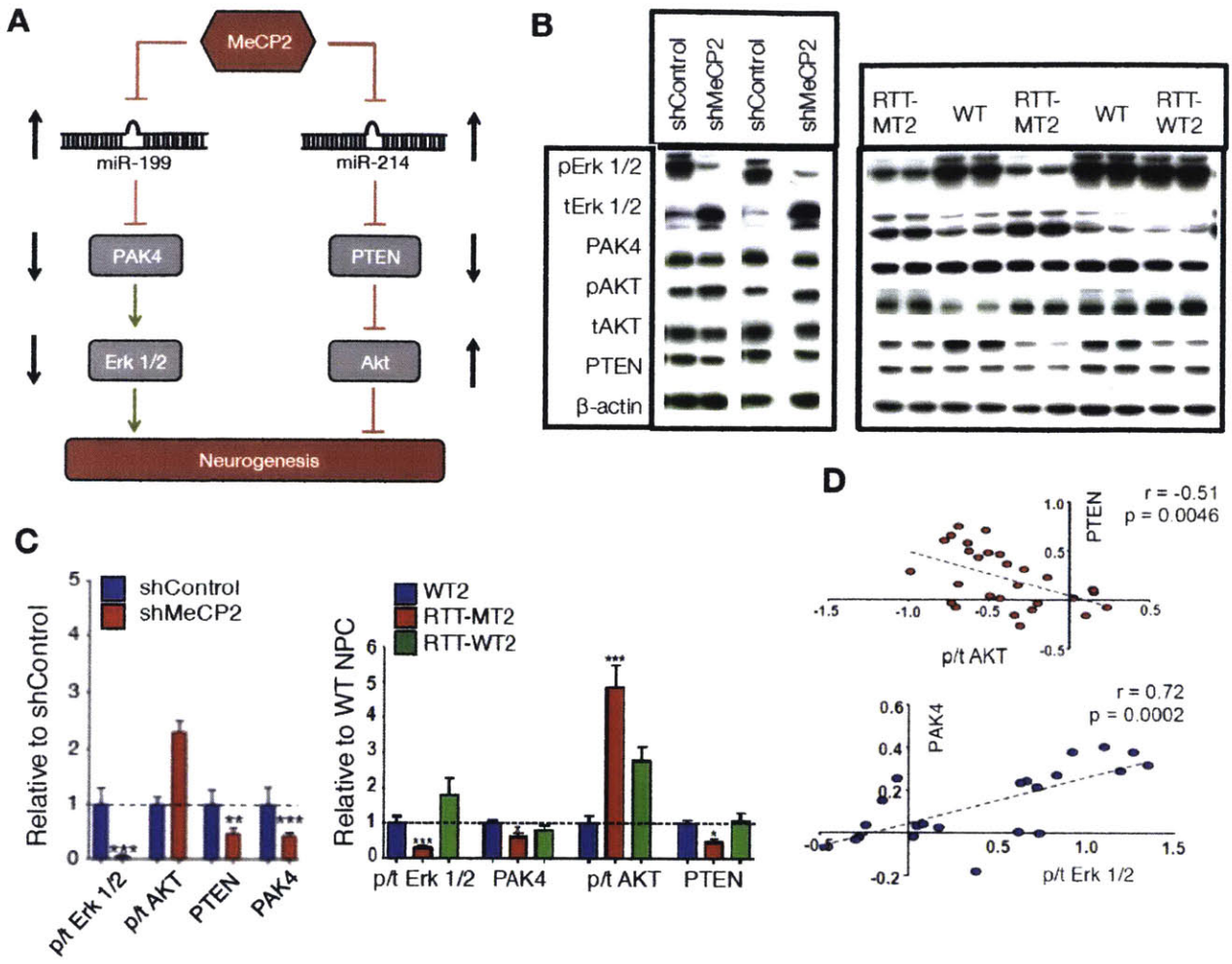

Figure 6: Pathway regulation downstream of MeCP2 leads to deficits in neurogenesis.

(A) Presumptive signaling pathways downstream of MeCP2. Arrows on the left and right indicate up- or down-regulation in the absence of MeCP2. In the absence of MeCP2 (*red*), miR-199 and miR-214 are robustly upregulated. PAK4, inhibited by miR-199, is reduced as a result of miR-199 elevation. Downstream target of PAK4, ERK1/2, is reduced as a result of PAK4 decrease. PTEN, inhibited by miR-214, is decreased as a result of increased miR-214. PTEN inhibits AKT, which is upregulated as a result of reduced PTEN. The misregulation of both pathways converges at the regulation of neurogenesis (*red*), aberrant in the absence of MeCP2. *(B)* Representative Western blots showing levels of phosphorylated and total ERK1/2 (p/t ERK1/2) and AKT ratios (p/t AKT) as well as PTEN and PAK4 protein levels together with normalizer β-actin in NPs expressing meCP2 shRNA (shMECP2) or Control shRNA (shControl) (*left*) as well as in WT2, RTT-WT2, and RTT-MT2 NPs (*right*). *(C)* Quantification of Western blot in shMECP2 (*red*) and shControl (*blue*) (*left*) and WT unaffected control (WT2 – *blue*), RTT-WT2 (*green*), and RTT-MT2 (*red*) (*right*). *(Graphs show mean ± SEM. **p < 0.01, ***p < 0.001, two-tailed one sample t-test (shMeCP2, shControl) or ANOVA (WT2, RTT-MT2, RTT-WT2) with Dunnett's multiple comparisons test). (D)* Correlation between

PTEN and p/t AKT levels (*top*) and PAK4 and p/t ERK1/2 (*bottom*) in WT2, RTT-WT2, RTT-Mut2 NPs. Each dot represents one sample *(blue dots for positive and red for negative correlations; Spearmann coefficients and p-values are shown in graphs.)*

Immature RTT neurons express elevated levels of miR-199 and miR-214; downstream pathways are partially conserved from NPs

Having established a plausible mechanism linking miR-199 and miR-214 to the observed deficits in neurogenesis, we tested whether the pathway misregulation observed in the NP stage extends to immature neurons as well. The Nanostring nCounter miRNA screen was performed in three-week differentiated neurons (**Figure 7A**). As observed in the RTT NP population, miR-199 and miR-214 were robustly upregulated, as confirmed via PCR in RTT patient samples (**Figure 7B**). We tested whether protein levels of the pathway components downstream of miR-199 and miR-214 (**Figure 6A**) are misregulated in neurons and found that despite consistent reductions in miRNA targets PTEN and PAK4, there were no significant changes in either AKT or ERK activation (**Figure 7C**). These results suggest that additional factors may contribute to the activation of AKT and ERK during later human neuronal development. Indeed, whereas significant positive and negative correlations were observed between PAK4 and activated ERK, and PTEN and activated AKT, respectively, at the NP stage, (**Figure 6D**), after three weeks of differentiation the correlation between PAK4 and activated ERK is diminished and the negative correlation between PTEN and AKT inverts to become positive (**Figure 7D**).

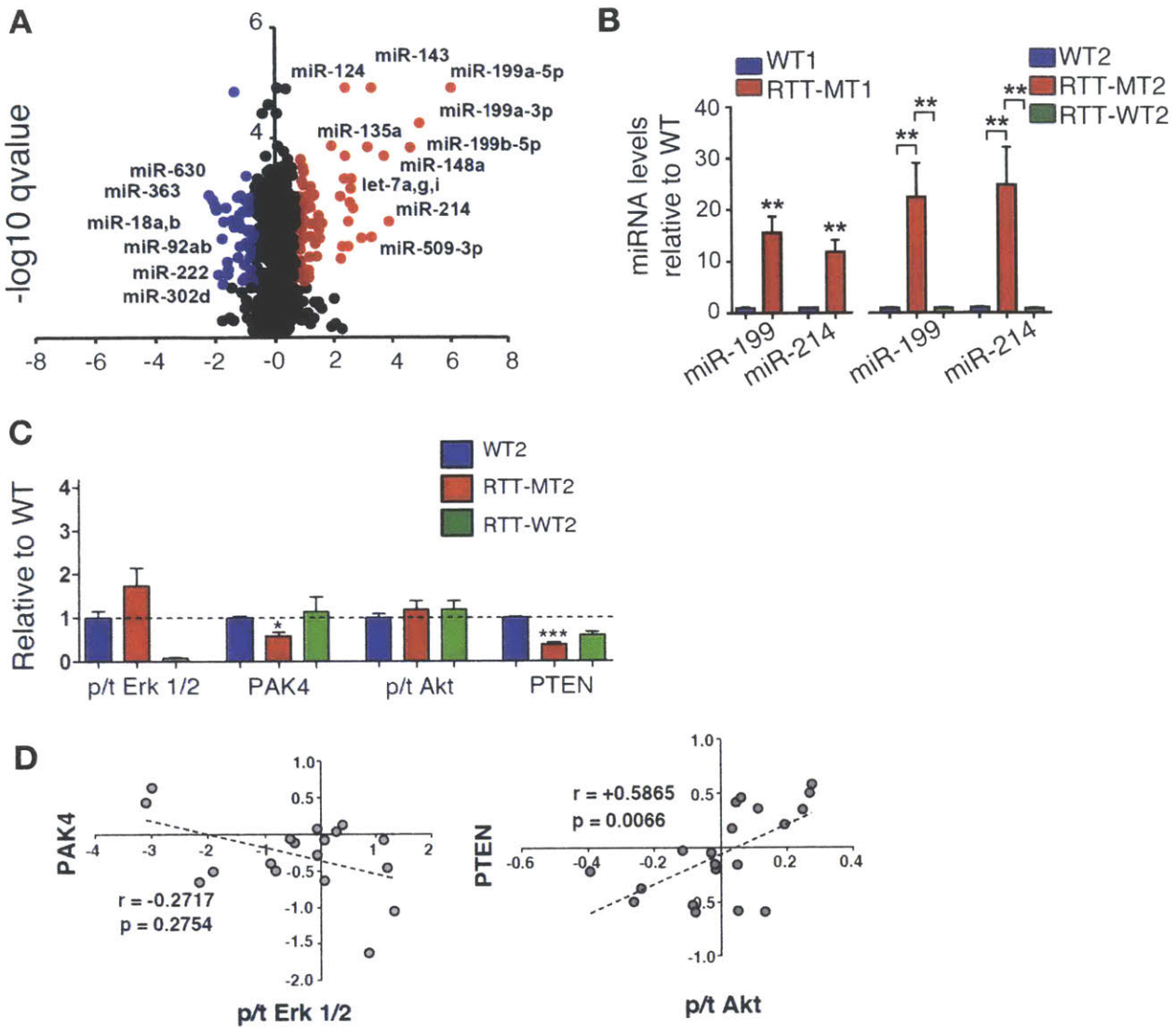

Figure 7: miR-199 and miR-214 remain upregulated in immature neurons; downstream pathway partially conserved.

(A) Volcano plot showing miRNA fold changes relative to WT1 (x-axis is log transformed) based on NanoString miRNA profiling in RTT-MT1 immature neurons (three weeks *in vitro*). Y-axis shows q-value significance. miRNAs with more than 2-fold increase and $q < 0.05$ are highlighted in blue (reduced) and red (increased). *(B)* Validation of Nanostring miRNA profiling results for upregulated miR-199/214 miRNAs using mature miRNA-specific qRT-PCR in patient-derived mutants (RTT-MT1, RTT-MT2 – *red*) and respective controls (WT1, WT2 – *blue* and RTT-WT2 – *green*). *(All values are shown as mean ± SEM relative to WT control ratios. **$p < 0.01$, Wilcoxon Signed Rank Test (WT1, RTT-MT1) or ANOVA (WT2, RTT-WT2, RTT-MT2) with Sidak's multiple comparisons test). (C)* Quantification of Western blot in three-week-old neurons measures phosphorylated and total ERK1/2 (p/t ERK1/2)

and AKT ratios (p/t AKT), as well as PTEN and PAK4 protein levels and normalizer β-actin, in WT2 (*blue*), RTT-WT2 (*green*) and RTT-MT2 (*red*). *(Graphs show mean ± SEM. **p < 0.01, ***p < 0.001, ANOVA (WT2, RTT-WT2, RTT-MT2) with Dunnett's multiple comparisons test). (D)* Correlation between PAK4 and p/t ERK1/2 (*left*) and PTEN and p/t AKT levels (*right*) in WT2, RTT-MT2, RTT-WT2 neurons at three weeks *in vitro*. *(Spearman's coefficients and p-values are shown in the graphs.)*

Inhibition of miR-199 or miR-214 ameliorates pathway deficits

Due to the complexity of signaling interactions involved, we sought to establish causality with respect to the observed enrichment of miR-199 and miR-214 levels during early prenatal neurogenesis and downstream pathway regulation. Indeed, such effects could feasibly be an epiphenomenon of delayed neuronal differentiation brought about by additional MeCP2-regulated pathways independent of miR-199/miR-214. In order to elucidate any potential mechanistic role(s) of miR-199/miR-214 dysregulation, we employed nucleofection to transfect shMECP2 NPs with plasmids encoding small RNA sequences that inhibit endogenous miR-199 or miR-214, as well as negative control miRNA inhibitors. This approach addressed whether miR-199 and/or miR-214 exerts an inhibitory effect on PAK4 and PTEN, respectively, and whether they influence the observed neuronal differentiation deficits in human neurons via differential effects on ERK and AKT signaling. Indeed, we found that miR-199 inhibition was able to significantly reverse the PAK4 reductions seen in shMeCP2 neurons (**Figure 8A**) and the reductions in PTEN levels in shMeCP2 immature neurons were significantly ameliorated by miR-214 inhibition (**Figure 8B**). In addition, the effects of miR-199 and miR-214 inhibition were specific for their targets, as no significant changes in PTEN or PAK4 were observed following miR-199 and miR-214 inhibition, respectively. Measurements of phosphorylated and total ERK and AKT via western blotting revealed that miR-199 inhibition in shMECP2 NPs resulted in the normalization of ERK activation exclusively, whereas inhibition of miR-214 in shMeCP2 NPs resulted in reduced AKT activation with no effects on ERK signaling (**Figure 8C-E**). Collectively, these data suggest that in MeCP2-deficient NPs, upregulation of miR-199 and miR-214

differentially regulates ERK and AKT signaling, respectively. To determine whether increased miR-214 and miR-199 levels are responsible for the observed MECP2 deficiency-related abnormalities in neuronal differentiation, we tested whether inhibiting these miRNAs via nucleofection in shMECP2 NPs could increase the expression of neuronal markers such as MAP2 and DCX. Indeed, both miR-199 and miR-214 single miRNA inhibition significantly increased MAP2 and DCX levels in immature MeCP2-shRNA neurons (**Figure 8F, G**), in addition to improving the observed alterations in neuronal maturity (**Figure 8H**). These results strongly suggest that the dysregulation in miR-214 and miR-199 as a result of MeCP2 deficiency is an important component of the molecular machinery underlying the alterations in neuronal differentiation.

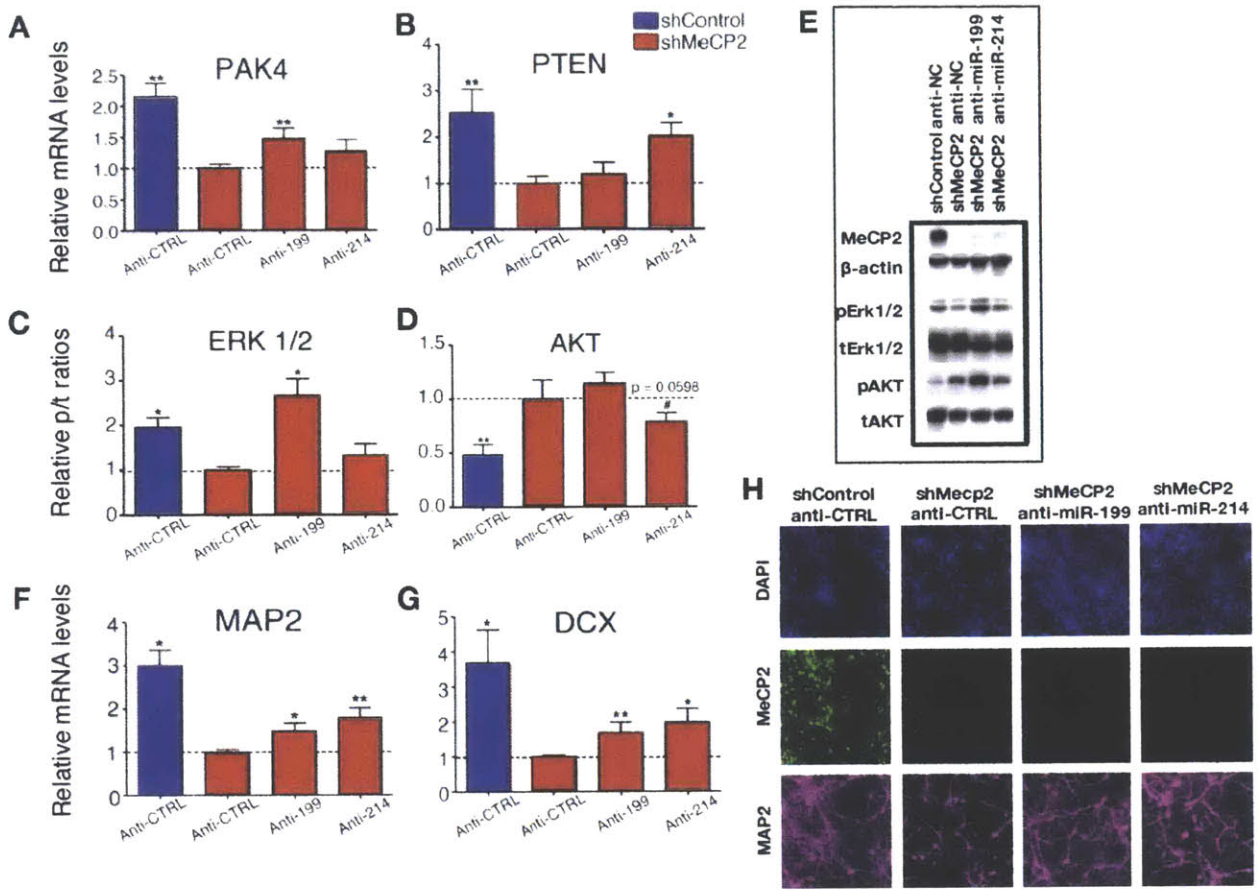

Figure 8: Partial amelioration of pathway deficits following inhibition of miR-199 or miR-214.

Nucleofection of miR-199 or miR-214 inhibitors ("anti-199" and "anti-214," respectively) in shMeCP2 expressing NPs (*red bars*), as well nucleofection of a negative miRNA control inhibitor ("anti-CTRL") in both shControl (*blue bars*) and shMeCP2 (*red bars*). *(A-B)* Levels of *PAK4* mRNA *(A)* and *PTEN* mRNA *(B)* in neurons harvested after nucleofection in shControl and shMeCP2 NPs. (C-D) Levels of phosphorylated and total ERK1/2 protein *(C)* and phosphorylated and total AKT protein *(D)* in NPs harvested after nucleofection. Graphs based on Western blot shown in *(E):* phosphorylated and total ERK1/2 (pERK1/2 and tERK1/2) and AKT (pAKT and tAKT), along with MECP2 protein levels and normalizer β-actin. *(F-G)* Levels of *MAP2 (F)* and *DCX (G)* mRNA in three-week nucleofected neuronal samples. *(All graphs show mean ± SEM. *p < 0.05 ,**p < 0.01, #0.10 < p <0.05, two-tailed one sample t-test). (H)* Representative immunostaining for MAP2 and MECP2 in three-week anti-miRNA / anti-CTRL nucleofected neurons.

Developmental trajectories of miR-199 and miR-214 differ in human versus mouse

Having observed deficits in RTT mouse neurogenesis as well as human neurons (**Figure 3**), we tested whether miR-199 and miR-214 are upregulated in MeCP2-deficient mouse NPs/neurons as they are in human cells. We measured the expression of both miRNAs in the brains of embryonic, perinatal, and postnatal (cortex-specific) WT and *Mecp2* mutant mice (both male null and female heterozygous mice) (**Figure 9A, B**). Our results revealed a transient, robust expression of both miR-199 and miR-214 around embryonic day E12.5, validating the observed upregulation of both miRNAs during the early stages of embryonic neurogenesis in an MeCP2-reduced or deficient context. Levels of both miRNAs subsequently dropped rapidly, and diminished at birth and four postnatal weeks in WT mice. Notably, expression of miR-199/miR214 in the brain of *Mecp2* mutant mice (n = three male null and three female heterozygote mice) displayed the same developmental expression peak during early neurogenesis.

We next sought to determine if the developmental expression patterns of miR-199 and miR-214 are similar in human and mouse neurons. We established that both miRNAs are upregulated in human (**Figure 4B-C; Figure 7B-C**) and mouse (**Figure 9A-B**) MeCP2-deficient cells during neurogenesis. Given the current inability of iPSC-derived neuronal cultures to reach a level of maturity reminiscent of the human postnatal brain, we re-analyzed the expression of the three miR-199 family miRNAs and miR-214 based on publicly available RNA sequencing results from the Brainspan Atlas of the Developing Brain. This data included multiple brain regions from human postmortem

brains from infancy to early adulthood (see also: Methods). Our results revealed miR-199 (miR-199a,b-3p) as by far the most highly expressed in the human postnatal brain among the four miRNAs queried, yet with different developmental trajectories between hippocampus (HIP), ventrolateral prefrontal cortex (VFC) and dorsolateral prefrontal cortex (DFC) (**Figure 9C-E**). miR-214 is expressed at low and slightly increasing levels throughout postnatal development in all three brain regions (**Figure 9C-E**).

Interestingly, whereas miRNAs 199 and 214 are highly expressed during neurogenesis in mouse and human NPs, their developmental trajectories differ in a postnatal context. The expression of both miRNAs is nearly abolished in the postnatal mouse, whereas human brain regions express miR-199 robustly and miR-214 at low albeit increasing levels throughout life. The developmentally restricted expression pattern of miRNAs in the WT mouse brain has been shown before (Mineno et al., 2006), yet is in contrast in this instance to the observed developmental patterns in human neuronal cultures and human postmortem brain. These results suggest potentially different roles of miR-199 and miR-214 in human versus mouse, further emphasizing the importance of employing a human neuronal cell line to identify miRNA signatures of RTT.

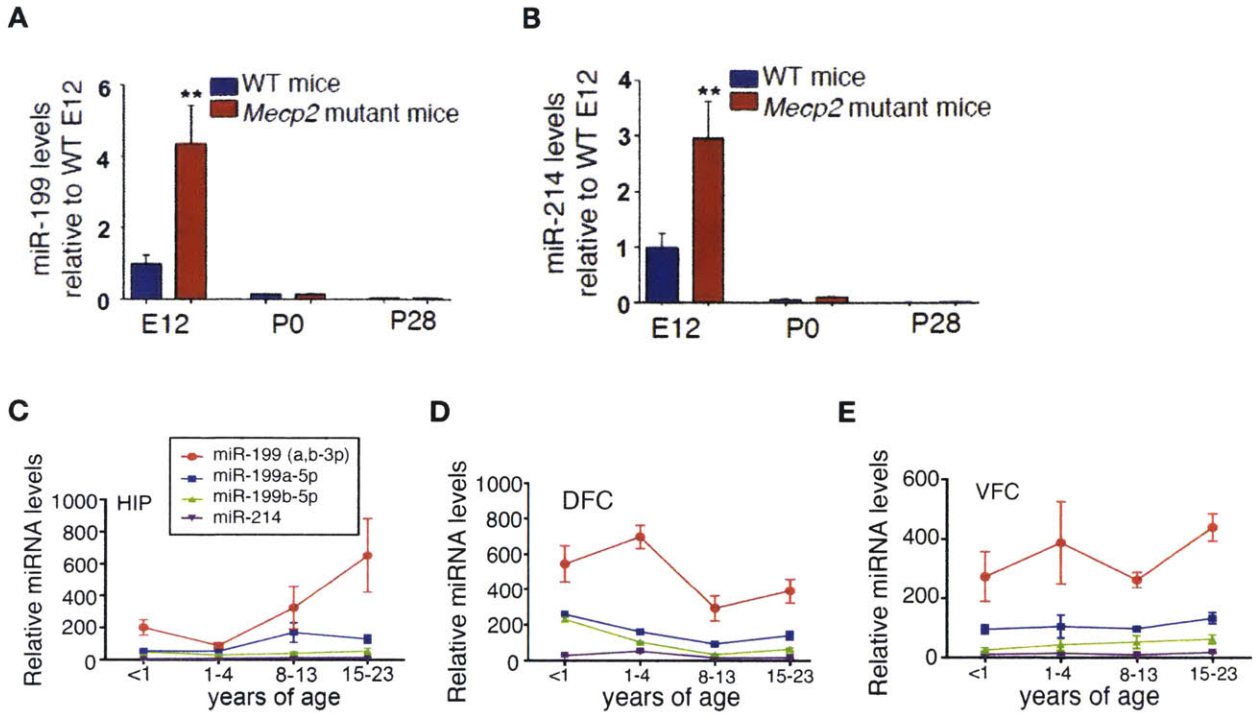

Figure 9: Developmental expression of miR-199 and miR-214 in healthy humans and Mecp2 control and mutant mice.

(A-B) Relative miR-199a-3p *(A)* and miR-214 *(B)* levels in embryonic (E12), perinatal (P0), and postnatal (P28) brains from WT and *Mecp2* mutant mice. All data are shown as relative to E12 WT. *(C-E)* Plotted values represent mean ± SEM Average RPKM (Reads Per Kilobase of transcript per Million mapped reads) values for miR-199 (miR-199a,b-3p), miR-199a-5p, miR-199b-5p, and miR-214 during four postnatal developmental periods (<1 year, 1-4 years, 8-13 years, and 15-23 years). Results from three different brain regions are displayed on separate graphs: HIP = hippocampus *(C)*; DFC = Dorsolateral prefrontal cortex *(D)*; VFC = ventrolateral prefrontal cortex *(E)*. Graphs were generated based on publically available data from the Brainspan Atlas of the Developing Brain database (see also: Methods). *(Graphs show mean ± SEM. *p < 0.05, **p < 0.01, two-tailed Mann Whitney test).*

Discussion

Mutations and altered expression of MECP2 have been linked to ASD, intellectual disability, schizophrenia, and other neuropsychiatric disorders of developmental origin other than RTT (Hammer et al., 2002; Gonzales and Lasalle, 2010). However, the vast majority of the existing literature has focused on the role of MECP2 in postnatal brain maturation and plasticity, and little is known about its effects in prenatal brain development. Our findings provide a novel mechanism downstream of MeCP2 that may contribute to critical prenatal components of the pathogenesis of neurodevelopmental disorders.

Mouse models with an embryonic (*Nestin-cre*) deletion of *Mecp2* recapitulate the majority of RTT symptomatology, whereas postnatal deletion such as in the case of CamKIIa-cre *Mecp2* mutant mice results only in a subset of RTT-related symptoms (Akbarian et al., 2001; Chen et al., 2001; Guy et al., 2001). Such severe effects of prenatal-specific disruption of Mecp2 support our proposed model. Furthermore, prenatal brain-specific overexpression of Mecp2 results in complete rescue, whereas Mecp2 overexpression via postnatal neuron-specific promoters cannot fully rescue the observed phenotype (Luikenhuis et al., 2004; Giacometti et al., 2007). However, rescue of Mecp2 expression in lox-stop *Mecp2* mutant adolescent mice can notably improve survival and ameliorate RTT-related symptoms (Giacometti et al., 2007; Guy et al., 2007). Additionally, numerous therapeutic approaches have been shown to partially rescue RTT phenotypes. The most notable examples have been those aimed at restoring BDNF and IGF1 and β-adrenergic receptor signaling, which also hold clinical

promise (Chang et al., 2006; Ogier et al., 2007; Tropea et al., 2009; Kline et al., 2010; Pini et al., 2012; Castro et al., 2013; 2014; Khwaja et al., 2014; Mellios et al., 2014). Such cases of postnatal amelioration of RTT phenotypes, however, do not exclude the possibility of a prenatal component of RTT, but rather underscore the reversibility of RTT symptomatology.

Neuropathological analysis of the brains of RTT patients has revealed increased cell density and diminished cellular size and dendritic complexity, in addition to reduced early neuronal marker expression (Armstrong, 1995; Bauman et al., 1995). Furthermore, multiple studies in mouse models of RTT have revealed alterations in neuronal maturation and dendritic and spine morphology in adolescent or adult mice (Shahbazian et al., 2002; Kishi and Macklis, 2004; Fukuda et al., 2005; Leng et al., 2009; Castro et al., 2014). Notably, our data in newborn *Mecp2* mutant mice also demonstrate a significant reduction in cortical thickness, which by necessity must be a result of aberrant prenatal brain development. Our findings of increased BrdU incorporation in MeCP2-deficient human neuronal cultures and migration deficits in mouse further support this notion and provide an alternative explanation for the observed alterations in postnatal neuronal morphology. However, due to the strong existing evidence of the role of MeCP2 in postnatal brain maturation and plasticity and the postnatal peak in developmental expression of MeCP2, our proposed model is most likely to be the first part of a "two-hit" scenario that incorporates both pre- and post-natal contributions to RTT pathophysiology. In such a case, future experiments

utilizing miR-199 and miR-214 prenatal-specific knockdown and transgenic overexpression will be needed to fully validate our proposed mechanism.

One limitation of our findings is that they are unable to fully conclude whether the observed aberrant neuronal differentiation in RTT neurons and *Mecp2* mutant mice is a result of a delay in neurogenesis or of an initial premature increase in early neurogenesis which can subsequently result in compensatory reductions in mid- and late-stage neurogenesis. The known differential effects of ERK and AKT on prenatal neurogenesis, however, point toward the latter. Such a premature increase in early neurogenesis followed by a depletion of neurogenic capacity can explain the aberrant early neuronal maturation and dendritic arborization in MeCP2-deficient neurons, as it would severely impact the precise developmental timing needed for the complex and interrelated prenatal brain developmental stages. Furthermore, our findings of transient and opposite disruptions in ERK and AKT signaling during early neurogenesis in human patient-derived neuronal cultures are of particular interest, as reductions in both ERK and AKT activation are observed in certain brain regions of adult symptomatic *Mecp2* mutant mice (Ricciardi et al., 2011; Castro et al., 2014). On a similar note, the dissociation between ERK and AKT activation from the changes in miR-199/PAK4 and miR-214/PTEN expression observed in three-week differentiated iPSC-derived neurons suggests the presence of compensatory influences on the activation of these two central molecular hubs.

It is known that too much or too little MECP2 can result in neurodevelopmental defects including RTT-related phenotypes. Thus we would predict that reductions in miR-

199/214 miRNAs could also be deleterious. Indeed, knockout mice lacking *Dnm3os*, the transcript antisense to Dynamin 3 gene that encodes pri-miR-199a-2 and pri-miR-214 (Watanabe et al., 2008) show body growth abnormalities. On a similar note, a recent paper reported that miR-199a-2 knockout mice display some RTT/neurodevelopmental disorder-like symptoms (Tsujimura et al., 2015), supporting the hypothesis of dosage dependency of MECP2-related miR-199 expression with respect to normal brain development. However, the same study claims small decreases in one of the miR-199 members in mouse E17 or P0 brain-derived hippocampal cultures, and provides *in vitro* evidence for additional effectors downstream of miR-199. Our results show that mouse miR-199 and miR-214 are developmentally restricted to early prenatal brain development (E12-E14), and thus we believe that any potential brain region-specific miR-199 changes at later mouse developmental stages will not have a significant physiological effect. However, more studies in mouse RTT models are needed to determine the role of miR-199 and miR-214 on the observed behavioral disease-related phenotypes.

Given the plethora of neuropsychiatric diseases with potential links to MECP2, our findings of aberrant prenatal neuronal differentiation via alterations in prenatal brain-enriched miRNAs such as miR-199 and miR-214 could have implications for additional neurodevelopmental disorders other than RTT, particularly following the growing reports of genetic linkage of ASDs and schizophrenia with additional molecules involved in prenatal neurogenesis (Gulsuner et al., 2013; Casanova and Casanova, 2014). It is tempting to speculate that early disruptions in brain development could

result in increased susceptibility to subtle postnatal deleterious effects on brain maturation and plasticity, thus contributing to the full pathogenesis of neurodevelopmental disorders.

Methods

Neural Differentiation of iPSC Clones

Neural differentiation was performed as described previously (**Chapter 2**). Briefly, for the first set of RTT patient and control (RTT-MT1 and WT1), neural differentiation was accomplished via magnetic activated cell sorting (MACS) of dissociated EBs, followed by fluorescence activated cell sorting (FACS) to enrich an NP population. For RTT patient 2 and WT2 samples (RTT-MT2, RTT-WT2, and WT2), iPSCs were differentiated into NPs and then neurons as previously described via dual SMAD inhibition (Shi et al., 2012).

Branching Analysis

shRNA Control and shRNA MeCP2 NPCs were differentiated for 19 days. A small portion (~10%) of cells were infected with a lentiviral GFP construct to allow for sparse labeling and detection of neurites. Neurons were fixed after 19 days in 4% PFA for 30 minutes at 4°C. Cells were subsequently stained with Rb anti-MECP2 (Cell Signaling 3456S) to confirm positive or negative MECP2 expression in shRNA Control and shRNA MECP2 cells, respectively. Branching was traced semi-automatically and quantified in ImageJ using the NeuronJ plug-in described by (Meijering et al., 2004).

RNA extraction and quantification

RNA extraction was performed using the miRNeasy Mini Kit (Qiagen). cDNA synthesis for large RNAs was done using SuperScript VILO cDNA Synthesis Kit (Invitrogen) and used as PCR template to examine both allele-specific transcription mRNA and pri-miRNA expression. Mature miRNA reverse transcription and miRNA and mRNA qRT-PCR were done as shown before through the use of Taqman miRNA assays (Mellios et al., 2011).

For genotyping, RNA was extracted with miRNeasy Mini Kit (Qiagen). cDNA was used as PCR template to examine the allele-specific transcription of *MECP2*. PCR products were purified and sequenced by Genewiz, Inc.

Primers for PCR and sequencing:

For GM11273, R106W: forward GCAGGCAAAGCAGAGACATC; reverse CTTTGGGAGATTTGGGCTTC

For GM07982, V247X: forward GTGTGCAGGTGAAAAGGGTC; reverse GCTGCTCTCCTTGCTTTTCC

For NanoString miRNA profiling, miRNAs were processed with the NanoString nCounter system (NanoString, Seattle, Washington, USA) per vendor instructions. Data archiving, normalization, analysis and file export were performed using nSolver software. Probe intensity data between samples was normalized using nSolver

Software (Nanostring) utilizing the geometric means of the top 300 most highly expressed miRNAs. P-values were determined using Microsoft Excel using the installed T-Test macro between n=3 replicates of data. The Benjamini-Hochberg multiple testing correction was used for q-value calculations with False Discovery Rate (FDR) < 0.05.

miRNA measurements performed in mice employed male *Mecp2*$^{-/y}$ mice, female *Mecp2*$^{-/+}$ mice, and WT littermates. Embryos and neonates were obtained by breeding heterozygous females of C57BL/6 background (Guy et al., 2001) with WT C57BL/6 male mice.

Protein detection and BrdU labeling

Samples for protein isolation were homogenized and dissociated in RIPA buffer (Sigma) with protease and phosphatase inhibitors (Roche). Western blotting was performed as previously described (Mellios et al., 2014) using 7.5 μg total protein per well; bands were visualized using Kodak Biomax MR Film and ImageJ were used for analysis. The following primary antibodies were used: MeCP2 (1:1000, Cell Signaling), pERK1/2, tERK1/2, pAKT, tAKT, PAK4, PTEN (all 1:1000, Cell Signaling) and β-actin (1:120,000, Sigma Aldrich).

For BrdU pulse labelling, BrdU (final concentration = 10μM) was added to the culture media and treated for 3 hours. Cells were fixed with 4% PFA for 30 mins at 4°C. Prior to standard immunostaining, cells were treated with HCl (1N) for 30 mins at 45°C.

For immunocytochemistry, all cells were fixed for 20 mins with 4% PFA and permeabilized with 0.1% triton X100 (Sigma) for 10 mins. Primary antibodies were incubated in PBS with 1% BSA at 4°C overnight: human anti-PAX6 (1:100 Developmental Studies Hybridoma Bank), anti-Nestin (1:600 Millipore), anti-Musashi (1:600 Millipore), anti-SOX1 (1:100 Novus), anti-Tuj1 (1:500 Millipore), anti-MAP2 (1:1500, Encor Biotechnology), anti-GFAP (1:1000 Sigma), anti-TBR1 (1:200, Abcam), anti-MECP2 (1:200, Cell Signaling), mouse anti-TBR1 (1:200, Abcam), anti-CTIP2 (1:200, Abcam), anti-PAX6 (1:600 Millipore), as well as anti-GFP (1:500, life technologies). Alexa Fluor secondary antibodies were used at 1:500 (Life Technologies) for 1 hour at room temperature. Covesrlips were affixed with ProLong Gold antifade reagent with DAPI (Life Technology) and imaged with a Zeiss Axiovert microscope equipped with a Zeiss Axiocam digital camera.

In utero electroporation

In utero electroporation was performed as described previously (Ip et al., 2011). Briefly, the uteri of E13 pregnant mice anaesthetized with pentobarbital were exposed and placed on humidified gauze pads. Plasmids mixed with 0.05% Fast Green (Sigma) were injected into the lateral ventricle of the recipient embryos. Indicated plasmids were mixed at the following concentrations: shRNA plasmids, 1μg/μl; pCAG-Venus

plasmid, 0.5μg/μl. Immediately after DNA injection, four 50-ms electrical pulses (30V) were applied at 1-s intervals using a 5-mm electrode and an electroporator (EM830, BTX) to electroporate plasmids into the lateral cortex. The uterine horns were returned to the abdominal cavity, and the abdomen wall and skin were quickly sutured. All surgical procedures were completed within 45 min, after which the mice recovered under a heating lamp until waking up. Mice were housed in a vivarium (one pregnant mouse per cage) with a 12/12-h light/dark cycle.

Nucleofection

shControl and shMeCP2 NPs were plated (D0) in 6-well plates (Corning) at $4x10^5$ per laminin (1 mg/mL; Sigma Aldrich)-coated well in DMEM (Life Technologies) / Ham's F-12 (Cellgro) media supplemented with B27 (Life Technologies), basic Fibroblast Growth Factor (20 ng/mL; Peprotech), Epidermal Growth Factor (20 ng/mL; Sigma Aldrich), Heparin (5 μg/mL; Sigma Aldrich), and puromycin (0.8 μg/mL; Sigma Aldrich) to select for cells stably expressing either the shRNA or control construct. Nucleofection was performed according to the manufacturer's instructions using the Lonza Human Stem Cell Nucleofector Kit 2 when cells reached confluence (approximately $1x10^6$ cells per well; D2). Plasmids (anti-miR-199, anti-miR-214, and anti-control miArrest™ miRNA Inhibitors) were obtained from Genecopoeia; 5 μg DNA was used per reaction. All plasmids co-expressed mCherry as well for to control for transfection efficiency. Cells were immediately re-plated and supplemented with Rho-associated protein kinase (ROCK) inhibitor (10 μM; Tocris) to enhance survival post-nucleofection. A half change of media was performed the following day. NPs were checked for fluorescence,

indicating successful expression of the construct, and harvested for analysis at D4 (NPs) or at D21 (neurons).

Developmental miRNA expression in human postmortem brains

Expression profiles of miRNAs of interest across human brain development were created using publically available data from the 'Brainspan Atlas of the Developing Brain' (http://www.brainspan.org/). Briefly, previously published raw data (Ziats and Rennert, 2014) was downloaded and miRNAs of interest to this study were extracted. Average RPKM values for each developmental period assessed were plotted with their standard deviations. Results from six different brain regions were available and are displayed on separate graphs: DFC = Dorsolateral prefrontal cortex; VFC = ventrolateral prefrontal cortex; HIP = hippocampus. For each brain region studied, expression values were grouped into four developmental stages as used previously (Ziats and Rennert, 2014): Infancy = less than 1 year old (yo); Early Childhood = 1yo-4yo; Late Childhood = 8yo - 13yo; Adolescence/ young adulthood = 15yo - 23yo. Plotted values represent the average +/- standard deviation Reads Per Kilobase Million (RPKM) for each miRNA, which is a normalized measure of expression from RNA-seq data, and is further described on the Brainspan website.

Supplementary Tables

miRNA	Fold change NP1	q-value NP1	Fold change NP2	q-value NP2	Fold change Neuron1	q-value Neuron1	Fold change Neuron2	q-value Neuron2	Rank high to low
hsa-miR-9-5p	1.6421	0.14067	0.4071	0.02507	0.9807	0.90010	0.4709	0.00417	1
hsa-miR-19b-3p	0.6776	0.40972	1.4745	0.02929	0.3710	0.01642	1.6036	0.06918	2
hsa-miR-125b-5p	1.3329	0.46873	0.4417	0.00302	2.4757	0.02985	0.5646	0.01551	3
hsa-miR-20a-5p+hsa-miR-20b-5p	0.4973	0.03314	1.5550	0.13821	0.2514	0.00887	1.8095	0.03024	4
hsa-miR-16-5p	0.6938	0.38422	0.7408	0.22632	0.3486	0.01856	1.1740	0.31016	5
hsa-miR-135a-5p	1.0503	0.84839	0.4927	0.01249	2.1698	0.00618	0.4931	0.02789	6
hsa-miR-130a-3p	1.5047	0.37815	0.9975	0.95357	0.7132	0.08169	0.9666	0.84772	7
hsa-miR-99a-5p	1.2064	0.29431	0.3682	0.02164	0.7932	0.21055	0.4872	0.00691	8
hsa-miR-93-5p	0.9029	0.78709	0.9956	0.96527	0.6375	0.01393	1.0203	0.87954	9
hsa-miR-15b-5p	1.3856	0.58778	0.8514	0.27043	1.3177	0.07064	0.9046	0.34978	10
hsa-miR-363-3p	0.4755	0.18413	2.0314	0.00573	0.1155	0.00877	3.2606	0.00643	11
hsa-miR-27b-3p	1.9252	0.22230	0.8276	0.12973	1.4956	0.05570	1.1019	0.55164	12
hsa-miR-26a-5p	1.5604	0.10895	0.7679	0.35456	1.4215	0.08842	1.1889	0.49858	13
hsa-miR-25-3p	0.9758	0.95105	0.9603	0.66218	0.8420	0.07326	0.8823	0.27269	14
hsa-miR-92a-3p	0.2814	0.10895	1.3614	0.37057	0.1453	0.00887	1.7747	0.02548	15
hsa-miR-181a-5p	1.3520	0.19924	0.6549	0.05736	1.4398	0.07934	0.4158	0.01162	16
hsa-miR-125a-5p	1.2849	0.37275	0.6543	0.03605	1.1206	0.42379	0.5784	0.01551	17
hsa-miR-374a-5p	1.5567	0.19924	1.3033	0.14151	0.9867	0.90737	1.4010	0.06918	18
hsa-miR-106a-5p+hsa-miR-17-5p	0.7355	0.31568	1.2296	0.55506	0.3572	0.00780	1.6710	0.03379	19
hsa-miR-340-5p	0.7439	0.11128	0.5977	0.07581	0.4733	0.03414	0.7093	0.02541	20
hsa-miR-106b-5p	1.4328	0.47055	0.9395	0.68181	1.5635	0.01642	1.1060	0.32363	21
hsa-miR-301a-3p	0.6338	0.12049	0.8804	0.18329	0.4419	0.01573	0.7478	0.06865	22
hsa-miR-135b-5p	4.2617	0.03514	1.0405	0.75853	20.2605	0.00399	0.9236	0.51603	23
hsa-miR-15a-5p	0.4801	0.34253	0.6804	0.13821	0.3460	0.00586	0.7469	0.03028	24
hsa-miR-99b-5p	1.4356	0.36466	0.7263	0.02127	0.9841	0.89898	0.6890	0.02789	25
hsa-miR-92b-3p	0.3686	0.03423	0.7246	0.18573	0.1718	0.00920	1.2867	0.32339	26
hsa-miR-19a-3p	0.7291	0.18413	1.0932	0.28646	0.3438	0.01626	1.3478	0.17551	27
hsa-miR-107	0.8852	0.68921	0.7165	0.03269	0.6219	0.00661	1.0087	0.95174	28
hsa-let-7a-5p	16.8546	0.01985	0.0333	0.03139	9.0745	0.00377	0.2268	0.00196	29
hsa-let-7c-5p	5.4634	0.02979	0.0501	0.00148	2.0222	0.00399	0.3424	0.00181	30
hsa-miR-221-3p	0.3193	0.03925	1.1595	0.24710	0.1066	0.00614	1.2828	0.22752	31
hsa-miR-18a-5p	0.7518	0.21735	1.0875	0.57123	0.1657	0.00399	1.3734	0.13304	32
hsa-miR-374b-5p	1.1583	0.46657	1.3203	0.04144	0.9141	0.57615	1.6256	0.07389	33
hsa-miR-21-5p	0.3051	0.29431	0.5957	0.05759	0.2428	0.01128	0.7444	0.02644	34
hsa-miR-130b-3p	0.6895	0.40972	1.2955	0.08547	0.3609	0.00586	1.3632	0.10713	35
hsa-miR-191-5p	1.0690	0.90472	0.8052	0.23761	2.0741	0.00399	0.7352	0.04353	36
hsa-miR-1260a	0.6882	0.37275	0.9751	0.81858	0.9498	0.75179	1.1864	0.50789	37
hsa-miR-218-5p	1.8234	0.18413	0.6167	0.05636	5.8744	0.00399	0.7199	0.06918	38

hsa-miR-30c-5p	1.0635	0.74172	0.9302	0.65036	0.4314	0.02736	1.1254	0.39559	39
hsa-miR-100-5p	1.1974	0.51323	0.5124	0.00506	0.8555	0.29822	0.9118	0.31244	40
hsa-miR-30b-5p	1.4061	0.20208	0.7429	0.25218	1.5402	0.07271	1.1466	0.59572	41
hsa-let-7i-5p	12.7691	0.01626	0.0406	0.00386	11.6006	0.00344	0.2720	0.00065	42
hsa-let-7e-5p	2.0510	0.22218	0.1919	0.00506	1.3451	0.02364	0.4889	0.00879	43
hsa-miR-32-5p	1.0095	0.98833	0.8704	0.23761	1.1305	0.03414	0.8790	0.28954	44
hsa-miR-148b-3p	0.7325	0.43619	0.9374	0.55547	1.1518	0.12046	0.7675	0.08780	45
hsa-miR-18b-5p	0.6222	0.41058	2.5959	0.03907	0.1188	0.00399	4.6923	0.01093	46
hsa-miR-361-5p	0.7520	0.22218	1.0644	0.24283	0.6982	0.14678	1.1970	0.28954	47
hsa-miR-335-5p	1.0565	0.89046	0.7360	0.21973	2.8399	0.00399	0.9439	0.56706	48
hsa-miR-34a-5p	0.2396	0.19281	1.6451	0.07581	0.1529	0.01145	1.3286	0.06891	49
hsa-miR-324-5p	0.9561	0.88879	0.7109	0.17387	0.7147	0.06456	0.9060	0.47208	50
hsa-miR-24-3p	0.3999	0.05144	1.0188	0.76772	0.2001	0.01660	1.1598	0.34318	51
hsa-miR-331-3p	0.6585	0.32665	0.7978	0.26848	0.4660	0.02641	0.9024	0.46300	52
hsa-miR-423-3p	0.8251	0.46226	0.8713	0.19737	0.4354	0.00887	1.0115	0.93439	53
hsa-miR-590-5p	3.1909	0.02031	0.9884	0.88332	2.6515	0.03198	1.0328	0.87954	54
hsa-miR-149-5p	2.0577	0.26628	0.9561	0.70925	3.7891	0.03652	0.8315	0.09726	55
hsa-miR-342-3p	1.0225	0.89413	0.7744	0.03907	2.2536	0.02725	0.6130	0.03917	56
hsa-miR-301b-3p	0.6986	0.47355	1.1340	0.44448	0.3519	0.00887	1.1226	0.60206	57
hsa-miR-132-3p	0.8172	0.18413	0.2973	0.02669	0.5772	0.01099	0.5863	0.00879	58
hsa-let-7g-5p	22.3817	0.00929	0.0254	0.02455	11.5901	0.00641	0.2635	0.00243	59
hsa-miR-23a-3p	1.4689	0.19924	0.8788	0.27043	1.3312	0.03472	0.6374	0.04185	60
hsa-miR-103a-3p	0.5536	0.27605	1.1385	0.25338	0.5394	0.02033	0.9176	0.67266	61
hsa-miR-219a-2-3p	0.6489	0.40627	13.6445	0.00386	0.2193	0.00649	18.0731	0.00181	62
hsa-miR-423-5p	1.1814	0.66652	0.7417	0.08547	1.2139	0.11237	0.7978	0.12921	63
hsa-miR-454-3p	0.8184	0.53981	0.8668	0.12973	0.4883	0.01839	0.8450	0.14458	64
hsa-miR-204-5p	0.4271	0.32589	0.2361	0.00579	3.6252	0.06168	0.5303	0.06918	65
hsa-miR-551b-3p	0.6284	0.40972	0.7431	0.09229	0.6888	0.02358	0.9923	0.96615	66
hsa-miR-128-3p	1.6171	0.23932	0.6873	0.37057	2.7920	0.00586	1.1723	0.19189	67
hsa-miR-219a-5p	1.3362	0.30496	1.1678	0.05736	0.6903	0.07326	2.8662	0.00879	68
hsa-miR-23b-3p	0.7675	0.29431	0.8568	0.08547	1.0221	0.89898	0.8054	0.17700	69
hsa-miR-494-3p	2.4449	0.19270	1.0658	0.94787	1.2003	0.52950	1.9702	0.00691	70
hsa-miR-30a-5p	0.4034	0.25264	0.7701	0.05736	0.1763	0.00377	0.8439	0.24972	71
hsa-miR-598-3p	1.4619	0.20462	0.9067	0.49887	1.6595	0.00344	0.8475	0.21952	72
hsa-miR-216a-5p	7.7046	0.04120	0.8819	0.28646	6.6746	0.01128	0.6173	0.07938	73
hsa-miR-181b-5p+hsa-miR-181d-5p	1.0788	0.76760	0.6851	0.14151	0.7641	0.15885	0.5283	0.01551	74
hsa-miR-421	0.9287	0.76839	1.2339	0.17470	0.4900	0.00377	1.6007	0.01162	75
hsa-miR-151a-5p	1.8784	0.27605	0.8624	0.54793	3.0284	0.00586	0.9541	0.64448	76
hsa-miR-140-5p	1.1146	0.76839	0.8043	0.15687	0.8747	0.38322	0.7658	0.05346	77
hsa-miR-197-3p	1.2838	0.52492	0.6780	0.18329	1.0270	0.89898	0.8466	0.28954	78
hsa-miR-630	1.2616	0.21748	0.9931	0.94787	0.0955	0.00887	1.3394	0.33259	79

hsa-miR-1246	1.7391	0.05762	1.0567	0.88808	0.4582	0.00377	1.0134	0.93439	80
hsa-miR-708-5p	0.5196	0.32941	0.7669	0.14151	0.7476	0.06346	0.8996	0.60206	81
hsa-miR-151a-3p	1.3667	0.52889	0.9309	0.69345	1.2086	0.42893	0.9986	0.98692	82
hsa-miR-148a-3p	12.2372	0.02197	1.5780	0.02164	35.8258	0.00338	1.2263	0.25898	83
hsa-let-7d-5p	18.9066	0.01984	0.0346	0.00573	11.0221	0.00344	0.2293	0.00181	84
hsa-miR-222-3p	0.5469	0.18039	1.1923	0.01336	0.1275	0.01627	1.2329	0.27269	85
hsa-let-7b-5p	4.1561	0.01985	0.0957	0.01442	8.4288	0.01099	0.1069	0.00126	86
hsa-miR-29c-3p	0.7234	0.42506	1.0030	0.95779	1.1127	0.13787	1.1699	0.14956	87
hsa-miR-296-5p	2.1078	0.05762	1.1781	0.28738	2.5820	0.03061	1.2253	0.04660	88
hsa-miR-26b-5p	1.8929	0.05296	0.7706	0.27437	1.5476	0.02548	0.7616	0.04243	89
hsa-miR-544a	4.0600	0.02979	0.6681	0.35084	3.1459	0.01642	0.6315	0.19681	90
hsa-miR-30e-5p	2.1252	0.18039	0.8710	0.22314	1.3123	0.08610	0.8389	0.14490	91
hsa-miR-22-3p	2.2939	0.04120	1.1624	0.56306	3.8498	0.01465	1.1987	0.30959	92
hsa-miR-199a-3p+hsa-miR-199b-3p	5.8801	0.01555	4.9632	0.00573	120.1920	0.00377	8.2341	0.01152	93
hsa-miR-137	0.8419	0.76587	0.5361	0.02164	1.2394	0.18251	0.9189	0.56287	94
hsa-miR-30d-5p	1.5598	0.16938	0.9380	0.50268	1.2206	0.17264	0.7579	0.13304	95
hsa-miR-660-5p	0.7458	0.20524	1.4965	0.04421	0.5711	0.11799	0.8661	0.26851	96
hsa-miR-29a-3p	0.2099	0.00685	0.9736	0.91082	0.5080	0.03506	1.0544	0.74612	97
hsa-miR-455-3p	1.2282	0.58778	1.6087	0.01730	1.1168	0.25913	1.8258	0.00417	98
hsa-miR-484	3.0053	0.03715	0.7339	0.08547	1.2373	0.06201	1.4620	0.17828	99
hsa-miR-199b-5p	4.1758	0.03423	2.1834	0.04421	89.4105	0.00399	3.7474	0.00691	100
hsa-miR-345-5p	0.8772	0.61355	0.8397	0.50515	0.5650	0.01660	1.1024	0.59628	101
hsa-miR-124-3p	3.1597	0.02197	0.3993	0.01544	9.7027	0.00377	0.7793	0.14417	102
hsa-miR-425-5p	0.9101	0.84839	1.0695	0.60861	1.2693	0.02894	1.0055	0.97978	103
hsa-miR-485-3p	4.0036	0.00685	1.1557	0.49701	3.2933	0.00586	1.2250	0.04766	104
hsa-miR-1180-3p	0.4683	0.19924	0.7396	0.12973	0.8707	0.65755	0.6865	0.06702	105
hsa-miR-362-3p	0.8592	0.61355	1.5223	0.15687	0.6993	0.06965	0.8301	0.18176	106
hsa-miR-320c	0.6156	0.46873	0.8397	0.50268	0.3651	0.03414	1.4194	0.12226	107
hsa-let-7f-5p	4.4758	0.02197	0.0642	0.00386	5.8567	0.02065	0.3821	0.04191	108
hsa-miR-450a-5p	2.5660	0.01985	1.4171	0.03329	12.4522	0.00887	1.4848	0.01018	109
hsa-miR-217	15.2682	0.00685	0.8786	0.37481	2.3748	0.04533	0.5640	0.03807	110
hsa-miR-98-5p	6.3971	0.00685	0.0407	0.00597	10.4537	0.00586	0.2253	0.00127	111
hsa-miR-488-3p	2.6009	0.02084	0.6371	0.07581	3.7652	0.01128	0.5796	0.00643	112
hsa-miR-29b-3p	0.4550	0.29431	1.1964	0.50515	0.9054	0.73879	1.3926	0.00869	113
hsa-miR-186-5p	1.5477	0.40819	0.6978	0.27437	1.3111	0.05762	0.8775	0.47170	114
hsa-miR-365a-3p+hsa-miR-365b-3p	0.5398	0.34909	1.4071	0.27437	2.8120	0.01128	1.9204	0.00643	115
hsa-miR-592	0.8799	0.73770	0.3159	0.00002	2.1314	0.03996	0.5687	0.03148	116
hsa-miR-455-5p	1.7219	0.13463	1.2981	0.09473	2.2080	0.01523	1.5041	0.03069	117
hsa-miR-101-3p	1.9421	0.17919	1.1261	0.75864	2.8738	0.00399	0.9414	0.76496	118
hsa-miR-133a-3p	0.9164	0.84370	1.7847	0.00603	0.5392	0.02164	1.5133	0.01162	119
hsa-miR-125a-3p	2.4303	0.11128	0.9563	0.45960	1.5927	0.09060	0.9156	0.31883	120

hsa-miR-885-5p	1.2467	0.30826	0.2662	0.02127	2.4870	0.00377	0.3591	0.01228	121
hsa-miR-769-5p	0.9579	0.70736	0.7995	0.09816	0.8637	0.48863	0.7984	0.06264	122
hsa-miR-196a-5p	2.2590	0.16931	0.9690	0.84009	2.2584	0.09325	1.2904	0.25898	123
hsa-miR-95-3p	2.3717	0.11128	0.4460	0.01288	8.4534	0.00344	0.6397	0.09801	124
hsa-miR-192-5p	1.1963	0.38422	0.9279	0.60861	1.4247	0.46558	0.9073	0.65772	125
hsa-miR-532-5p	1.2498	0.38113	1.7446	0.00889	0.7201	0.17024	0.9558	0.62425	126
hsa-miR-181c-5p	1.3975	0.40627	0.6429	0.09473	3.2464	0.00399	0.4256	0.00758	127
hsa-miR-199a-5p	31.5711	0.01073	2.1888	0.04766	369.1766	0.00399	4.1072	0.00691	128
hsa-miR-504-5p	1.2907	0.40949	1.4078	0.00951	0.4520	0.04963	1.4207	0.01743	129
hsa-miR-7-5p	1.3051	0.18413	0.7625	0.21973	10.3902	0.03414	0.8145	0.12253	130
hsa-miR-28-5p	0.7828	0.40827	1.1995	0.24710	0.4994	0.00641	1.0666	0.60042	131
hsa-miR-579-5p	2.3303	0.24327	0.9123	0.70090	1.7203	0.18269	0.9268	0.46497	132
hsa-miR-210-3p	1.3269	0.46226	0.7800	0.18573	1.7791	0.08522	1.2487	0.05859	133
hsa-miR-424-5p	0.8991	0.82756	1.5501	0.09473	8.0705	0.02041	2.0247	0.00758	134
hsa-miR-27a-3p	1.1825	0.59331	1.0825	0.59067	0.6545	0.01660	1.0356	0.87500	135
hsa-miR-185-5p	0.9305	0.89046	1.0124	0.94216	0.8760	0.11139	1.0043	0.97714	136
hsa-miR-1297	0.4031	0.43712	0.8514	0.60652	0.5761	0.08293	0.9468	0.83083	137
hsa-miR-362-5p	0.9865	0.88245	1.8578	0.07048	0.5826	0.02176	0.8421	0.19681	138
hsa-miR-1469	0.9313	0.86853	0.9222	0.77655	0.3245	0.00629	1.0043	0.97991	139
hsa-miR-145-5p	1.5537	0.13463	3.2152	0.02044	9.4460	0.00344	5.3009	0.01972	140
hsa-miR-324-3p	0.9680	0.89637	0.6508	0.40756	0.5883	0.01642	0.8614	0.76132	141
hsa-miR-582-5p	2.0302	0.00929	0.3694	0.00579	1.1583	0.11801	0.8777	0.46413	142
hsa-miR-574-5p	0.5935	0.11128	1.1663	0.40481	0.4796	0.02072	1.0049	0.97714	143
hsa-miR-873-3p	0.5167	0.22907	1.1408	0.71508	1.5442	0.18477	1.0264	0.85145	144
hsa-miR-574-3p	0.8907	0.62394	1.4902	0.09816	1.4813	0.06070	1.0123	0.95553	145
hsa-miR-744-5p	1.5749	0.38113	1.0240	0.94769	0.8121	0.08114	0.9162	0.54877	146
hsa-miR-1283	0.0458	0.18039	1.3905	0.68181	1.8021	0.38970	1.7326	0.34318	147
hsa-miR-490-3p	18.4600	0.01626	0.9285	0.60861	16.4204	0.00661	0.9266	0.78869	148
hsa-miR-129-2-3p	1.2832	0.22218	0.2913	0.01288	0.8437	0.38970	1.1698	0.22464	149
hsa-miR-33a-5p	0.7610	0.38422	0.7102	0.11157	0.7284	0.54516	0.7616	0.17855	150
hsa-miR-122-5p	0.7062	0.10895	1.3157	0.28646	0.5516	0.01145	0.9596	0.90237	151
hsa-miR-664a-3p	0.5477	0.18412	0.9604	0.65556	0.4923	0.06346	0.7773	0.03379	152
hsa-miR-193b-3p	0.4538	0.06155	1.3323	0.00653	0.5623	0.01511	1.5326	0.07898	153
hsa-miR-126-3p	1.4897	0.36193	1.0707	0.76423	1.5305	0.15231	0.7588	0.03028	154
hsa-miR-219a-1-3p	0.3138	0.10307	0.6745	0.23761	0.1472	0.00586	1.5625	0.07031	155
hsa-miR-505-3p	0.6505	0.42949	0.7938	0.12973	2.5660	0.00887	0.8772	0.13942	156
hsa-miR-378i	0.7713	0.19924	0.9196	0.62188	1.0826	0.62878	0.8364	0.10713	157
hsa-miR-532-3p	1.1129	0.52828	1.0262	0.91712	0.6767	0.06456	1.1513	0.08423	158
hsa-miR-200a-3p	0.5730	0.46226	1.0116	0.95045	0.8081	0.52015	0.9502	0.71284	159
hsa-miR-500a-5p+hsa-miR-501-5p	0.8760	0.54103	1.4228	0.02669	0.7027	0.07290	0.8709	0.02383	160
hsa-miR-548a-5p	1.8864	0.10507	1.1320	0.60861	3.2194	0.04942	0.9785	0.93439	161

hsa-miR-561-5p	1.1730	0.44759	0.8795	0.37057	0.6344	0.01622	1.0626	0.74145	162
hsa-miR-96-5p	1.1416	0.52828	1.5404	0.05636	1.7086	0.06795	0.9836	0.95174	163
hsa-miR-28-3p	0.7018	0.38113	1.0205	0.81724	0.3580	0.02000	1.3032	0.01580	164
hsa-miR-548i	1.7763	0.08373	1.1323	0.68999	1.3554	0.05011	0.9401	0.72817	165
hsa-miR-152-3p	1.2491	0.59756	1.1129	0.35914	2.0813	0.01642	0.8786	0.26278	166
hsa-miR-509-3p	9.5756	0.02405	1.1002	0.76765	23.0318	0.00684	1.3895	0.13897	167
hsa-miR-320a	1.4172	0.25264	0.7959	0.29865	0.9360	0.72718	0.8540	0.47208	168
hsa-miR-302d-3p	0.1247	0.10895	2.4263	0.00606	0.1464	0.00586	1.5068	0.13897	169
hsa-miR-1298-5p	1.3211	0.29431	0.7724	0.05736	2.2708	0.13672	0.1113	0.01190	170
hsa-miR-518f-3p	2.0822	0.19924	0.8761	0.50268	1.5537	0.01993	0.7376	0.11465	171
hsa-miR-146a-5p	1.6291	0.36423	0.8825	0.45913	0.9903	0.90737	0.8121	0.06801	172
hsa-miR-520d-5p+hsa-miR-527+hsa-miR-518a-5p	1.2925	0.43619	0.8845	0.75415	1.2209	0.47088	1.4837	0.04243	173
hsa-miR-302a-3p	0.2064	0.02221	6.4666	0.00559	0.2470	0.01627	2.0360	0.01152	174
hsa-miR-1290	2.6469	0.00685	0.8763	0.68999	0.2521	0.01512	1.2443	0.26326	175
hsa-miR-382-5p	1.6990	0.36466	1.8658	0.09910	3.7048	0.02041	1.3630	0.14458	176
hsa-miR-155-5p	1.3552	0.38422	1.0536	0.82107	0.9284	0.79461	1.1938	0.07518	177
hsa-miR-302e	0.8488	0.40972	0.7991	0.07581	0.5647	0.06346	0.9359	0.56287	178
hsa-miR-548b-3p	0.8175	0.72137	0.9126	0.60861	0.9582	0.76185	0.8804	0.43113	179
hsa-miR-1908-5p	0.4637	0.11128	0.9581	0.75770	0.4245	0.10096	0.6420	0.01162	180
hsa-miR-766-3p	0.9750	0.94445	0.9620	0.81858	1.2364	0.11139	1.0796	0.12598	181
hsa-miR-548h-5p	1.3439	0.29146	0.8103	0.40549	0.2084	0.06978	0.4465	0.02494	182
hsa-miR-302b-3p	0.1493	0.02221	5.7054	0.00573	0.2041	0.00490	2.1873	0.06862	183
hsa-miR-551a	0.9415	0.78709	1.2686	0.45142	0.6727	0.40148	1.1831	0.50149	184
hsa-miR-376a-3p	0.9649	0.85280	2.6704	0.01249	0.6809	0.01573	1.9166	0.01551	185
hsa-miR-129-5p	0.7334	0.40819	0.3416	0.00579	4.2912	0.00377	0.8572	0.38775	186
hsa-miR-34b-3p	1.2280	0.46226	1.0763	0.81858	0.8224	0.13961	0.8973	0.38775	187
hsa-miR-652-3p	0.7058	0.37438	0.7602	0.15687	0.6469	0.07474	1.0791	0.50149	188
hsa-miR-508-5p	0.7853	0.35156	1.2763	0.18329	0.2669	0.00377	1.1218	0.67266	189
hsa-miR-449a	1.1183	0.69191	2.4358	0.02164	1.3036	0.54282	1.1429	0.04243	190
hsa-miR-495-3p	1.1226	0.73770	2.2317	0.06848	1.0744	0.48916	2.0220	0.00691	191
hsa-miR-328-3p	0.8000	0.36193	0.8979	0.55709	1.0871	0.20894	0.8408	0.26851	192
hsa-miR-10a-5p	1.3123	0.37275	0.9986	0.98875	2.2601	0.04034	1.3371	0.07255	193
hsa-miR-190b	0.8428	0.73445	0.7885	0.55941	1.2138	0.49299	0.9421	0.81680	194
hsa-miR-1271-5p	1.6816	0.18413	0.7246	0.24710	1.3057	0.33304	0.7952	0.46497	195
hsa-miR-503-5p	1.2084	0.69772	1.2539	0.05759	2.3875	0.03414	1.5510	0.01018	196
hsa-miR-629-5p	0.8947	0.46226	0.7282	0.10327	0.6065	0.02108	0.9403	0.23458	197
hsa-miR-493-3p	1.1353	0.44759	0.9904	0.94787	0.6903	0.19834	1.0263	0.91883	198
hsa-miR-194-5p	1.6359	0.18039	0.8029	0.27437	2.0943	0.05834	0.6083	0.04123	199
hsa-miR-361-3p	1.0613	0.68072	0.8144	0.08140	1.5183	0.02769	0.9918	0.91421	200
hsa-miR-188-5p	1.2629	0.36398	0.7474	0.06848	0.6009	0.06189	0.9354	0.32029	201
hsa-miR-651-5p	0.4946	0.18413	1.1768	0.22314	0.5729	0.02641	1.2624	0.06651	202

hsa-miR-542-3p	0.7692	0.29175	1.6381	0.15026	1.1718	0.14295	3.6117	0.02494	203
hsa-miR-1973	0.5243	0.00685	1.1862	0.52857	0.5092	0.00586	1.2570	0.30959	204
hsa-miR-526a+hsa-miR-518c-5p+hsa-miR-518d-5p	0.8917	0.38422	1.3327	0.37705	0.9138	0.13511	0.8230	0.26851	205
hsa-miR-2117	0.8401	0.48666	1.0967	0.68999	0.6355	0.06304	1.1410	0.53937	206
hsa-miR-105-5p	0.9930	0.98833	0.9745	0.92940	3.3003	0.01660	0.9199	0.77348	207
hsa-miR-302c-3p	0.3974	0.08991	2.1672	0.05736	0.3139	0.00734	1.7071	0.01205	208
hsa-miR-891a-5p	1.2581	0.40562	1.4258	0.17601	1.3503	0.14004	1.2738	0.26489	209
hsa-miR-1247-5p	0.1160	0.18413	2.6119	0.12973	0.3938	0.06346	5.6812	0.00243	210
hsa-miR-214-3p	7.6219	0.02031	1.3497	0.18329	41.2357	0.00399	1.7899	0.06891	211
hsa-miR-516a-3p+hsa-miR-516b-3p	1.2799	0.44100	0.9628	0.87519	1.2598	0.23347	1.0616	0.72817	212
hsa-miR-542-5p	1.5518	0.16464	0.8484	0.68181	1.5176	0.03996	0.9032	0.30959	213
hsa-miR-200c-3p	0.6551	0.23223	1.3618	0.18329	0.9956	0.99360	0.8072	0.14956	214
hsa-miR-577	0.9316	0.87838	0.9532	0.50969	0.8891	0.67262	0.8651	0.10530	215
hsa-miR-1307-3p	1.5243	0.06459	1.0664	0.75061	1.0775	0.87952	0.8457	0.27269	216
hsa-miR-1226-3p	0.6720	0.29431	0.8570	0.57625	0.8111	0.34357	0.7994	0.30959	217
hsa-miR-339-3p	0.6655	0.18413	1.2540	0.32023	0.5533	0.02728	0.9951	0.97383	218
hsa-miR-1206	1.3352	0.37227	1.4000	0.18329	1.4581	0.06875	0.8962	0.53175	219
hsa-miR-1200	1.2991	0.29431	1.0778	0.52857	0.8188	0.34935	1.1449	0.72971	220
hsa-miR-34c-5p	0.8038	0.58216	0.8845	0.44448	0.7973	0.14295	1.1963	0.48189	221
hsa-miR-140-3p	0.6238	0.29571	1.2330	0.00653	0.5955	0.11198	0.8986	0.25892	222
hsa-miR-769-3p	0.9244	0.84839	1.0512	0.80628	0.3972	0.04053	0.9389	0.57330	223
hsa-miR-597-5p	0.9325	0.81845	1.0362	0.89154	0.7646	0.17264	0.7951	0.18259	224
hsa-miR-143-3p	4.8759	0.01152	46.1579	0.13821	23.3776	0.00377	55.2295	0.00065	225
hsa-miR-539-5p	1.3316	0.43619	0.9017	0.75864	1.0529	0.85938	1.3171	0.39044	226
hsa-miR-183-5p	1.1522	0.84370	1.8706	0.17387	1.4959	0.09001	1.2404	0.21208	227
hsa-miR-1287-3p	1.3373	0.29146	0.9401	0.76423	1.2081	0.14088	1.1602	0.23458	228
hsa-miR-767-5p	0.8116	0.27544	0.9637	0.49745	2.6812	0.03652	0.9522	0.81439	229
hsa-miR-563	7.8157	0.00881	1.1808	0.47564	1.6309	0.08660	1.0661	0.65772	230
hsa-miR-1305	0.7257	0.22230	1.2490	0.15061	0.2774	0.00641	0.9536	0.75908	231
hsa-miR-138-5p	1.2841	0.44759	0.9190	0.25927	2.1919	0.00661	0.8773	0.14490	232
hsa-miR-376c-3p	1.0748	0.79861	2.2178	0.04149	0.6275	0.04155	1.3606	0.01376	233
hsa-miR-450b-5p	0.9129	0.69169	1.0188	0.91712	1.2112	0.35594	1.3006	0.32339	234
hsa-miR-655-3p	0.7822	0.18413	0.7963	0.26961	1.2947	0.23321	0.5804	0.06794	235
hsa-miR-1261	1.3314	0.59512	0.9926	0.97539	1.3120	0.09505	1.0240	0.91421	236
hsa-miR-208b-3p	0.5154	0.11128	1.0754	0.80180	1.9054	0.09576	0.7334	0.06862	237
hsa-miR-142-3p	0.8587	0.69035	1.2126	0.24710	1.4035	0.11801	0.7518	0.09382	238
hsa-miR-891b	0.6807	0.14290	1.0862	0.68999	2.0525	0.13787	1.2298	0.10530	239
hsa-miR-1-3p	1.1309	0.62394	1.9120	0.08547	3.9292	0.01145	2.7383	0.01743	240
hsa-miR-337-5p	1.2199	0.40819	1.1293	0.68999	0.9378	0.87264	0.8618	0.43447	241
hsa-miR-545-3p	1.4528	0.14649	1.2731	0.21125	1.8374	0.06065	1.1658	0.40384	242
hsa-miR-590-3p	0.8927	0.63968	1.0509	0.87519	0.7134	0.04963	0.9388	0.52649	243

hsa-miR-758-3p+hsa-miR-411-3p	2.8861	0.00886	1.0382	0.76765	4.1935	0.04431	1.0765	0.76496	244
hsa-miR-196b-5p	1.1420	0.59331	1.0312	0.81858	0.6621	0.14193	0.6379	0.27269	245
hsa-miR-1268a	0.8456	0.57744	0.9345	0.43820	0.6550	0.17327	1.0803	0.72381	246
hsa-miR-136-5p	0.6580	0.18413	1.4193	0.07643	0.8517	0.47363	1.0570	0.47208	247
hsa-miR-656-3p	1.1413	0.76760	1.2506	0.39026	1.0583	0.88200	1.1395	0.22752	248
hsa-miR-491-5p	2.3026	0.19924	0.9050	0.68999	1.8763	0.01520	0.7598	0.26253	249
hsa-miR-548a-3p	0.8817	0.41382	0.8163	0.52204	1.0626	0.62503	1.0422	0.87954	250
hsa-miR-626	1.4113	0.59531	0.8818	0.63029	2.1772	0.03802	0.9106	0.73998	251
hsa-miR-195-5p	1.4573	0.29146	1.0257	0.81724	1.3406	0.22001	1.2866	0.25898	252
hsa-miR-1915-3p	1.4048	0.29146	0.6031	0.15393	1.0851	0.53748	0.7918	0.19681	253
hsa-miR-628-5p	0.5656	0.20025	0.8778	0.43834	1.1125	0.52015	0.8114	0.06891	254
hsa-miR-600	0.6557	0.07199	0.8691	0.26444	0.5562	0.06456	0.8570	0.59288	255
hsa-miR-515-3p	1.6509	0.19924	1.3036	0.09750	1.1291	0.72715	1.0117	0.96537	256
hsa-miR-302f	0.8704	0.47276	1.2405	0.21973	1.0305	0.90737	1.0062	0.95553	257
hsa-miR-526b-5p	1.2618	0.14649	1.2310	0.15687	1.2988	0.37418	1.0459	0.86029	258
hsa-miR-379-5p	0.9953	0.98193	1.3129	0.32774	1.0030	0.99635	1.1107	0.45390	259
hsa-miR-190a-5p	0.5939	0.20524	1.0538	0.76040	0.4701	0.09416	1.0952	0.64448	260
hsa-miR-517c-3p+hsa-miR-519a-3p	1.3193	0.70321	1.0186	0.84902	1.1111	0.19655	1.0706	0.74291	261
hsa-miR-627-3p	1.0405	0.84929	1.1134	0.75864	1.1785	0.58358	0.7633	0.15333	262
hsa-miR-625-5p	1.0662	0.89575	0.7848	0.29865	0.6375	0.23572	0.8295	0.14417	263
hsa-miR-490-5p	1.7808	0.11316	1.5548	0.28738	2.6147	0.00399	0.9280	0.76132	264
hsa-miR-154-5p	0.4785	0.29431	0.6809	0.37057	0.6709	0.20639	0.7589	0.23044	265
hsa-miR-876-3p	0.5241	0.19924	0.7664	0.32680	1.9403	0.08169	0.9746	0.88942	266
hsa-miR-34c-3p	0.8064	0.62394	1.0447	0.52517	0.8458	0.29822	0.9910	0.96537	267
hsa-miR-153-3p	0.7865	0.68072	0.8307	0.57065	1.3449	0.20991	0.7399	0.42396	268
hsa-miR-337-3p	1.3653	0.20025	1.2794	0.37057	1.0961	0.59653	1.1935	0.38775	269
hsa-miR-299-3p	0.8786	0.38422	1.1055	0.37705	0.9582	0.75774	1.4921	0.17551	270
hsa-miR-571	0.7135	0.24702	0.8016	0.50515	0.3928	0.08169	0.7399	0.18990	271
hsa-miR-10b-5p	2.1879	0.00715	1.1829	0.35354	0.8599	0.65394	1.0475	0.67156	272
hsa-miR-1537-3p	5.5044	0.29146	1.2663	0.55709	1.3881	0.55723	0.7660	0.12767	273
hsa-miR-548g-3p	1.3610	0.20025	1.3954	0.05759	0.9862	0.97550	1.2941	0.17006	274
hsa-miR-593-3p	0.6264	0.10507	0.9009	0.67860	0.7210	0.39644	1.3563	0.02541	275
hsa-miR-377-3p	0.9690	0.89575	1.4989	0.22304	0.7168	0.11839	1.2878	0.18176	276
hsa-miR-372-3p	1.2314	0.69191	1.4001	0.02693	0.9994	0.99743	0.8160	0.27269	277
hsa-miR-501-3p	1.1329	0.54103	0.8182	0.50268	0.9151	0.37533	1.0259	0.72817	278
hsa-miR-208a-3p	0.8957	0.54310	1.0547	0.88984	0.6885	0.30259	1.0317	0.93322	279
hsa-miR-584-5p	0.6697	0.27544	0.9485	0.73860	1.0383	0.91302	1.1781	0.20893	280
hsa-miR-591	0.6923	0.43619	1.0754	0.81724	0.7435	0.31030	0.9069	0.43113	281
hsa-miR-520e	1.5832	0.29146	0.7777	0.35694	1.5750	0.07271	0.7169	0.19681	282
hsa-miR-369-3p	1.4563	0.29431	1.3818	0.37057	1.5414	0.14402	0.7895	0.14417	283
hsa-miR-1205	0.6212	0.18413	0.9032	0.44448	0.4578	0.10682	0.8697	0.54900	284

hsa-miR-761	0.8597	0.61355	1.4229	0.22304	0.7146	0.19108	0.7891	0.06794	285
hsa-miR-339-5p	0.7910	0.56866	1.0428	0.86745	0.4275	0.00887	0.9660	0.86029	286
hsa-miR-514a-3p	0.8791	0.47085	1.4699	0.29960	1.0590	0.81296	0.8790	0.53674	287
hsa-miR-146b-5p	0.6852	0.36466	0.8207	0.40549	1.1454	0.58707	1.3400	0.15905	288
hsa-miR-641	0.7872	0.36218	1.1182	0.43834	0.8131	0.49269	0.7814	0.19586	289
hsa-miR-770-5p	1.0032	0.98999	0.9037	0.45899	1.3714	0.14034	0.7749	0.29625	290
hsa-miR-640	0.2089	0.02403	0.7509	0.28173	0.2655	0.01239	0.9247	0.45520	291
hsa-miR-142-5p	1.3956	0.14649	0.8100	0.60861	1.2652	0.05762	1.1397	0.76132	292
hsa-miR-520c-3p	1.6753	0.21647	1.0897	0.62188	0.5680	0.07459	0.8207	0.43113	293
hsa-miR-215-5p	1.1829	0.84839	1.1054	0.36869	1.5829	0.06283	0.9426	0.80103	294
hsa-miR-33b-5p	0.8980	0.87838	1.2331	0.40549	0.5214	0.06304	0.8453	0.40612	295
hsa-miR-330-5p	1.2212	0.15384	0.9726	0.92940	0.7837	0.25880	0.9357	0.67266	296
hsa-miR-499a-5p	1.1502	0.51070	1.1547	0.59879	1.6503	0.02032	0.8558	0.31055	297
hsa-miR-572	1.1828	0.76587	1.0884	0.58429	1.9200	0.15927	1.0965	0.74552	298
hsa-miR-877-5p	1.0031	0.99403	0.9473	0.65556	0.9362	0.90737	1.1017	0.12102	299
hsa-miR-1203	0.9898	0.98203	1.4341	0.18303	0.9968	0.98472	0.8437	0.31016	300

Supplementary Table 1: Statistical analysis of Nanostring miRNA profiling.

Table showing fold changes and q-values (see: Methods) for the top 300 most highly expressed miRNAs in RTT-MT1 relative to WT1 NPs and immature neurons (three weeks *in vitro*) ("NP1" and "Neuron1") and RTT-MT2 relative to RTT-WT2 NPs and immature neurons (three weeks *in vitro*) ("NP2" and "Neuron2"). miRNAs are ranked from the highest to lowest in average expression with their rank shown in the table.

KEEG Pathway	Gene number	P-Value	Fisher Exact
Endocytosis	28	0.000005	0.000002
Regulation of actin cytoskeleton	28	0.000092	0.000037
Axon guidance	20	0.000130	0.000043
Wnt signaling pathway	19	0.002500	0.001000
MAPK signaling pathway	28	0.002800	0.001400
Calcium signaling pathway	19	0.012000	0.006100
Focal adhesion	20	0.022000	0.012000
Ubiquitin mediated proteolysis	15	0.026000	0.012000
Neurotrophin signaling pathway	14	0.026000	0.012000
mTOR signaling pathway	8	0.029000	0.009400
Hedgehog signaling pathway	8	0.041000	0.015000
TGF-beta signaling pathway	10	0.063000	0.028000
ErbB signaling pathway	10	0.063000	0.028000
Glioma	8	0.070000	0.028000
Adherens junction	9	0.075000	0.033000
Cell adhesion molecules (CAMs)	13	0.078000	0.041000
Insulin signaling pathway	13	0.089000	0.048000
Glycerophospholipid metabolism	8	0.096000	0.042000
Long-term potentiation	8	0.096000	0.042000

Supplementary Table 2: Pathway analysis of predicted targets of miR-199 and miR-214.

In silico analysis of the predicted targets of significantly altered miR-199 and miR-214 miRNAs using Targetscan were subjected to KEEG pathway analysis on DAVID bioinformatics database. Only brain-related pathways are shown. Number of genes predicted to be targeted by either miR-199 or miR-214, p-values, and Fisher exact test calculations are shown.

Acknowledgements:

We would like to thank Ting Fu, Tatiana Karadimitriou, Chuong Le, Anita Liu, Jonathan Woodson, Arooshi Kumar, and Brian Rodriguez for excellent technical support as well as members of the Jaenisch, Haggarty, and Sur laboratories for helpful discussion. This work was supported by NIH grant MH085802 (MS), 2R01MH104610-15 (RJ), and the Simons Foundation Autism Research Initiative (MS, RJ), NIH/NIMH R01MH095088 (SJH), Pitt-Hopkins Research Foundation (SJH), FRAXA Research Foundation (SJH).

Adapted from Mellios et al. -- July 2016 Submitted to Molecular Psychiatry

Contributions

Tissue culture was performed by Danielle Feldman, Showming Kwok, Ph.D., Steven Sheridan, Ph.D., and technical assistant Bess Rosen. miRNA screening and analysis was performed by Steven Sheridan, Ph.D. and Nikolaos Mellios, Ph.D. PCR experiments were performed by Nikolaos Mellios, Ph.D. Immunocytochemistry and morphological analyses were performed by Danielle Feldman. Proliferation assay and associated analyses were performed by Danielle Feldman and Jacque Ip. Mouse experiments were performed by Jacque Ip. Western blotting was performed by technical assistant Bess Rosen.

References

Akbarian S, Chen RZ, Gribnau J, Rasmussen TP, Fong H, Jaenisch R, Jones EG (2001) Expression pattern of the Rett syndrome gene MeCP2 in primate prefrontal cortex. Neurobiol Dis 8:784–791.

Amir RE, Van den Veyver IB, Wan M, Tran CQ, Francke U, Zoghbi HY (1999) Rett syndrome is caused by mutations in X-linked MECP2, encoding methyl-CpG-binding protein 2. Nat Genet 23:185–188.

Andoh-Noda T, Akamatsu W, Miyake K, Matsumoto T, Yamaguchi R, Sanosaka T, Okada Y, Kobayashi T, Ohyama M, Nakashima K, Kurosawa H, Kubota T, Okano H (2015) Differentiation of multipotent neural stem cells derived from Rett syndrome patients is biased toward the astrocytic lineage. Mol Brain 8:136.

Armstrong DD (1995) The neuropathology of Rett syndrome--overview 1994. Neuropediatrics 26:100–104.

Bauman ML, Kemper TL, Arin DM (1995) Microscopic observations of the brain in Rett syndrome. Neuropediatrics 26:105–108.

Bedogni F, Cobolli Gigli C, Pozzi D, Rossi RL, Scaramuzza L, Rossetti G, Pagani M, Kilstrup-Nielsen C, Matteoli M, Landsberger N (2015) Defects During Mecp2 Null Embryonic Cortex Development Precede the Onset of Overt Neurological Symptoms. Cereb Cortex.

Casanova EL, Casanova MF (2014) Genetics studies indicate that neural induction and early neuronal maturation are disturbed in autism. Front Cell Neurosci 8:827.

Castro J, Garcia RI, Kwok S, Banerjee A, Petravicz J, Woodson J, Mellios N, Tropea D, Sur M (2014) Functional recovery with recombinant human IGF1 treatment in a mouse model of Rett Syndrome. Proc Natl Acad Sci USA 111:9941–9946.

Castro J, Mellios N, Sur M (2013) Mechanisms and therapeutic challenges in autism spectrum disorders. Current Opinion in Neurology 26:154–159.

Chang Q, Khare G, Dani V, Nelson S, Jaenisch R (2006) The disease progression of Mecp2 mutant mice is affected by the level of BDNF expression. Neuron 49:341–348.

Chen RZ, Akbarian S, Tudor M, Jaenisch R (2001) Deficiency of methyl-CpG binding protein-2 in CNS neurons results in a Rett-like phenotype in mice. Nat Genet 27:327–331.

Cheng T-L, Wang Z, Liao Q, Zhu Y, Zhou W-H, Xu W, Qiu Z (2014a) MeCP2 suppresses nuclear microRNA processing and dendritic growth by regulating the

DGCR8/Drosha complex. Dev Cell 28:547–560.

Coolen M, Bally-Cuif L (2009) MicroRNAs in brain development and physiology. Curr Opin Neurobiol 19:461–470.

Einspieler C, Kerr AM, Prechtl HFR (2005) Is the Early Development of Girls with Rett Disorder Really Normal? Pediatr Res 57:696–700.

Farra N, Zhang W-B, Pasceri P, Eubanks JH, Salter MW, Ellis J (2012) Rett syndrome induced pluripotent stem cell-derived neurons reveal novel neurophysiological alterations. Mol Psychiatry 17:1261–1271.

Fernandes TG, Duarte ST, Ghazvini M, Gaspar C, Santos DC, Porteira AR, Rodrigues GMC, Haupt S, Rombo DM, Armstrong J, Sebastião AM, Gribnau J, Garcia-Cazorla À, Brüstle O, Henrique D, Cabral JMS, Diogo MM (2015) Neural commitment of human pluripotent stem cells under defined conditions recapitulates neural development and generates patient-specific neural cells. Biotechnol J 10:1578–1588.

Forero DA, van der Ven K, Callaerts P, Del-Favero J (2010) miRNA genes and the brain: implications for psychiatric disorders. Human Mutation 31:1195–1204.

Fornari F, Milazzo M, Chieco P, Negrini M, Calin GA, Grazi GL, Pollutri D, Croce CM, Bolondi L, Gramantieri L (2010) MiR-199a-3p regulates mTOR and c-Met to influence the doxorubicin sensitivity of human hepatocarcinoma cells. Cancer Res 70:5184–5193.

Fukuda T, Itoh M, Ichikawa T, Washiyama K, Goto Y-I (2005) Delayed maturation of neuronal architecture and synaptogenesis in cerebral cortex of Mecp2-deficient mice. J Neuropathol Exp Neurol 64:537–544.

Giacometti E, Luikenhuis S, Beard C, Jaenisch R (2007) Partial rescue of MeCP2 deficiency by postnatal activation of MeCP2. Proc Natl Acad Sci USA 104:1931–1936.

Gonzales ML, Lasalle JM (2010) The role of MeCP2 in brain development and neurodevelopmental disorders. Curr Psychiatry Rep 12:127–134.

Gulsuner S, Walsh T, Watts AC, Lee MK, Thornton AM, Casadei S, Rippey C, Shahin H, Nimgaonkar VL, Go RCP, Savage RM, Swerdlow NR, Gur RE, Braff DL, King M-C, McClellan JM (2013) Spatial and Temporal Mapping of De Novo Mutations in Schizophrenia to a Fetal Prefrontal Cortical Network. Cell 154:518–529.

Guy J, Gan J, Selfridge J, Cobb S, Bird A (2007) Reversal of neurological defects in a mouse model of Rett syndrome. Science 315:1143–1147.

Guy J, Hendrich B, Holmes M, Martin JE, Bird A (2001) A mouse Mecp2-null mutation

causes neurological symptoms that mimic Rett syndrome. Nat Genet 27:322–326.

Hammer S, Dorrani N, Dragich J, Kudo S, Schanen C (2002) The phenotypic consequences of MECP2 mutations extend beyond Rett syndrome. Ment Retard Dev Disabil Res Rev 8:94–98.

Hébert SS, Mandemakers W, Papadopoulou AS, DeStrooper B (2009) microRNAs in Sporadic Alzheimer's Disease and Related Dementias. Berlin, Heidelberg: Springer Berlin Heidelberg.

Hou J, Lin L, Zhou W, Wang Z, Ding G, Dong Q, Qin L, Wu X, Zheng Y, Yang Y, Tian W, Zhang Q, Wang C, Zhang Q, Zhuang S-M, Zheng L, Liang A, Tao W, Cao X (2011) Identification of miRNomes in human liver and hepatocellular carcinoma reveals miR-199a/b-3p as therapeutic target for hepatocellular carcinoma. Cancer Cell 19:232–243.

Imamura O, Pagès G, Pouysségur J, Endo S, Takishima K (2010) ERK1 and ERK2 are required for radial glial maintenance and cortical lamination. Genes to Cells 15:1072–1088.

Ip JPK, Shi L, Chen Y, Itoh Y, Fu W-Y, Betz A, Yung W-H, Gotoh Y, Fu AKY, Ip NY (2011) α2-chimaerin controls neuronal migration and functioning of the cerebral cortex through CRMP-2. Nat Neurosci 15:39–47.

Jindra PT, Bagley J, Godwin JG, Iacomini J (2010) Costimulation-dependent expression of microRNA-214 increases the ability of T cells to proliferate by targeting Pten. J Immunol 185:990–997.

Kerr AM (1995) Early clinical signs in the Rett disorder. Neuropediatrics 26:67–71.

Khwaja OS et al. (2014) Safety, pharmacokinetics, and preliminary assessment of efficacy of mecasermin (recombinant human IGF-1) for the treatment of Rett syndrome. Proc Natl Acad Sci USA 111:4596–4601.

Kim J-E, O'Sullivan ML, Sanchez CA, Hwang M, Israel MA, Brennand K, Deerinck TJ, Goldstein LSB, Gage FH, Ellisman MH, Ghosh A (2011) Investigating synapse formation and function using human pluripotent stem cell-derived neurons. Proc Natl Acad Sci USA 108:3005–3010.

Kim S, Lee UJ, Kim MN, Lee E-J, Kim JY, Lee MY, Choung S, Kim YJ, Choi Y-C (2008) MicroRNA miR-199a* regulates the MET proto-oncogene and the downstream extracellular signal-regulated kinase 2 (ERK2). J Biol Chem 283:18158–18166.

Kishi N, Macklis JD (2004) MECP2 is progressively expressed in post-migratory neurons and is involved in neuronal maturation rather than cell fate decisions. Mol Cell Neurosci 27:306–321.

Kline DD, Ogier M, Kunze DL, Katz DM (2010) Exogenous brain-derived neurotrophic factor rescues synaptic dysfunction in Mecp2-null mice. Journal of Neuroscience 30:5303–5310.

Kosik KS (2006) The neuronal microRNA system. Nat Rev Neurosci 7:911–920.

Krichevsky AM, Sonntag K-C, Isacson O, Kosik KS (2006) Specific microRNAs modulate embryonic stem cell-derived neurogenesis. Stem Cells 24:857–864.

Krol J, Loedige I, Filipowicz W (2010) The widespread regulation of microRNA biogenesis, function and decay. Nat Rev Genet 11:597–610.

Leng J, Jiang L, Chen H, Zhang X (2009) Brain-derived neurotrophic factor and electrophysiological properties of voltage-gated ion channels during neuronal stem cell development. Brain Res 1272:14–24.

Leonard H, Bower C (1998) Is the girl with Rett syndrome normal at birth? Dev Med Child Neurol 40:115–121.

Lewis BP, Shih I-H, Jones-Rhoades MW, Bartel DP, Burge CB (2003) Prediction of mammalian microRNA targets. Cell 115:787–798.

Li L-M, Hou D-X, Guo Y-L, Yang J-W, Liu Y, Zhang C-Y, Zen K (2011) Role of microRNA-214-targeting phosphatase and tensin homolog in advanced glycation end product-induced apoptosis delay in monocytes. J Immunol 186:2552–2560.

Li Y, Wang H, Muffat J, Cheng AW, Orlando DA, Lovén J, Kwok S-M, Feldman DA, Bateup HS, Gao Q, Hockemeyer D, Mitalipova M, Lewis CA, Vander Heiden MG, Sur M, Young RA, Jaenisch R (2013) Global transcriptional and translational repression in human-embryonic-stem-cell-derived Rett syndrome neurons. Cell Stem Cell 13:446–458.

Luikenhuis S, Giacometti E, Beard CF, Jaenisch R (2004) Expression of MeCP2 in postmitotic neurons rescues Rett syndrome in mice. Proceedings of the National Academy of Sciences 101:6033–6038.

Marchetto MCN, Carromeu C, Acab A, Yu D, Yeo GW, Mu Y, Chen G, Gage FH, Muotri AR (2010) A model for neural development and treatment of Rett syndrome using human induced pluripotent stem cells. Cell 143:527–539.

Meijering E, Jacob M, Sarria JCF, Steiner P, Hirling H, Unser M (2004) Design and validation of a tool for neurite tracing and analysis in fluorescence microscopy images. Cytometry Part A 58A:167–176.

Mellios N, Sugihara H, Castro J, Banerjee A, Le C, Kumar A, Crawford B, Strathmann J, Tropea D, Levine SS, Edbauer D, Sur M (2011) miR-132, an experience-dependent microRNA, is essential for visual cortex plasticity. Nat Genet 14:1240–

1242.

Mellios N, Sur M (2012) The Emerging Role of microRNAs in Schizophrenia and Autism Spectrum Disorders. Front Psychiatry 3:39.

Mellios N, Woodson J, Garcia RI, Crawford B, Sharma J, Sheridan SD, Haggarty SJ, Sur M (2014) β2-Adrenergic receptor agonist ameliorates phenotypes and corrects microRNA-mediated IGF1 deficits in a mouse model of Rett syndrome. Proc Natl Acad Sci USA 111:9947–9952.

Mineno J, Okamoto S, Ando T, Sato M, Chono H, Izu H, Takayama M, Asada K, Mirochnitchenko O, Inouye M, Kato I (2006) The expression profile of microRNAs in mouse embryos. Nucleic Acids Res 34:1765–1771.

Neul JL, Kaufmann WE, Glaze DG, Christodoulou J, Clarke AJ, Bahi-Buisson N, Leonard H, Bailey MES, Schanen NC, Zappella M, Renieri A, Huppke P, Percy AK, Members listed in the Appendix FTRC (2010) Rett syndrome: Revised diagnostic criteria and nomenclature. Ann Neurol 68:944–950.

Neul JL, Lane JB, Lee H-S, Geerts S, Barrish JO, Annese F, Baggett LM, Barnes K, Skinner SA, Motil KJ, Glaze DG, Kaufmann WE, Percy AK (2014) Developmental delay in Rett syndrome: data from the natural history study. J Neurodev Disord 6:20.

Neul JL, Zoghbi HY (2004) Rett syndrome: a prototypical neurodevelopmental disorder. Neuroscientist 10:118–128.

Ogier M, Wang H, Hong E, Wang Q, Greenberg ME, Katz DM (2007) Brain-derived neurotrophic factor expression and respiratory function improve after ampakine treatment in a mouse model of Rett syndrome. Journal of Neuroscience 27:10912–10917.

Peltier J, Conway A, Keung AJ, Schaffer DV (2011) Akt Increases Sox2 Expression in Adult Hippocampal Neural Progenitor Cells, but Increased Sox2 Does Not Promote Proliferation. Stem Cells and Development 20:1153–1161.

Peltier J, O'Neill A, Schaffer DV (2007) PI3K/Akt and CREB regulate adult neural hippocampal progenitor proliferation and differentiation. Dev Neurobiol 67:1348–1361.

Petazzi P, Akizu N, García A, Estarás C, Martínez de Paz A, Rodríguez-Paredes M, Martínez-Balbás MA, Huertas D, Esteller M (2014) An increase in MECP2 dosage impairs neural tube formation. Neurobiol Dis 67:49–56.

Pini G, Scusa MF, Congiu L, Benincasa A, Morescalchi P, Bottiglioni I, Di Marco P, Borelli P, Bonuccelli U, Della-Chiesa A, Prina-Mello A, Tropea D (2012) IGF1 as a Potential Treatment for Rett Syndrome: Safety Assessment in Six Rett Patients.

Autism Research and Treatment 2012:1–14.

Pucilowska J, Puzerey PA, Karlo JC, Galán RF, Landreth GE (2012) Disrupted ERK signaling during cortical development leads to abnormal progenitor proliferation, neuronal and network excitability and behavior, modeling human neuro-cardio-facial-cutaneous and related syndromes. Journal of Neuroscience 32:8663–8677.

Ricciardi S, Boggio EM, Grosso S, Lonetti G, Forlani G, Stefanelli G, Calcagno E, Morello N, Landsberger N, Biffo S, Pizzorusso T, Giustetto M, Broccoli V (2011) Reduced AKT/mTOR signaling and protein synthesis dysregulation in a Rett syndrome animal model. Human Molecular Genetics 20:1182–1196.

Samuels IS, Karlo JC, Faruzzi AN, Pickering K, Herrup K, Sweatt JD, Saitta SC, Landreth GE (2008) Deletion of ERK2 mitogen-activated protein kinase identifies its key roles in cortical neurogenesis and cognitive function. Journal of Neuroscience 28:6983–6995.

Schanen C, Francke U (1998) A severely affected male born into a Rett syndrome kindred supports X-linked inheritance and allows extension of the exclusion map. Am J Hum Genet 63:267–269.

Shahbazian MD, Sun Y, Zoghbi HY (2002) Balanced X chromosome inactivation patterns in the Rett syndrome brain. Am J Med Genet 111:164–168.

Shi Y, Kirwan P, Livesey FJ (2012) Directed differentiation of human pluripotent stem cells to cerebral cortex neurons and neural networks. Nat Protoc 7:1836–1846.

Szulwach KE, Li X, Smrt RD, Li Y, Luo Y, Lin L, Santistevan NJ, Li W, Zhao X, Jin P (2010) Cross talk between microRNA and epigenetic regulation in adult neurogenesis. J Cell Biol 189:127–141.

Trappe R, Laccone F, Cobilanschi J, Meins M, Huppke P, Hanefeld F, Engel W (2001) MECP2 mutations in sporadic cases of Rett syndrome are almost exclusively of paternal origin. Am J Hum Genet 68:1093–1101.

Tropea D, Giacometti E, Wilson NR, Beard C, McCurry C, Fu DD, Flannery R, Jaenisch R, Sur M (2009) Partial reversal of Rett Syndrome-like symptoms in MeCP2 mutant mice. Proc Natl Acad Sci USA 106:2029–2034.

Tsujimura K, Abematsu M, Kohyama J, Namihira M, Nakashima K (2009) Neuronal differentiation of neural precursor cells is promoted by the methyl-CpG-binding protein MeCP2. Experimental Neurology 219:104–111.

Tsujimura K, Irie K, Nakashima H, Egashira Y, Fukao Y, Fujiwara M, Itoh M, Uesaka M, Imamura T, Nakahata Y, Yamashita Y, Abe T, Takamori S, Nakashima K (2015) miR-199a Links MeCP2 with mTOR Signaling and Its Dysregulation Leads to Rett Syndrome Phenotypes. Cell Rep 12:1887–1901.

Urdinguio RG, Fernandez AF, Lopez-Nieva P, Rossi S, Huertas D, Kulis M, Liu C-G, Croce CM, Calin GA, Esteller M (2010) Disrupted microRNA expression caused by Mecp2 loss in a mouse model of Rett syndrome. Epigenetics 5:656–663.

Wang J, Zhou M, Wang X, Yang X, Wang M, Zhang C, Zhou S, Tang N (2014) Impact of Ketamine on Learning and Memory Function, Neuronal Apoptosis and Its Potential Association with miR-214 and PTEN in Adolescent Rats Homayouni R, ed. PLoS ONE 9:e99855.

Wang Y-S, Wang Y-H, Xia H-P, Zhou S-W, Schmid-Bindert G, Zhou C-C (2012) MicroRNA-214 regulates the acquired resistance to gefitinib via the PTEN/AKT pathway in EGFR-mutant cell lines. Asian Pac J Cancer Prev 13:255–260.

Watanabe T, Sato T, Amano T, Kawamura Y, Kawamura N, Kawaguchi H, Yamashita N, Kurihara H, Nakaoka T (2008) Dnm3os, a non-coding RNA, is required for normal growth and skeletal development in mice. Dev Dyn 237:3738–3748.

Williams EC, Zhong X, Mohamed A, Li R, Liu Y, Dong Q, Ananiev GE, Mok JCC, Lin BR, Lu J, Chiao C, Cherney R, Li H, Zhang S-C, Chang Q (2014) Mutant astrocytes differentiated from Rett syndrome patients-specific iPSCs have adverse effects on wild-type neurons. Human Molecular Genetics 23:2968–2980.

Wu H, Tao J, Chen PJ, Shahab A, Ge W, Hart RP, Ruan X, Ruan Y, Sun YE (2010) Genome-wide analysis reveals methyl-CpG-binding protein 2-dependent regulation of microRNAs in a mouse model of Rett syndrome. Proc Natl Acad Sci USA 107:18161–18166.

Yang H, Kong W, He L, Zhao JJ, O'Donnell JD, Wang J, Wenham RM, Coppola D, Kruk PA, Nicosia SV, Cheng JQ (2008) MicroRNA Expression Profiling in Human Ovarian Cancer: miR-214 Induces Cell Survival and Cisplatin Resistance by Targeting PTEN. Cancer Res 68:425–433.

Yang T-S, Yang X-H, Wang X-D, Wang Y-L, Zhou B, Song Z-S (2013) MiR-214 regulate gastric cancer cell proliferation, migration and invasion by targeting PTEN. Cancer Cell International 13:68.

Ziats MN, Rennert OM (2014) Identification of differentially expressed microRNAs across the developing human brain. Mol Psychiatry 19:848–852.

Chapter IV

Aberrant neurogenesis in a 3D human model of Rett Syndrome

Abstract

Rett Syndrome (RTT) is an X-linked neurodevelopmental disorder traditionally characterized by a postnatal onset that involves developmental stagnation and regression including the loss of motor and language skills. RTT is most often due to mutations in the gene encoding Methyl CpG binding protein 2 (MeCP2), expressed throughout the course of neurogenesis and into adulthood. Whereas the focus surrounding MeCP2 has been largely on postnatal brain function, we sought to better understand the roles of this pleiotropic gene during early neurogenesis and how its absence during this time can contribute to the more well-characterized late stage RTT pathology. We generated isogenic patient-derived cerebral organoids to assay neuronal development in a human 3D MeCP2-deficient context. RTT organoids develop gross morphological deficits suggestive of delayed differentiation during the earliest stages of neuroepithelial cell expansion and division. We extended these findings by demonstrating halted progression into the stages of intermediate progenitor and post-mitotic neuron. Our results suggest a delay at a key timepoint in neurodevelopment during which the subventricular zone expands with intermediate progenitor cells destined to populate the cortex. Such a lag in development could have wide-ranging consequences with respect to proper cortical lamination and connectivity later in development, key phenotypes associated with RTT albeit not previously thought related to early development.

Introduction

iPSC modeling of RTT

Rett Syndrome (RTT) is an X-linked neurodevelopmental disorder caused by mutations in the gene encoding Methyl CpG binding protein 2 (MeCP2). MeCP2 is a pleiotropic regulator of gene expression and as such, a holistic view of its functions has been difficult to grasp (Lyst and Bird, 2015). Whereas mouse models have informed us of various behavioral, physiological, and molecular signatures of RTT, they lack the phenotypic subtlety and genetic background necessary for a full understanding of human RTT pathogenesis (Calfa et al., 2011; Feldman et al., 2016). Human stem cell models of RTT—generated via the reprogramming of patient cells or genome editing—have shed light on deficits in human RTT neurons including aberrant transcription (Chen et al., 2013; Li et al., 2013), impaired neuronal maturation and electrophysiological function (Kim et al., 2011a; Farra et al., 2012; Li et al., 2013; Tang et al., 2016), and up- or down- regulation of key signaling pathways and activity-related genes (Li et al., 2013). The vast majority of stem cell-based studies have focused on post-mitotic neurons in order to shed light on the postnatal mechanisms of RTT. However, recent clinical literature has begun to suggest an earlier onset of RTT (Fehr et al., 2010; 2011; Marschik et al., 2013; Neul et al., 2014; Tarquinio et al., 2015). Mounting evidence has emerged for the various roles of MeCP2 in neurogenesis (Stancheva et al., 2003; Coverdale et al., 2004; Tsujimura et al., 2009; Petazzi et al., 2014; Bedogni et al., 2015; Gao et al., 2015), including a study that demonstrated a differentiation bias of neural stem cells towards the astrocytic lineage in a RTT patient-derived stem cell model (Andoh-Noda et al., 2015). The processes of lineage

determination of NPs varies significantly in rodent (lissencephalic) versus primate (gyrencephalic) neurogenesis with respect to the absolute and relative number of NP subtype, the type of cell division performed by NP subtypes, and the length of both cell cycle and neurogenesis (Florio and Huttner, 2014). Thus, in order to gain a full understanding of RTT patient pathology during neurogenesis, it is crucial to study human cells. We previously demonstrated early deficits in human MeCP2-deficient immature neurons and neural progenitors (NPs) including increased proliferation, impaired migration, reduced dendritic branching, and altered expression of key miRNA-regulated signaling pathways (**Chapter 3**). Here we sought to better understand RTT physiology during neurogenesis using a 3D model that recapitulates the development of the human cortex (Lancaster et al., 2013; Lancaster and Knoblich, 2014a)

Cerebral organoids serve as a model of human neurogenesis in vitro

Human cerebral organoids are unique in their development of progenitor-rich zones akin to ventricular / subventricular zones from which NPs migrate radially to generate the layers of the cortex (Lancaster et al., 2013). The ventricular zone (VZ) is formed by neuroepithelial cells (NECs) during neurogenesis; it is a germinal layer at the apical boundary of the cortical wall that contains the cell bodies of apical progenitors (APs) that divide at the ventricular surface (Florio and Huttner, 2014). Progenitor cells in the VZ undergo several modes of cell division: symmetrical division that expands the NP pool, asymmetrical divisions that give rise to a single neuron and a single proliferative cell, and symmetrical terminal divisions that produce two post-mitotic neurons.

Symmetric progenitor divisions are more frequent during early stages of neurogenesis, whereas the majority of late-stage divisions are asymmetric and produce a daughter cell that migrates to the basally located germinal layer known as the SVZ (Noctor et al., 2004). The SVZ contains intermediate progenitor cells and develops into two distinct germinal zones in primates known as the inner SVZ (iSVZ) and the outer SVZ (oSVZ). The former largely resembles the SVZ of lissencephalic rodents, whereas the oSVZ, specific to gyrencephalic species, thickens considerably during neurogenesis and eventually contains up to four times as many progenitors as the VZ and SVZ combined (Smart et al., 2002; Florio and Huttner, 2014). Thus, basal / SVZ progenitors, also capable of undergoing symmetric cell division, may serve to increase the number of neurons generated from apical / VZ progenitors (Götz and Huttner, 2005). Indeed, the majority of neocortical neurons in primates are generated by divisions of cells in the SVZ (Smart et al., 2002; LaMonica et al., 2013; Florio and Huttner, 2014). Human cerebral organoids are further unique in their corticogenesis modeling capability as they generate an oSVZ-like region when generated from human (and not mouse) embryonic stem cells (ESCs) (Lancaster et al., 2013). Accordingly, they have been used to model neurogenesis-relevant human pathologies such as Zika virus infection (Dang et al., 2016; Garcez et al., 2016; Qian et al., 2016) and microcephaly (Lancaster et al., 2013).

Whereas our work and others have demonstrated a role for MeCP2 in human neurogenesis (Andoh-Noda et al., 2015), and a delay in neuronal maturation in its absence (Marchetto et al., 2010; Kim et al., 2011b), it remains unclear at what point(s)

and to what degree NP maturation is impaired in RTT. We used RTT patient-derived cerebral organoids to model neurogenesis in 3D, demonstrating unprecedented gross morphological and expression-based deficits that inform our understanding of the earliest stages of RTT.

Results

Cerebral organoids as a model of corticogenesis in vitro

We established the presence of key molecular and phenotypic signatures of RTT during various stages of human neurogenesis in Chapter 2. In order to further investigate in a 3D context, we generated isogenic cerebral organoids from RTT patient 2 (**Chapter 2**) separated on the basis of X-inactivation (XCI). Key to the use of cerebral organoids as a model of corticogenesis is their development of progenitor-rich ventricle-like zones (**Figure 1A**) from which NPs migrate radially from the apical ("a") to the basal ("b") surface and beyond to form the layers of the cortex in an inside-out fashion in which the newest neurons climb past the previously settled layer (Rakic, 1974).

We utilized electroporation to assess this migration process in organoids. By electroporating a GFP construct into the center of a WT organoid, we were able to track the migration of cells that received the plasmid from the center of the PAX6(+) ventricle to the MAP2(+) surrounding zone (**Figure 1B**). Additionally, we demonstrated the ability to map the fate of the electroporated cells, as seen in a Tbr1(+) (layer VI)

cortical neuron that migrated from a ventricle (**Figure 1C**). Of note, we also detected a small number of GAD67(+) cells, demonstrating the presence of an inhibitory neuron population in wild type organoids.

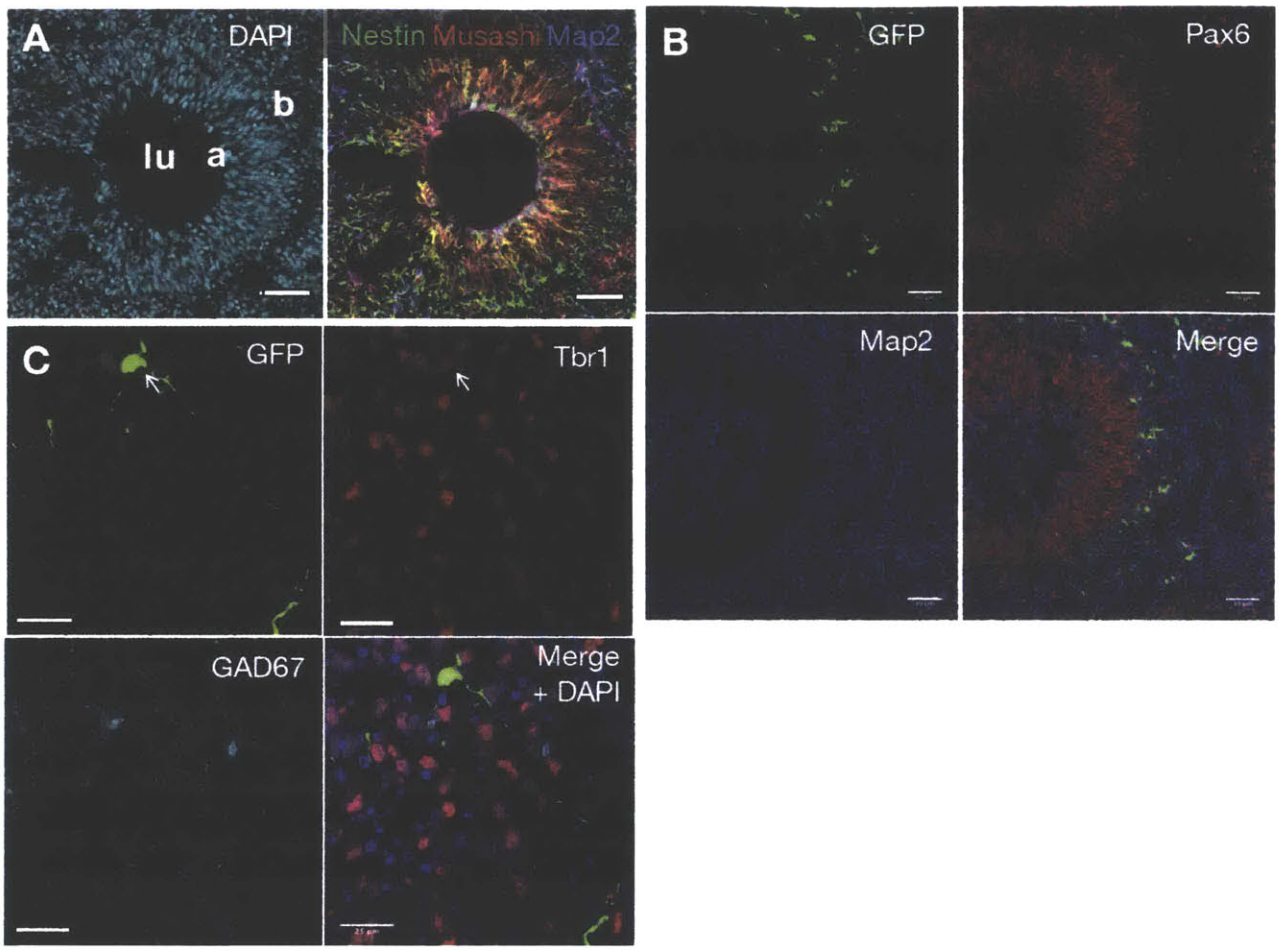

Figure 1: Cerebral organoids as a 3D model for human neurogenesis and corresponding deficits in RTT

(A) Cerebral organoids develop progenitor-rich, ventricle-like zones. DAPI stain (*left*) demonstrates the clear delineation of the ventricle structure including the lumen ("lu") and apical and basal surfaces ("a" and "b," respectively). Immunocytochemical staining (*right*) shows an enrichment of progenitor markers Musashi (*red*) and Nestin (*green*) in the ventricular region, with surrounding MAP2(+) neurons (*blue*) directly outside the ventricle. *(Scale bar = 50 μM.)* (B) Representative image 7 days after the electroporation of GFP (*green; top, left*) into the ventricle region delineated by PAX6(+) progenitors (*red; top, right*). Note the MAP2(+) neurons that surround the ventricle but do not overlap with the progenitor zone (*blue; bottom, left*). Note the migration of GFP(+) cells into the MAP2(+) region in the merged image (*bottom, right*). *(Scale bar = 50 μM.) (C)* Representative image demonstrating the fate determination of electroporated (GFP(+)) cells (*green; top, left*). The GFP(+) neuron is Tbr1(+) (*red; top, right*), suggesting a layer VI cortical neuron identity. Note the presence of GAD67(+) cells as well (*cyan; bottom, left*), representative of an inhibitory neuron population in organoids. *(Scale bar = 25 μM.)*

Generation of patient-derived cerebral organoids

We next sought to examine early neurogenesis in the context of RTT patients. Given that embryonic or perinatal postmortem tissue from patients is not available, we developed organoids from our isogenic RTT patient 2 line (harboring a nonsense mutation in the transcription repressor domain; see: **Chapter 2**). Of note, RTT patient-derived organoids did not successfully neuralize using the previously described protocol used to generate WT2 organoids (Lancaster et al., 2013). Thus we modified the existing protocol to include dual-SMAD inhibition as described previously (Shi et al., 2012) during the neural induction phase (**Figure 2A**) in order to increase the yield of high-quality organoids with a robust neural identity. Both RTT-WT2 and RTT-MT2 organoids formed embryoid bodies (**Figure 2B, top**) and developed an extended neuroepithelial morphology post-neural induction (**Figure 2B, middle**). After 4 weeks in culture, both RTT-WT2 and RTT-MT2 organoids had grown extensively and robustly developed ventricle-like zones throughout their respective structures (**Figure 2B, bottom**).

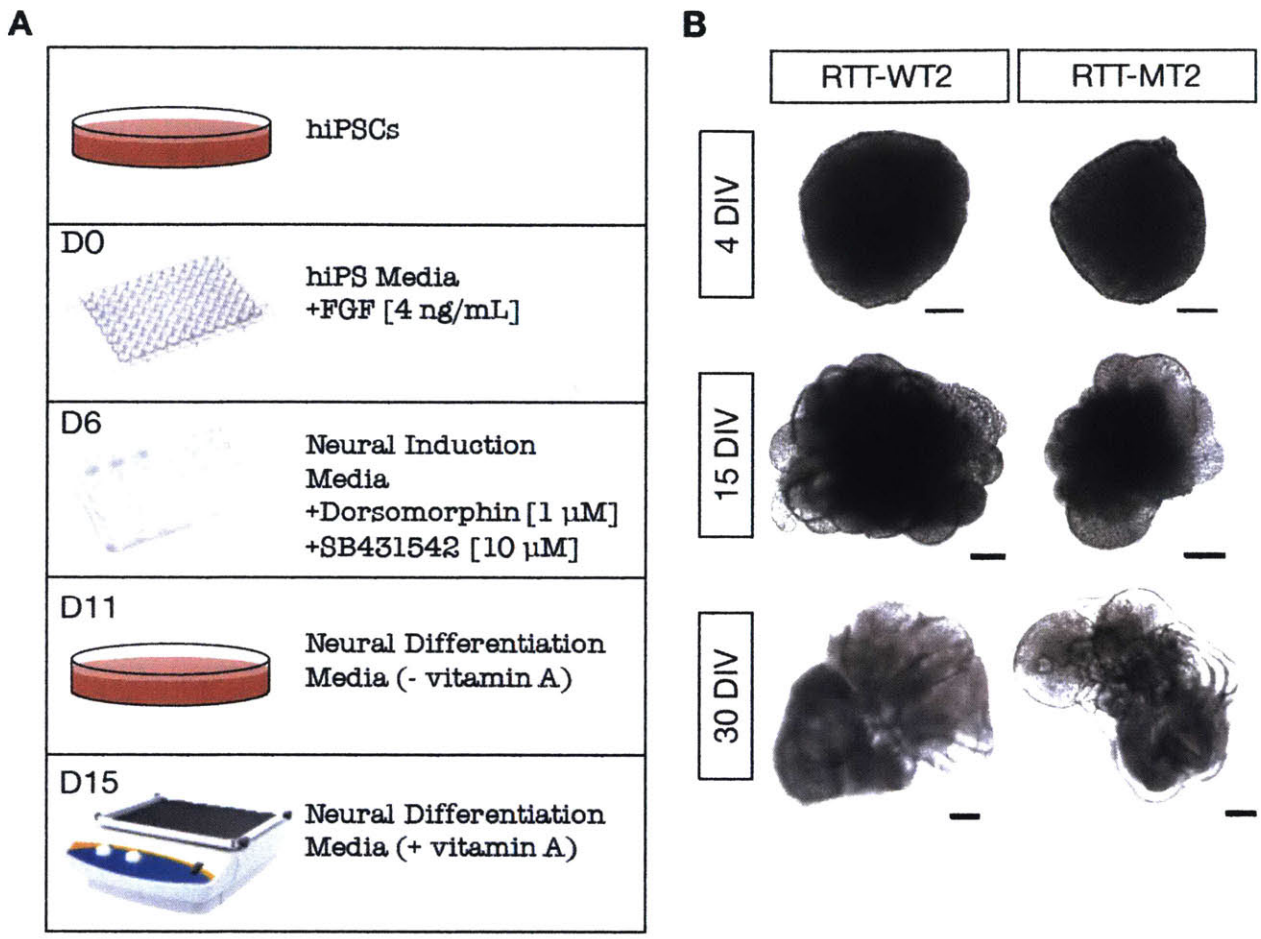

Figure 2: Generation of RTT patient-derived cerebral organoids

(A) RTT organoids were generated using a modified version of the protocol described by (Lancaster and Knoblich, 2014b). RTT iPSCs were used to generate embryoid bodies (Day 0) in a non-adherent plate, which were transferred on Day 6 to neural induction media supplemented with dual SMAD inhibiting factors Dorsomorphin and SB431542. The organoids were subsequently transferred to matrigel droplets in order to provide structural support for expansion in addition to growth factors; media was switched to neural differentiation media lacking vitamin A (Day 11). After branching into the matrigel droplet, the organoids were structurally sound enough to be moved to a shaker (Day 15); media was changed to contain vitamin A (retinol), which is converted into retinoic acid and promotes neuronal differentiation. *(B)* Representative images of the timeline of development in both RTT-WT2 (*left*) and RTT-MT2 (*right*) organoids. The isogenic pair successfully formed healthy EBs (*4 DIV*; *top*), and went on to develop a robust neuroepithelial identity post-dual SMAD inhibition (*15 DIV*; *middle*). Both RTT-WT2 and RTT-MT2 organoids expanded rapidly upon matrigel embedding and grew to develop ventricles visible in intact organoids (*30 DIV; bottom*). *(Images acquired via light microscopy. Scale bar (4 DIV; 15 DIV) = 100 μM. Scale bar (30 DIV) = 200 μM.)*

MeCP2-deficient NPs exhibit impaired neuronal migration from the ventricles of cerebral organoids

To assess neuronal migration in an MeCP2-deficient context, we first electroporated WT iPSC-derived 3D cerebral organoids with an MECP2 shRNA "shMeCP2" (or control construct "shControl") together with GFP (to visualize transfected neurons and control for efficiency of electroporation) (**Figure 3A**). After 7 days of electroporation, most of the control neurons attained a unipolar/bipolar shape and migrated out of the PAX6(+) proliferative zone. MeCP2-depleted cells did not migrate as far and remained in the ventricle-like PAX6(+) proliferative zones within the cerebral organoids. (**Figure 3B**). We next assayed NP migration in RTT patient-derived organoids. We electroporated a GFP construct in addition to non-migratory fluorescent beads, which served as a marker of injection site within the ventricle (**Figure 3C**). As predicted, we found that migratory NPs in RTT-MT2 organoids remained closer to the ventricle than NPs in RTT-WT2 organoids (**Figure 3D**). These results, in support of our previous findings of delayed migration in *Mecp2*-deficient mouse neurons (**Chapter 3; Figure 3A**), provide evidence for migration deficits during human neurogenesis in the context of RTT.

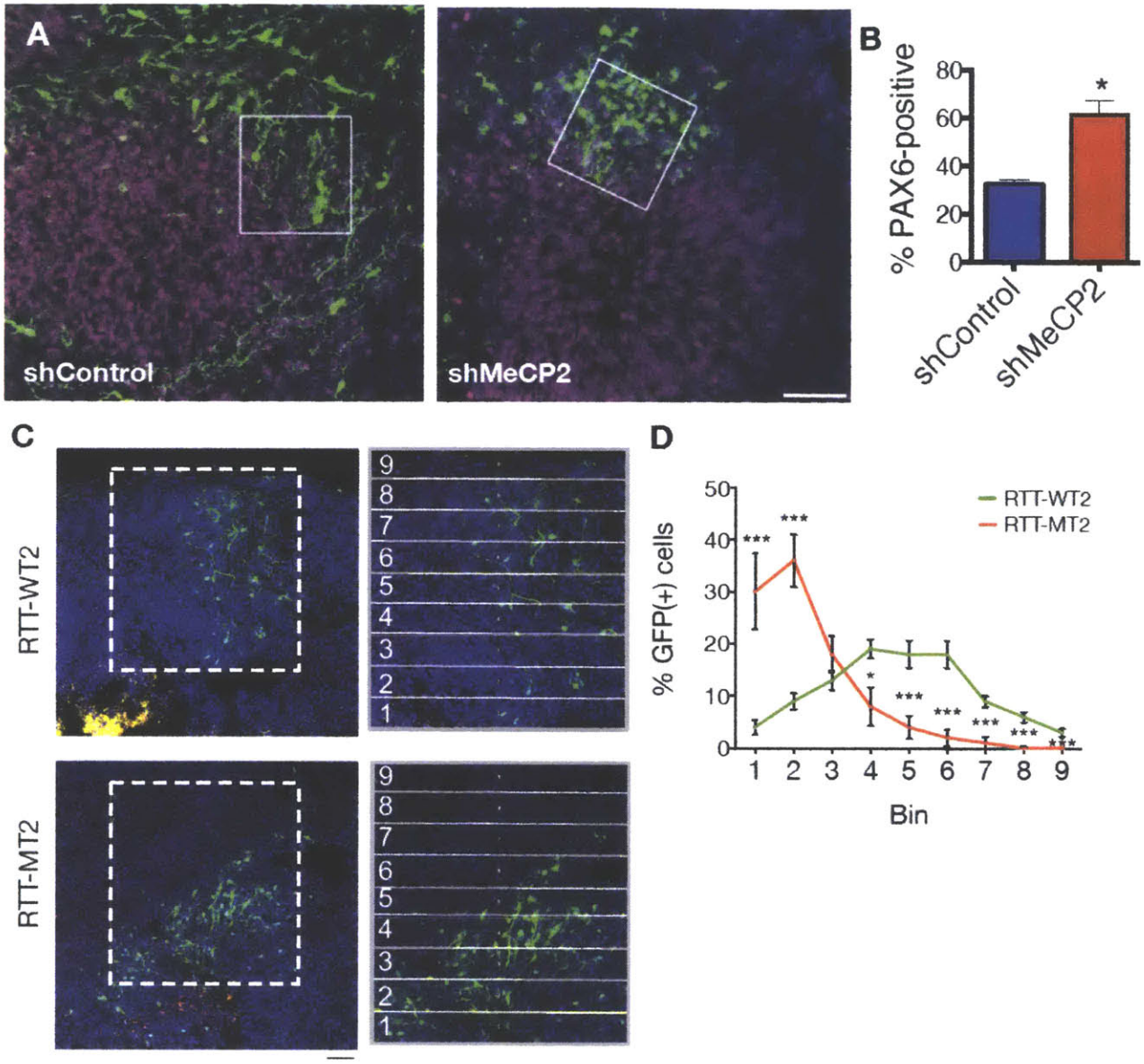

Figure 3: MeCP2-deficient NPs exhibit impaired neuronal migration from the ventricles of cerebral organoids

(A) Human iPSC-derived WT organoids co-electroporated with GFP plus a control shRNA ("shControl," *left*) or an shRNA targeting MECP2 ("shMeCP2," *right*) and examined after seven days. Representative images depict impaired migration of GFP(+) cells (*green*) from the PAX6(+) ventricle (*purple*) in the MeCP2-deficient context (*right*). *(Scale bar = 100 μM.) (B)* Quantification of the percentages of Pax6(+) / GFP(+) cells reveals an increase in the number of electroporated cells that remained as progenitors in the shMeCP2 group. More than 100 GFP(+) neurons from three organoids were examined in each group. *(Graph shows mean ± S.E.M. *p < 0.05; two-tailed Student's t-test.) (C)* RTT-WT2 and RTT-MT2

organoids were electroporated with GFP and non-migratory fluorescent beads. Electroporated GFP(+) cells in RTT-MT2 organoids exhibit reduced migration distance as compared to cells in RTT-WT2 organoids. Fluorescent beads are used to mark the ventricle. The right panel indicates the inset and the divided bins from the adjacent ventricle. *(Scale bar= 100 μM.) (D)* Significant reduction of migration distance in electroporated GFP+ cells in RTT-MT2 organoids. More than 700 GFP+ cells from seven organoids were examined in each group. *(Bars in all graphs represent mean ± S.E.M. *p < 0.05; ***p < 0.005; two-tailed Student's t-test.)*

MeCP2-deficient organoids exhibit expanded ventricle-like zones at 5.5 weeks of differentiation in vitro

A robust morphological phenotype was observed following 5.5 weeks of organoid differentiation, in which RTT-MT2 organoids exhibited increased ventricular area at the expense of neuron-rich regions (**Figure 4A**). We quantified the area of ventricle-like regions and unsurprisingly found a significantly higher percentage of ventricular area in the RTT-MT2 organoids (**Figure 4B**). Accordingly, measurements of total DAPI area were performed to serve as an inverse quantification of the total amount of space occupied by ventricular lumens. As expected, RTT-MT2 organoids had a significantly decreased DAPI-filled area relative to RTT-WT2 organoids indicative of more open space within the mutant organoids (**Figure 4C**). In addition to the number of ventricles, the type of ventricles in RTT-MT2 organoids appeared distinct from those in RTT-WT2 organoids. The ventricle walls of the latter appeared thicker in width, as defined by the distance from the apical to the basal surface. We quantified the mean ventricle wall thickness and found a significant decrease in RTT-MT2 organoids (**Figure 4D**). Notably, the distribution of ventricle wall thicknesses across both groups and the relative frequencies were significantly altered in RTT-MT2 organoids versus RTT-WT2 (**Figure 4E, F**).

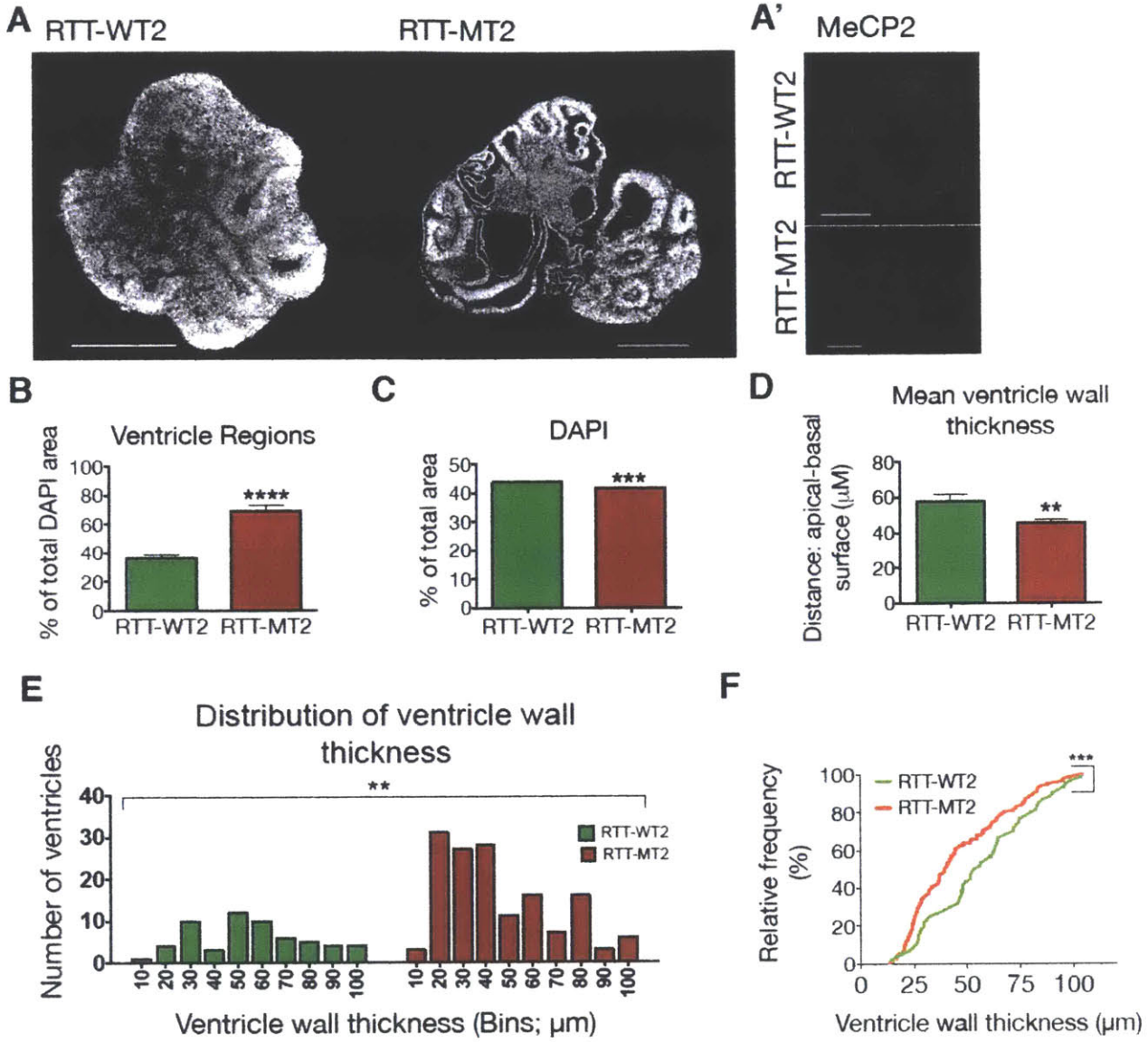

Figure 4: RTT-MT2 organoids exhibit gross morphological deficits indicative of delayed maturation

(A) DAPI immunofluorescence reveals structural differences (i.e., expanded ventricular zones) in RTT-MT2 (*left*) versus RTT-WT2 (*right*) patient-derived organoids. (A') Immunocytochemical staining of MeCP2 confirms the respective presence and absence of protein in RTT-WT2 (*red, top*) and RTT-MT2 (*red—not seen, bottom*) organoids. *(Scale bar = 500 μM.)* (B) Quantification of DAPI as a percentage of total area in order to reflect the inverse of the ventricular lumen area in RTT-WT2 versus RTT-MT2 organoids. *(n = 42 slices distributed across 3 organoids (RTT-WT2) and 64 slices distributed across 4 organoids (RTT-MT2)).* (C) Quantification of ventricular zones as a percentage of overall DAPI content reveals a significant increase in the percentage of ventricular zones in RTT-MT2 organoids

*(n = 6 slices taken from 3 organoids (RTT-WT2) and 8 slices taken from 4 organoids (RTT-MT2)). (Graphs B-C show mean ± SEM. ***p < 0.001, ****p < 0.0001, two-tailed Student's t-test.) (D)* RTT-MT2 organoids exhibit a reduction in mean ventricle wall thickness, defined as the distance between apical and basal surfaces of the ventricle. *(Graph shows mean ± SEM. n = 60 ventricles measured across 6 slices taken from 3 organoids (RTT-WT2) and 148 ventricles measured across 8 slices taken from 4 organoids (RTT-MT2). **p < 0.01, Mann-Whitney test.) (E-F)* Assessment of the distribution of ventricle wall thickness via contingency plot (*E*) and cumulative distribution (*F*) reveals significant differences in RTT-MT2 versus RTT-WT2 organoids. *(n = 60 ventricles measured across 6 slices taken from 3 organoids (RTT-WT2) and 148 ventricles measured across 8 slices taken from 4 organoids (RTT-MT2). **p < 0.01, ***p < 0.001, Chi-square test (E) and Kolmogorov-Smirnov test (F)).*

RTT-MT2 organoids exhibit aberrant expression of neuronal markers

Our morphological analyses suggested impaired neuronal differentiation in RTT-MT2 organoids. We sought to gain a better understanding of the respective developmental stages of RTT-WT2 and RTT-MT2 organoids at 5.5 weeks *in vitro*. We performed immunostaining experiments to determine the expression levels of dendritic marker Microtubule-associated protein 2 (MAP2), early neuronal marker Doublecortin (DCX), and the sequentially expressed early NP marker PAX6, intermediate progenitor marker Tbr2, and first born cortical neuron (layer VI) marker Tbr1 (**Figure 5A**). We found reductions in the levels of neuronal markers MAP2 and DCX (**Figure 5B, C**). Concurrently, RTT-MT2 organoids expressed a larger population of NP marker PAX6(+) cells (**Figure 5D**), and a smaller population of cells expressing Tbr2 (**Figure 5E**) and Tbr1 (**Figure 5F**), suggestive of impaired neurogenesis in RTT patient-derived 3D cerebral organoids. Intriguingly, our monolayer cultures also revealed many rosette-like structures in RTT-MT2 vs. RTT-WT2 neurons at three weeks *in vitro* (**Chapter 2: Figure 1A**), which coincides with the observed increased proliferative capacity of mutant cultures. Taken together, these findings provide strong evidence for severe alterations in early human neuronal development as a result of MECP2 deficiency.

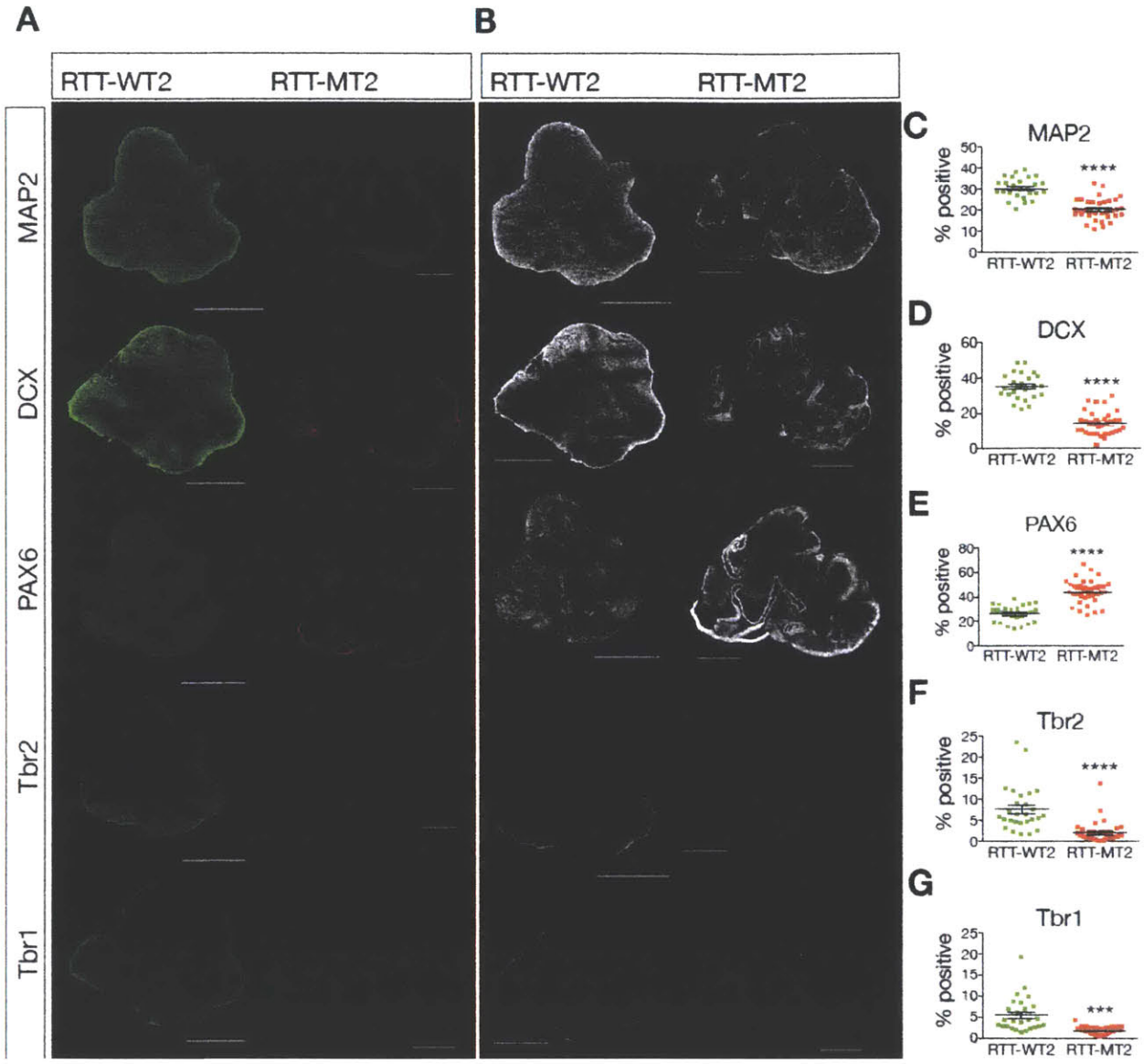

Figure 5: Immunocytochemical characterization reveals stunted neuronal differentiation in RTT-MT2 organoids at 5.5 weeks *in vitro*.

(A) Representative immunostaining in RTT-WT2 (*left, green*) and RTT-MT2 (*right, red*) organoids for (*from top to bottom*) MAP2 (dendrites), DCX (immature neurons), PAX6 (early neural progenitors), TBR2 (intermediate neural progenitors), and Tbr1 (early-born layer VI cortical neurons). Note the small amounts of Tbr2 and Tbr1 present in RTT-MT2 organoids. *(B)* Representative thresholded images of the staining performed in (*A*). *(Scale bar = 500 μM). (C-G)* Quantification of the percentage of organoid expressing the aforementioned progenitor or neuronal marker (normalized to DAPI) revealed: 1) significant decrease in the expression of MAP2 in RTT-MT2 organoids *(n = 26 sections from a total of 11 organoids (RTT-WT2) and 33 sections from a total of 14 organoids (RTT-MT2), distributed across*

three independent organoid differentiation batches) (C); 2) significant reduction in DCX in RTT-MT2 organoids (*n = 25 sections from a total of 11 organoids (RTT-WT2) and 35 sections from a total of 14 organoids (RTT-MT2), distributed across three independent organoid differentiation batches) (D)*; 3) significant increase in the expression of PAX6 in RTT-MT2 organoids (*n = 26 sections from a total of 11 organoids (RTT-WT2) and 35 sections from a total of 14 organoids (RTT-MT2), distributed across three independent organoid differentiation batches) (E)*; 4) significant decrease in the expression of Tbr2 in RTT-MT2 organoids (*n = 27 sections from a total of 12 organoids (RTT-WT2) and 36 sections from a total of 14 organoids (RTT-MT2), distributed across three independent organoid differentiation batches) (F)*; and 5) a significant decrease in the expression of Tbr1 in RTT-MT2 *(n = 26 sections from a total of 11 organoids (RTT-WT2) and 34 sections from a total of 14 organoids (RTT-MT2), distributed across three independent organoid differentiation batches). (A total of 79 sections (RTT-WT2) and 103 sections (RTT-MT2) were analyzed for this experiment. ***p < 0.001, ** p< 0.0001 Two-tailed Student's t-test.)*

We performed a staining of astrocyte marker and calcium-binding protein S100B (Vives et al., 2003) in our patient-derived organoids at 7.5 weeks *in vitro* in order to determine if glial cells were beginning to emerge in either WT or MT organoids (**Figure 6A**). We found that in RTT-WT2 organoids, S100B staining was not strongly present in the ventricle, but rather stained a population of cells outside the ventricle. This aligns with previous findings that in the human fetal cortex, S100B is present mostly in the intermediate zone (between the SVZ and the cortical plate). It has also been shown to be absent from GFAP-expressing cells of the SVZ and its onset is suggested to align with the terminal maturation of cortical astrocytes (Raponi et al., 2007). Interestingly, the S100B staining in RTT-MT2 organoids exhibited a different pattern in which there was increased S100B staining almost exclusively at the apical surface of the ventricle (**Figure 6B**). Neither the location of the stain in RTT-MT2 organoids (apical boundary of the VZ) nor the morphology of the cells (long, thin processes toward the basal surface) align with the description of S100B(+) mature glia described in the literature or found in the RTT-WT2 organoids. However, radial glia are also known to express S100B along with other glial markers like GFAP and vimentin, observed during early neurogenesis in the mouse (E10-E12) (Götz and Huttner, 2005). S100B has also been detected in progenitor cells lining the ventricles of the adult ependyma (Vives et al., 2003). Both the staining pattern and morphology we observed closely matches that of radial glia, which originate at the apical surface of the VZ and, following thickening of the ventricle, elongate a thin process toward the basal surface (Rakic, 2003). At the time that radial glia emerge, the number of basal progenitors increases as well, which form the SVZ and are characteristically TBR2(+) (Götz and Huttner, 2005; Malatesta et al., 2008). The

morphology and distribution of S100B staining in the RTT-MT2 organoids suggest that these are radial glial cells as opposed to astrocytes, indicating the concurrent formation of the SVZ, which we identified in RTT-WT2 organoids to have taken place two weeks prior. Thus, whereas we have identified S100B(+) astrocytes in RTT-WT2 organoids at 7.5 weeks *in vitro*, RTT-MT2 organoids are still generating an SVZ at this point, indicative of a delay that supports our previous findings and a potential delay in the onset of astrogenesis.

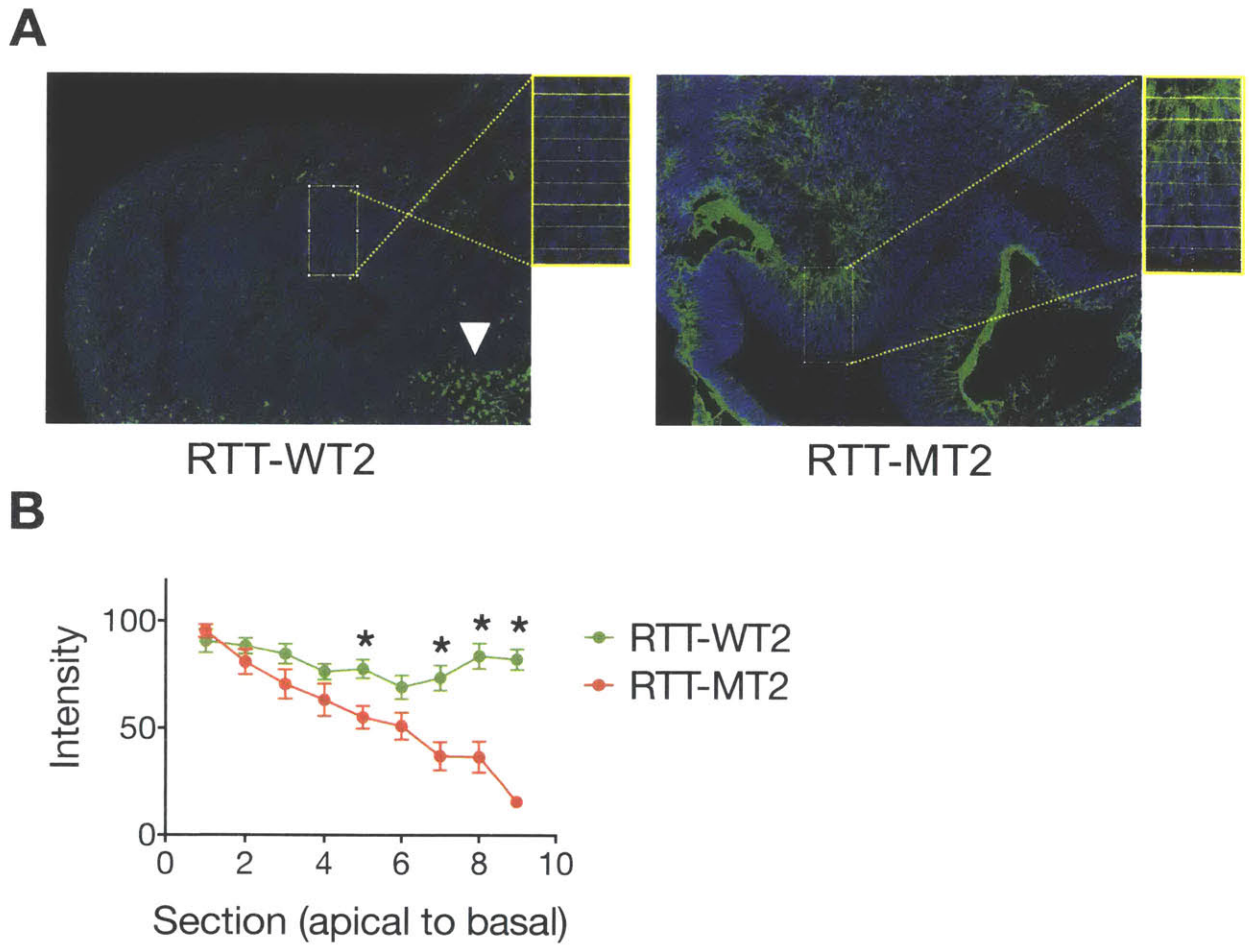

Figure 6: Characterization of S100B expression in RTT patient-derived organoids at 7.5 weeks *in vitro*

(A) RTT-WT2 (*left*) expresses S100B (*green*) minimally in the ventricular zone, and with increased intensity directly outside the ventricle (*white triangle*). RTT-MT2 (*right*) expresses S100B (*green*) most intensely lining the apical surface of the ventricular zone. Long processes extend from S100B(+) cells at the apical surface in the basal direction toward the presumptive SVZ. Boxes (insets) represent regions in which the distribution of S100B expression was quantified. *(B)* RTT-MT2 organoids express significantly increased S100B relative to WT in the basal region of the ventricle, where long processes extend from the cell bodies found at the apical surface. *(N = 1 differentiation round; 2 organoids per genotype; 8 WT ventricles and 9 mutant ventricles. *p < 0.05, Student's t-test.)*

Due to the intrinsic heterogeneity of cerebral organoids, we performed three individual differentiations and pooled sections / organoids from all batches. Representative images acquired from each organoid included in this study are shown in **Figure 7**.

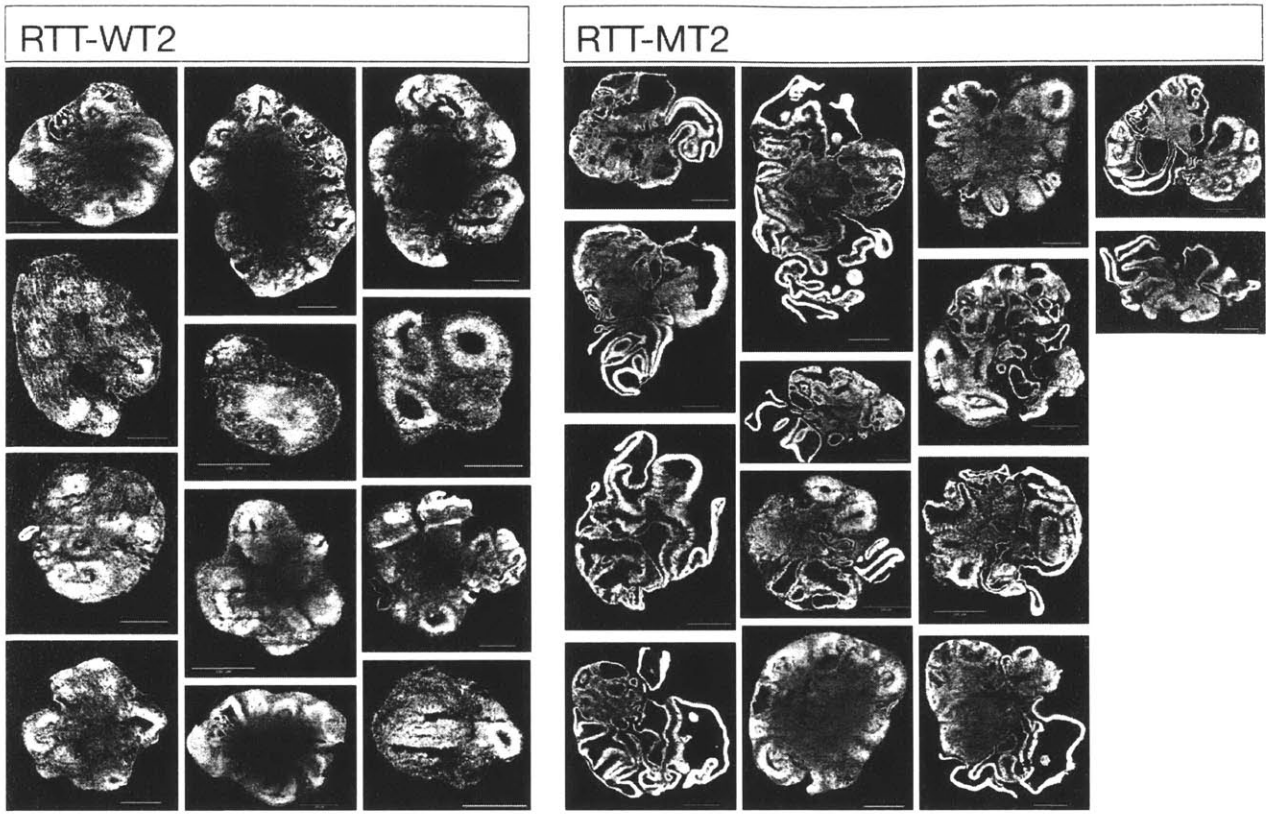

Figure 7: Representative sections from RTT-WT2 and RTT-MT2 organoids at 5.5 weeks *in vitro*

Representative DAPI immunofluorescence images acquired from each of the 12 RTT-WT2 organoids (*left*) and 14 RTT-MT2 organoids (*right*) used in this study. RTT-MT2 organoids exhibit a striking structure composed largely of thin ventricular zones, whereas RTT-WT2 organoids display both ventricular zones and dense, neuronal-rich regions. (*Scale bar = 500 μM.)*

Intact imaging of cerebral organoids

Our analyses of cerebral organoids thus far have been performed in sectioned tissue as opposed to intact 3D structures. Whereas there is much to glean from this information, it does not provide the full picture of an organoid as one cohesive unit. Intact imaging would be particularly useful for cerebral organoids as they are prone to a high degree of heterogeneity both inter- and intra-organoid. We have begun efforts to image 3D organoids in collaboration with the lab of Kwanghun Chung as described in their previous work (Murray et al., 2015). We immunostained for dendritic marker MAP2 in addition to a pan-Sodium channel antibody and found that, whereas the stains appears specific for their respective targets, they did not penetrate the organoid past ~100 μM (**Figure 8A**). We are currently working with the Chung lab to optimize this staining procedure in order to characterize intact cerebral organoids with respect to the developmental markers assayed in organoid slices.

We have concurrently been developing third harmonic generation (THG) imaging methods to assess the structure of label-free intact organoids throughout the time course of neurogenesis. THG belongs to a class of nonlinear microscopies that can generate micron-scale images from highly scattering materials (e.g., 3D tissues). It can be used to detect the interface between materials of different excitability such as the aqueous cytoplasm of cells and a nearby lipid membrane. THG imaging has been applied recently to the non-invasive monitoring of human adipose tissue (Chang et al., 2013), cell nuclei and cytoplasm in liver tissue (Lin et al., 2014), and subcortical structures within an intact mouse brain (Horton et al., 2013). THG imaging provides the

advantages of micron-scale resolution, label-free imaging, deep tissue penetration depth, and non-destructiveness. As such, we've sought to use THG imaging in human iPSC-derived organoids for label-free, non-destructive structural imaging. We have generated preliminary, proof-of-concept results demonstrating that a THG signal can be acquired throughout the entire depths of the cerebral organoid, fixed and imaged at 8 weeks post-differentiation (**Figure 8B**). We performed concurrent THG and 3-photon fluorescence imaging in organoids fixed and cleared as described above, and subsequently stained with tubulin marker Tuj1 (**Figure 8C**). Whereas the Tuj1 stain (*middle, red*) is no longer visible at a depth of 200 μM, the THG signal (*top, pseudo-colored green*) was acquired throughout the sample.

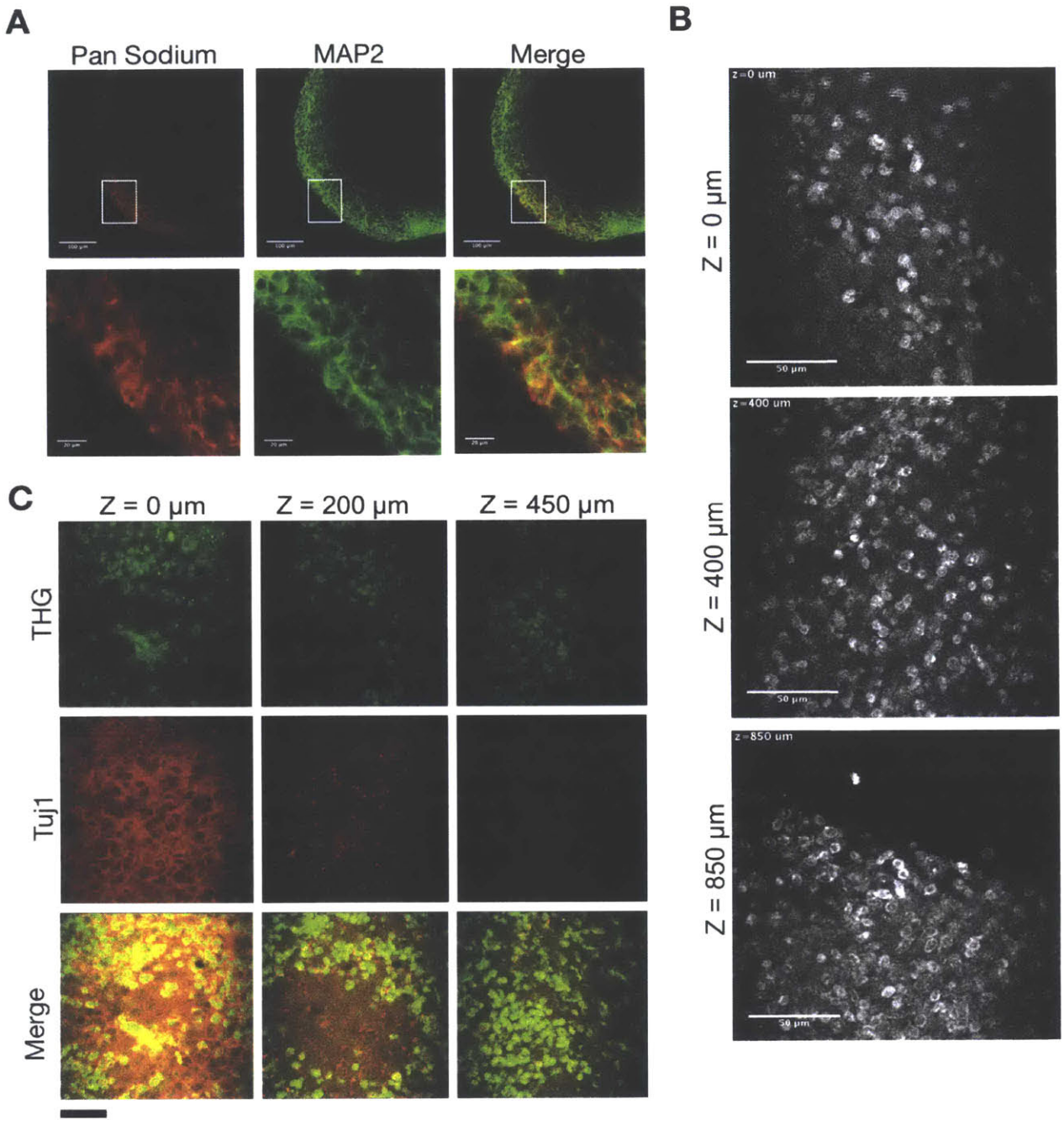

Figure 8: Intact imaging in 3D cerebral organoids

(A) Immunocytochemical staining of cleared organoids for pan-sodium channel (*red*) and dendritic marker MAP2 (*green*) and corresponding zoomed insets (*bottom*). Staining appears specific for its target albeit shallow in its penetration depth. *(Scale bar top = 100 µM; bottom = 20 µM). (B)* Representative example of THG imaging of WT organoid at 8 weeks *in vitro.* Signal extends from the top of the organoid (Z = 0 µM; *top*) to the bottom of the organoid (Z = 850 µM; *bottom*). Note the clear signal without attenuation throughout the organoid. *(Scale bar = 50*

μM). (C) Comparison of immunostaining (Tuj1) versus THG imaging in fixed and cleared WT organoids at 8 weeks *in vitro.* Tuj1 staining (*red, middle*) provides a clear image of tubulin structure (processes) at the surface of the organoid (Z = 0 μM) but does not penetrate past 200 μM. THG signal (*green, top*) remains consistent throughout. *(Scale bar = 50 μM).*

Discussion

Organoids successfully recapitulate key stages of human neurogenesis

We have demonstrated the ability to generate cerebral organoids that recapitulate key stages of neurogenesis such as progenitor-rich ventricle formation from which newborn neurons migrate. Impaired migration of MeCP2-deficient cells within WT organoids suggests a cell-autonomous defect in neuronal migration that supports our previous work in mouse (**Chapter 3**), among that of others (Bedogni et al., 2015). Interestingly, a recent study using cerebral organoids from patients with idiopathic ASD revealed a significant cell-specific acceleration in neuronal differentiation (Mariani et al., 2015), which was accompanied by increased levels of FOXG1, whose deficiency results in perturbed prenatal brain development and a congenital RTT-like phenotype ((Shoichet et al., 2005; Ariani et al., 2008; Das et al., 2014)).

Our findings of gross morphological alterations in RTT organoids include an increase in ventricular area, a decrease in mean ventricle wall thickness, and altered distribution of ventricle wall thickness in mutant organoids. The radial unit hypothesis (Rakic, 1988; 2009) suggests that two successive stages of neurogenesis determine the surface area and neocortical thickness, respectively. The former is established by proliferative divisions of NECs and the latter, termed the "differentiative phase," is the point at which asymmetric divisions generate neurons that migrate radially to the SVZ and then to the cortical plate to settle according to birth order (Rakic, 1974; Florio and Huttner, 2014). It is this switch from proliferative to differentiative divisions that causes the radial growth that thickens the SVZ and, subsequently, the cortical plate. Conversely,

increased lateral expansion of the ventricular zone corresponds to an increase in the number of NPs and an increase in self-amplifying divisions (Florio and Huttner, 2014). Our findings of increased ventricular area and decreased radial thickness support our previous findings of enhanced proliferation and decreased dendritic maturity in monolayer human MeCP2-deficient cultures (**Chapter 2**). Furthermore, these changes suggest a delay in the division switch that accompanies the formation and development of the SVZ. Of note, as SVZ expansion is uniquely different in human versus mouse neurogenesis (Florio and Huttner, 2014), it is likely that this phenotype would go unobserved in mouse (or other lissencephalic) models of RTT.

Our immunocytochemical analysis supports our morphological data that suggests a delay in RTT organoids during early neurogenesis and SVZ expansion. The observed decrease in neuronal markers MAP2 and DCX is unsurprising given our corresponding findings in monolayer human neuronal MeCP2-deficient cultures (**Chapter 2**). Whereas this aberration in expression suggests general delays in maturation, it does not independently point to a specific developmental stage during which RTT NPs are arrested. Thus, we performed staining of the sequentially expressed progenitor marker PAX6, intermediate progenitor marker Tbr2, and first-born layer VI cortical marker Tbr1. PAX6, increased in our RTT-MT2 organoids, has been shown to be critically responsible for progenitor cell proliferation during early cortical development, with identified direct targets that regulate the cell cycle such as *Cdk4*, *Cdk6*, *Mcm3*, *Cdca2*, *Cdca7,* and p27*kip1* (Sansom et al., 2009; Mi et al., 2013; Manuel et al., 2015b). PAX6 is particularly highly expressed in radial glial cells (RGCs), which are self-renewing and

can also give rise to basal progenitors in the SVZ, which are Tbr2(+). This Tbr2(+) SVZ population gives rise to Tbr1(+) post-mitotic neurons (LaMonica et al., 2013; Bizzotto and Francis, 2015). The expression of PAX6 is temporally graded, with the highest levels occurring during the onset of corticogenesis and extending to mid-stages, at which point Tbr2 expression rises (Manuel et al., 2015a). Whereas the sequential expression of PAX6, Tbr2, and Tbr1 in the developing neocortex is clearly delineated in rodents (Englund et al., 2005), the transitions are less sharp in primate neurogenesis, where a number of SVZ progenitors co-express PAX6 and Tbr2 during mid-stage neurogenesis (Florio and Huttner, 2014; Manuel et al., 2015a). We demonstrate here that RTT-MT2 organoids express a larger population of PAX6(+) cells and decreased populations of Tbr2 and Tbr1-postive cells relative to isogenic RTT-WT2 organoids. This expression pattern suggests once again that RTT-MT2 organoids develop an excess number of early progenitors at the expense of intermediate progenitors (i.e., lateral versus radial expansion) and, as a result, a decrease in the number of post-mitotic neurons. Interestingly, this pattern of elevated PAX6 and decreased Tbr2 / Tbr1 expression has been reported in the case of a disrupted apical adhesion complex composed of genes *DCHS1* and *FAT4* (Cappello et al., 2013). Mutations in either gene also resulted in increased progenitor proliferation, impaired neuronal migration, and reduced neuronal differentiation. This increase in progenitors does not result in a larger brain in patients with the analogous Van Maldergam syndrome, but rather a reduction of cortical gray matter volume and periventricular heterotopia, in which neurons remain clustered at the ventricular margins.

Human neurogenesis is both spatially and temporally expanded as compared to the relatively condensed process in mouse. For reference, the human ventricular zone at 8.5 gestational weeks is approximately three times larger than that of the analogous embryonic day 13.5 mouse ventricular zone (Tyler and Haydar, 2010). Despite these inter-species differences, we were able to recapitulate the migration deficits shown previously in mouse (**Chapter 2**) in human cerebral organoids. We expanded on these findings by identifying deficits in a key stage of neurogenesis during the formation and expansion of the SVZ. Further efforts to characterize the RTT VZ/SVZ population may aim to include comparison of *Tis21* expression, an anti-proliferative gene expressed exclusively in neuroepithelial cells that are about to switch from proliferative to neurogenic divisions (Iacopetti et al., 1999). Additionally, the balance of proliferation and differentiation can be probed by tracking the cleavage planes of VZ cells during mitosis (Florio and Huttner, 2014). The cleavage plane, determined primarily by the axis of the mitotic spindle (Lancaster and Knoblich, 2012), determines the self-renewing potential of the daughter cells (Konno et al., 2008). Mapping the neurogenic versus self-renewing potential of NPs in the RTT and WT VZ/SVZ throughout the course of neurogenesis will provide further insight into the RTT pathology that arises as a result of early insults to the NPs that will form the cerebral cortex.

Methods

Cerebral organoid generation

Cerebral organoids were generated from control WT cells (WT2) as previously described (Lancaster et al., 2013). Briefly, iPSCs were detached from irradiated MEFs and plated at $9x10^4$ per well of an ultralow attachment 96-well plate (Corning) in human ES media supplemented with FGF (4 ng/mL) and Rho associated protein kinase (ROCK) inhibitor (50 μM; Y-27632, Tocris) (Day 0). Embryoid bodies (EBs) were subsequently transferred to N2-based neural induction media (Day 6) in an ultra-low attachment 24-well plate (Corning). EBs were embedded in Matrigel droplets (Corning) on Day 11 and transferred to neural differentiation media supplemented with B27 without vitamin A (Gibco, Life Technologies). On Day 15, embedded EBs were transferred to a shaker and grown in neural differentiation media supplemented with B27 with vitamin A (Gibco, Life Technologies). Patient-derived organoids (RTT-MT2 and RTT-WT2) were generated as described above with the modification of the addition of dual-SMAD inhibition [10 μM SB431542 (Tocris Bioscience); 1 μM dorsomorphin (Stemgent)] during the neural induction phase in order to increase yield of high-quality organoids with a robust neural identity.

Electroporation

Organoids (specifically, the "ventricles" or progenitor zones) were electroporated with either a MECP2 shRNA construct (validated sequence from Sigma; TRCN0000330971) or control (SHC001, Sigma), each co-injected with a Venus construct (pCAGIG-Venus,

gift from Omar Durak and Prof. Li-Huei Tsai) at 8 weeks post-EB formation. Indicated plasmids were mixed at the following concentrations: shRNA/control plasmids, 1μg/μl; pCAG-Venus plasmid, 0.5μg/μl. Immediately after DNA injection into the organoid, four 50-ms electrical pulses (40V) were applied at 1-s intervals using a 5-mm electrode and an electroporator (EM830, BTX). After 7 days, organoids were fixed (4% paraformaldehyde (PFA)) and cryoprotected in 20% and 30% sucrose solutions, respectively, overnight. Fixed organoids were sliced on a cryostat (Leica, CM 3050 S) into 20 μM sections.

Immunocytochemistry

Cerebral organoids were fixed in 4% PFA for 3 hours at 4 °C and transferred to PBS. For slicing, organoids were embedded on ice in OCT (TissueTek) and sliced at 20 μM on a cryostat (Leica). Primary staining was performed overnight at 4 °C in 0.1% triton X100 (Sigma) and 3% bovine serum albumin (Sigma). Secondary staining was performed in the same buffer at room temperature for 1 hour (Alexa Fluor, Molecular Probes). Coverslips were affixed with ProLong Gold antifade reagent with DAPI (Life Technologies) and z-stacks were acquired using either a Leica TCS SP8 or a Zeiss Axiovert microscope. Analysis was performed in ImageJ.

Primary antibodies used: mouse α Map2 (Encor Biotechnology, 1:1000); chicken α Doublecortin (Aves Labs, 1:200); mouse α PAX6 (Millipore, 1:200); mouse α Pax6 (Developmental Studies Hybridoma Bank, 1:100); rabbit α TBR2 (Abcam, 1:400); rabbit α TBR1 (Abcam, 1:400); mouse α GAD67 (Abcam, 1:300).

Contributions

The organoid protocol was introduced to the Sur lab by Yun Li, Ph.D. (Jaenisch lab). Line-specific protocol optimization was performed by Danielle Feldman with the technical assistance of Stephanie Chou. Immunocytochemical analyses were performed by Danielle Feldman and Chloe Delepine, with the technical assistance of Stephanie Chou. Electroporation and associated analyses were performed by Jacque Ip, Danielle Feldman, and Stephanie Chou. Clearing of intact organoids and subsequent immunocytochemical analyses were performed by Danielle Feldman and Justin Swaney (Chung lab). THG imaging of intact organoids was performed by Murat Yildirim, Ph.D. in the lab of collaborator Chris Xu (Cornell University).

References

Andoh-Noda T, Akamatsu W, Miyake K, Matsumoto T, Yamaguchi R, Sanosaka T, Okada Y, Kobayashi T, Ohyama M, Nakashima K, Kurosawa H, Kubota T, Okano H (2015) Differentiation of multipotent neural stem cells derived from Rett syndrome patients is biased toward the astrocytic lineage. Mol Brain 8:136.

Ariani F, Hayek G, Rondinella D, Artuso R, Mencarelli MA, Spanhol-Rosseto A, Pollazzon M, Buoni S, Spiga O, Ricciardi S, Meloni I, Longo I, Mari F, Broccoli V, Zappella M, Renieri A (2008) FOXG1 is responsible for the congenital variant of Rett syndrome. Am J Hum Genet 83:89–93.

Bedogni F, Cobolli Gigli C, Pozzi D, Rossi RL, Scaramuzza L, Rossetti G, Pagani M, Kilstrup-Nielsen C, Matteoli M, Landsberger N (2015) Defects During Mecp2 Null Embryonic Cortex Development Precede the Onset of Overt Neurological Symptoms. Cereb Cortex.

Bizzotto S, Francis F (2015) Morphological and functional aspects of progenitors perturbed in cortical malformations. Front Cell Neurosci 9:30.

Calfa G, Percy AK, Pozzo-Miller L (2011) Experimental models of Rett syndrome based on Mecp2 dysfunction. Exp Biol Med (Maywood) 236:3–19.

Cappello S et al. (2013) Mutations in genes encoding the cadherin receptor-ligand pair DCHS1 and FAT4 disrupt cerebral cortical development. Nat Genet 45:1300–1308.

Chang T, Zimmerley MS, Quinn KP, Lamarre-Jouenne I, Kaplan DL, Beaurepaire E, Georgakoudi I (2013) Non-invasive monitoring of cell metabolism and lipid production in 3D engineered human adipose tissues using label-free multiphoton microscopy. Biomaterials 34:8607–8616.

Chen J, Lin M, Foxe JJ, Pedrosa E, Hrabovsky A, Carroll R, Zheng D, Lachman HM (2013) Transcriptome comparison of human neurons generated using induced pluripotent stem cells derived from dental pulp and skin fibroblasts. Kerkis I, ed. PLoS ONE 8:e75682.

Coverdale LE, Martyniuk CJ, Trudeau VL, Martin CC (2004) Differential expression of the methyl-cytosine binding protein 2 gene in embryonic and adult brain of zebrafish. Brain Res Dev Brain Res 153:281–287.

Dang J, Tiwari SK, Lichinchi G, Qin Y, Patil VS, Eroshkin AM, Rana TM (2016) Zika Virus Depletes Neural Progenitors in Human Cerebral Organoids through Activation of the Innate Immune Receptor TLR3. Cell Stem Cell.

Das DK, Jadhav V, Ghattargi VC, Udani V (2014) Novel mutation in forkhead box G1 (FOXG1) gene in an Indian patient with Rett syndrome. Gene 538:109–112.

Englund C, Fink A, Lau C, Pham D, Daza RAM, Bulfone A, Kowalczyk T, Hevner RF (2005) Pax6, Tbr2, and Tbr1 are expressed sequentially by radial glia, intermediate progenitor cells, and postmitotic neurons in developing neocortex. Journal of Neuroscience 25:247–251.

Farra N, Zhang W-B, Pasceri P, Eubanks JH, Salter MW, Ellis J (2012) Rett syndrome induced pluripotent stem cell-derived neurons reveal novel neurophysiological alterations. Mol Psychiatry 17:1261–1271.

Fehr S, Bebbington A, Ellaway C, Rowe P, Leonard H, Downs J (2011) Altered attainment of developmental milestones influences the age of diagnosis of rett syndrome. J Child Neurol 26:980–987.

Fehr S, Downs J, Bebbington A, Leonard H (2010) Atypical presentations and specific genotypes are associated with a delay in diagnosis in females with Rett syndrome. Am J Med Genet A 152A:2535–2542.

Feldman D, Banerjee A, Sur M (2016) Developmental Dynamics of Rett Syndrome. Neural Plasticity 2016:6154080–6154089.

Florio M, Huttner WB (2014) Neural progenitors, neurogenesis and the evolution of the neocortex. Development 141:2182–2194.

Gao H, Bu Y, Wu Q, Wang X, Chang N, Lei L, Chen S, Liu D, Zhu X, Hu K, Xiong J-W (2015) Mecp2 regulates neural cell differentiation by suppressing the Id1 to Her2 axis in zebrafish. J Cell Sci 128:2340–2350.

Garcez PP, Loiola EC, Madeiro da Costa R, Higa LM, Trindade P, Delvecchio R, Nascimento JM, Brindeiro R, Tanuri A, Rehen SK (2016) Zika virus impairs growth in human neurospheres and brain organoids. Science 352:816–818.

Götz M, Huttner WB (2005) The cell biology of neurogenesis. Nat Rev Mol Cell Biol.

Horton NG, Wang K, Kobat D, Clark CG, Wise FW, Schaffer CB, Xu C (2013) In vivo three-photon microscopy of subcortical structures within an intact mouse brain. Nature Photonics 7:205–209.

Iacopetti P, Michelini M, Stuckmann I, Oback B, Aaku-Saraste E, Huttner WB (1999) Expression of the antiproliferative gene TIS21 at the onset of neurogenesis identifies single neuroepithelial cells that switch from proliferative to neuron-generating division. Proceedings of the National Academy of Sciences 96:4639–4644.

Kim J-E, O'Sullivan ML, Sanchez CA, Hwang M, Israel MA, Brennand K, Deerinck TJ, Goldstein LSB, Gage FH, Ellisman MH, Ghosh A (2011a) Investigating synapse formation and function using human pluripotent stem cell-derived neurons. Proc Natl Acad Sci USA 108:3005–3010.

Kim K-Y, Hysolli E, Park I-H (2011b) Neuronal maturation defect in induced pluripotent stem cells from patients with Rett syndrome. Proc Natl Acad Sci USA 108:14169–14174.

Konno D, Shioi G, Shitamukai A, Mori A, Kiyonari H, Miyata T, Matsuzaki F (2008) Neuroepithelial progenitors undergo LGN-dependent planar divisions to maintain self-renewability during mammalian neurogenesis. Nat Cell Biol 10:93–101.

LaMonica BE, Lui JH, Hansen DV, Kriegstein AR (2013) Mitotic spindle orientation predicts outer radial glial cell generation in human neocortex. Nat Commun 4:1665.

Lancaster MA, Knoblich JA (2012) Spindle orientation in mammalian cerebral cortical development. Curr Opin Neurobiol 22:737–746.

Lancaster MA, Knoblich JA (2014) Generation of cerebral organoids from human pluripotent stem cells. Nat Protoc 9:2329–2340.

Lancaster MA, Renner M, Martin C-A, Wenzel D, Bicknell LS, Hurles ME, Homfray T, Penninger JM, Jackson AP, Knoblich JA (2013) Cerebral organoids model human brain development and microcephaly. Nature 501:373–379.

Li Y, Wang H, Muffat J, Cheng AW, Orlando DA, Lovén J, Kwok S-M, Feldman DA, Bateup HS, Gao Q, Hockemeyer D, Mitalipova M, Lewis CA, Vander Heiden MG, Sur M, Young RA, Jaenisch R (2013) Global transcriptional and translational repression in human-embryonic-stem-cell-derived Rett syndrome neurons. Cell Stem Cell 13:446–458.

Lin J, Zheng W, Wang Z, Huang Z (2014) Label-free three-dimensional imaging of cell nucleus using third-harmonic generation microscopy. Applied Physics Letters 105:103705.

Lyst MJ, Bird A (2015) Rett syndrome: a complex disorder with simple roots. Nat Rev Genet 16:261–275.

Malatesta P, Appolloni I, Calzolari F (2008) Radial glia and neural stem cells. Cell Tissue Res 331:165–178.

Manuel MN, Da Mi, Mason JO, Price DJ (2015) Regulation of cerebral cortical neurogenesis by the Pax6 transcription factor. Front Cell Neurosci 9:28.

Marchetto MCN, Carromeu C, Acab A, Yu D, Yeo GW, Mu Y, Chen G, Gage FH, Muotri AR (2010) A model for neural development and treatment of Rett syndrome using human induced pluripotent stem cells. Cell 143:527–539.

Mariani J, Coppola G, Zhang P, Abyzov A, Provini L, Tomasini L, Amenduni M, Szekely A, Palejev D, Wilson M, Gerstein M, Grigorenko EL, Chawarska K, Pelphrey KA, Howe JR, Vaccarino FM (2015) FOXG1-Dependent Dysregulation of

GABA/Glutamate Neuron Differentiation in Autism Spectrum Disorders. Cell 162:375–390.

Marschik PB, Kaufmann WE, Sigafoos J, Wolin T, Zhang D, Bartl-Pokorny KD, Pini G, Zappella M, Tager-Flusberg H, Einspieler C, Johnston MV (2013) Changing the perspective on early development of Rett syndrome. Res Dev Disabil 34:1236–1239.

Mi D, Carr CB, Georgala PA, Huang Y-T, Manuel MN, Jeanes E, Niisato E, Sansom SN, Livesey FJ, Theil T, Hasenpusch-Theil K, Simpson TI, Mason JO, Price DJ (2013) Pax6 exerts regional control of cortical progenitor proliferation via direct repression of Cdk6 and hypophosphorylation of pRb. Neuron 78:269–284.

Murray E, Cho JH, Goodwin D, Ku T, Swaney J, Kim S-Y, Choi H, Park Y-G, Park J-Y, Hubbert A, McCue M, Vassallo S, Bakh N, Frosch MP, Wedeen VJ, Seung HS, Chung K (2015) Simple, Scalable Proteomic Imaging for High-Dimensional Profiling of Intact Systems. Cell 163:1500–1514.

Neul JL, Lane JB, Lee H-S, Geerts S, Barrish JO, Annese F, Baggett LM, Barnes K, Skinner SA, Motil KJ, Glaze DG, Kaufmann WE, Percy AK (2014) Developmental delay in Rett syndrome: data from the natural history study. J Neurodev Disord 6:20.

Noctor SC, Martínez-Cerdeño V, Ivic L, Kriegstein AR (2004) Cortical neurons arise in symmetric and asymmetric division zones and migrate through specific phases. Nat Neurosci 7:136–144.

Petazzi P, Akizu N, García A, Estarás C, Martínez de Paz A, Rodríguez-Paredes M, Martínez-Balbás MA, Huertas D, Esteller M (2014) An increase in MECP2 dosage impairs neural tube formation. Neurobiol Dis 67:49–56.

Qian X et al. (2016) Brain-Region-Specific Organoids Using Mini-bioreactors for Modeling ZIKV Exposure. Cell 165:1238–1254.

Rakic P (1974) Neurons in Rhesus Monkey Visual Cortex: Systematic Relation between Time of Origin and Eventual Disposition. Science 183:425–427.

Rakic P (1988) Specification of cerebral cortical areas. Science 241:170–176.

Rakic P (2003) Developmental and evolutionary adaptations of cortical radial glia. Cereb Cortex 13:541–549.

Rakic P (2009) Evolution of the neocortex: a perspective from developmental biology. Nat Rev Neurosci 10:724–735.

Raponi E, Agenes F, Delphin C, Assard N, Baudier J, Legraverend C, Deloulme J-C (2007) S100B expression defines a state in which GFAP-expressing cells lose their

neural stem cell potential and acquire a more mature developmental stage. Glia 55:165–177.

Sansom SN, Griffiths DS, Faedo A, Kleinjan D-J, Ruan Y, Smith J, van Heyningen V, Rubenstein JL, Livesey FJ (2009) The Level of the Transcription Factor Pax6 Is Essential for Controlling the Balance between Neural Stem Cell Self-Renewal and Neurogenesis Hébert JM, ed. PLoS Genet 5:e1000511.

Shi Y, Kirwan P, Livesey FJ (2012) Directed differentiation of human pluripotent stem cells to cerebral cortex neurons and neural networks. Nat Protoc 7:1836–1846.

Shoichet SA, Kunde S-A, Viertel P, Schell-Apacik C, Voss von H, Tommerup N, Ropers H-H, Kalscheuer VM (2005) Haploinsufficiency of novel FOXG1B variants in a patient with severe mental retardation, brain malformations and microcephaly. Hum Genet 117:536–544.

Smart IHM, Dehay C, Giroud P, Berland M, Kennedy H (2002) Unique morphological features of the proliferative zones and postmitotic compartments of the neural epithelium giving rise to striate and extrastriate cortex in the monkey. Cereb Cortex 12:37–53.

Stancheva I, Collins AL, Van den Veyver IB, Zoghbi H (2003) A mutant form of MeCP2 protein associated with human Rett syndrome cannot be displaced from methylated DNA by notch in Xenopus embryos. Mol Cell.

Tang X, Kim J, Zhou L, Wengert E, Zhang L, Wu Z, Carromeu C, Muotri AR, Marchetto MCN, Gage FH, Chen G (2016) KCC2 rescues functional deficits in human neurons derived from patients with Rett syndrome. Proc Natl Acad Sci USA 113:751–756.

Tarquinio DC, Hou W, Neul JL, Lane JB, Barnes KV, O'Leary HM, Bruck NM, Kaufmann WE, Motil KJ, Glaze DG, Skinner SA, Annese F, Baggett L, Barrish JO, Geerts SP, Percy AK (2015) Age of diagnosis in Rett syndrome: patterns of recognition among diagnosticians and risk factors for late diagnosis. Pediatr Neurol 52:585–91.e2.

Tsujimura K, Abematsu M, Kohyama J, Namihira M, Nakashima K (2009) Neuronal differentiation of neural precursor cells is promoted by the methyl-CpG-binding protein MeCP2. Experimental Neurology 219:104–111.

Tyler WA, Haydar TF (2010) A new contribution to brain convolution: progenitor cell logistics during cortex development. Nat Neurosci 13:656–657.

Vives V, Alonso G, Solal AC, Joubert D, Legraverend C (2003) Visualization of S100B-positive neurons and glia in the central nervous system of EGFP transgenic mice. J Comp Neurol 457:404–419.

Chapter V

Future Directions

Characterizing late-stage cortical development in RTT organoids

We have demonstrated deficits in MeCP2-deficient human cells throughout the course of neurogenesis in both monolayer and 3D iPSC-derived cultures. Neurogenesis proceeds on a finely regulated timeline, the events of which are dependent upon the successes of prior events (Götz and Huttner, 2005; Florio and Huttner, 2014). Thus, our observed deficits including excessive proliferation, delayed migration, and stunted development of basal / subventricular zone (SVZ) progenitors are likely to have subsequent downstream effects including altered cell fate specification and cortical lamination. MeCP2 has been shown to inhibit astrocyte differentiation and promote neuronal differentiation of mouse stem cell-derived neurons *in vitro* (Tsujimura et al., 2009); accordingly, loss of MeCP2 accelerates astrogenesis (Okabe et al., 2010; Forbes-Lorman et al., 2014). The hypermethylation of astrocyte-specific promoters (i.e. *GFAP*) prevents astrocyte differentiation until mid-gestation (Qian et al., 2000; Takizawa et al., 2001; Namihira et al., 2004; Fan et al., 2005). MeCP2 binds these methylated regions and prevents the differentiation of NPs into astrocytes (Setoguchi et al., 2006; Kohyama et al., 2008). Further evidence of a role for MeCP2 in cell fate determination has been demonstrated in zebrafish (Gao et al., 2015), Xenopus (Stancheva et al., 2003), mesenchymal stem cell-derived neurons from a RTT patient (Squillaro et al., 2012), and olfactory neurons in the MeCP2-deficient mouse (Matarazzo et al., 2004). A logical next step from our observed findings would be to thoroughly track the emergence and maturation of upper cortical layers and astrocytes in RTT-WT2 and RTT-MT2 organoids based on gene and protein expression patterns.

Based on our previously observed deficits in cortical lamination (**Chapter 2; Figure 3**), and reports of reduced cortical density in adulthood (Kishi and Macklis, 2004), we expect that RTT-MT2 organoids will proceed to develop basal and intermediate progenitors, in addition to all six cortical layers, albeit in a delayed fashion that may result in aberrant formation. Whereas outer subventricular zone (oSVZ) progenitors largely give rise to the upper layers of the cortex, and we find aberrant SVZ development in RTT-MT2 organoids, we expect to find altered lamination in late stage organoids. Interestingly, previous experiments in postmortem human patient samples have demonstrated aberrant cortical formation including microdysgenesis (Jellinger and Seitelberger, 1986; Belichenko et al., 1997). Whereas organoids are subject to a great deal of inter- and intra-organoid variability, it would be preferable to track the development of the cortex in intact organoids with the use of clearing techniques (Murray et al., 2015) (see also: **Chapter 4**). Multiple rounds of staining in each organoid would provide a more cohesive picture of developmental progression that is currently unattainable with the use of thin sections.

Generating organoids that mimic RTT patient X-inactivation

Our RTT patient-derived organoids, despite harboring a clinically relevant mutation, lack a critical component of genetic accuracy: whereas RTT patients are mosaic with respect to their expression of MeCP2, our organoids are homogeneously WT or mutant. This model has informed our notions of early development in an MeCP2-deficient context, but it does not provide an accurate window into the developing RTT

brain. Future experiments should involve the study of mosaic RTT organoids, which can theoretically be accomplished via several routes. The use of naïve embryonic stem cells would be ideal in that they would undergo X-inactivation (XCI) to generate a mosaic organoid in a manner most closely related to that *in vivo*. However, the experimental feasibility of this approach is close to null. Alternatively, methods exist to reversibly reactivate the inactive X chromosome, using small molecule inhibitors of trans-acting X-inactivation factors (XCIFs) (Bhatnagar et al., 2014). Simulating XCI in our patient-derived iPSCs during the generation of organoids would inform our understanding of potential allelic skewing during early development, in addition to providing insight into potential growth advantages of one allele over another during organoid expansion. The most feasible approach, however, would likely be to mix stem cell cultures that express either the mutant or WT allele post-XCI. This mixing of lines and subsequent organoid generation would inform our understanding of relative growth patterns in WT versus mutant cells. Most importantly, this technique would provide a more accurate picture of the developing RTT brain. Existing literature has demonstrated non-cell autonomous effects of MeCP2 toxicity, suggesting that WT cells within mosaic organoids would not develop normally. However, differences in maturation, morphology, and potentially localization during early cortical patterning may be evident in WT versus mutant cells in mosaic organoids. Whereas microdysgenesis has been observed in a small number of RTT postmortem samples (Jellinger and Seitelberger, 1986), it is not clear whether the ectopic neurons are those that lack MeCP2.

Timeline of rescue in organoids

The reversibility of RTT phenotypes at mature stages of neuronal development suggests that the circuits involved in RTT pathogenesis are labile and immature, as opposed to degenerative (Chang et al., 2006; Guy et al., 2007; Tropea et al., 2009; Castro et al., 2014; Sztainberg et al., 2015). Whereas the demonstrated ameliorations of RTT phenotypes tend not to restore fully to WT levels, a question remains given the early developmental component of RTT described within whether earlier intervention may provide a more complete rescue of neuronal function and downstream maturation. Future efforts to restore proper cortical development in organoids can include previously established methods to overexpress MeCP2 or BDNF (Chang et al., 2006; Guy et al., 2007), or can alternatively attempt to target the pathways we have demonstrated to be transiently aberrantly regulated during neurogenesis. For example, inhibitors of the Akt pathway may prevent the excessive proliferation observed in both monolayer culture and in the lateral expansion of RTT-MT2 organoid ventricles. It remains unclear if an early push toward differentiative versus proliferative divisions in mutant cells would prevent and/or alleviate the delay in cortical development that may contribute to later stage pathology. Interestingly, pathway interventions that may speed maturation in RTT cells during early development could have the opposite effect at later stages when signaling signatures are reversed (Ricciardi et al., 2011). This has the potential to inform treatment efforts in both a specific manner, and as a proof-of-principle that suggests a need for timeline-specific pharmacological intervention in RTT syndrome.

References

Belichenko PV, Hagberg B, Dahlström A (1997) Morphological study of neocortical areas in Rett syndrome. Acta Neuropathol 93:50–61.

Bhatnagar S, Zhu X, Ou J, Lin L, Chamberlain L, Zhu LJ, Wajapeyee N, Green MR (2014) Genetic and pharmacological reactivation of the mammalian inactive X chromosome. Proceedings of the National Academy of Sciences 111:12591–12598.

Castro J, Garcia RI, Kwok S, Banerjee A, Petravicz J, Woodson J, Mellios N, Tropea D, Sur M (2014) Functional recovery with recombinant human IGF1 treatment in a mouse model of Rett Syndrome. Proc Natl Acad Sci USA 111:9941–9946.

Chang Q, Khare G, Dani V, Nelson S, Jaenisch R (2006) The disease progression of Mecp2 mutant mice is affected by the level of BDNF expression. Neuron 49:341–348.

Fan G, Martinowich K, Chin MH, He F, Fouse SD, Hutnick L, Hattori D, Ge W, Shen Y, Wu H, Hoeve ten J, Shuai K, Sun YE (2005) DNA methylation controls the timing of astrogliogenesis through regulation of JAK-STAT signaling. Development 132:3345–3356.

Florio M, Huttner WB (2014) Neural progenitors, neurogenesis and the evolution of the neocortex. Development 141:2182–2194.

Forbes-Lorman RM, Kurian JR, Auger AP (2014) MeCP2 regulates GFAP expression within the developing brain. Brain Res 1543:151–158.

Gao H, Bu Y, Wu Q, Wang X, Chang N, Lei L, Chen S, Liu D, Zhu X, Hu K, Xiong J-W (2015) Mecp2 regulates neural cell differentiation by suppressing the Id1 to Her2 axis in zebrafish. J Cell Sci 128:2340–2350.

Götz M, Huttner WB (2005) The cell biology of neurogenesis. Nat Rev Mol Cell Biol.

Guy J, Gan J, Selfridge J, Cobb S, Bird A (2007) Reversal of neurological defects in a mouse model of Rett syndrome. Science 315:1143–1147.

Jellinger K, Seitelberger F (1986) Neuropathology of Rett syndrome. Am J Med Genet Suppl 1:259–288.

Kishi N, Macklis JD (2004) MECP2 is progressively expressed in post-migratory neurons and is involved in neuronal maturation rather than cell fate decisions. Mol Cell Neurosci 27:306–321.

Kohyama J, Kojima T, Takatsuka E, Yamashita T, Namiki J, Hsieh J, Gage FH, Namihira M, Okano H, Sawamoto K, Nakashima K (2008) Epigenetic regulation of

neural cell differentiation plasticity in the adult mammalian brain. Proc Natl Acad Sci USA 105:18012–18017.

Matarazzo V, Cohen D, Palmer AM, Simpson PJ, Khokhar B, Pan S-J, Ronnett GV (2004) The transcriptional repressor Mecp2 regulates terminal neuronal differentiation. Molecular and Cellular Neuroscience 27:44–58.

Murray E, Cho JH, Goodwin D, Ku T, Swaney J, Kim S-Y, Choi H, Park Y-G, Park J-Y, Hubbert A, McCue M, Vassallo S, Bakh N, Frosch MP, Wedeen VJ, Seung HS, Chung K (2015) Simple, Scalable Proteomic Imaging for High-Dimensional Profiling of Intact Systems. Cell 163:1500–1514.

Namihira M, Nakashima K, Taga T (2004) Developmental stage dependent regulation of DNA methylation and chromatin modification in a immature astrocyte specific gene promoter. FEBS Lett 572:184–188.

Okabe Y, Kusaga A, Takahashi T, Mitsumasu C, Murai Y, Tanaka E, Higashi H, Matsuishi T, Kosai K-I (2010) Neural development of methyl-CpG-binding protein 2 null embryonic stem cells: a system for studying Rett syndrome. Brain Res 1360:17–27.

Qian X, Shen Q, Goderie SK, He W, Capela A, Davis AA, Temple S (2000) Timing of CNS Cell Generation. Neuron 28:69–80.

Ricciardi S, Boggio EM, Grosso S, Lonetti G, Forlani G, Stefanelli G, Calcagno E, Morello N, Landsberger N, Biffo S, Pizzorusso T, Giustetto M, Broccoli V (2011) Reduced AKT/mTOR signaling and protein synthesis dysregulation in a Rett syndrome animal model. Human Molecular Genetics 20:1182–1196.

Setoguchi H, Namihira M, Kohyama J, Asano H, Sanosaka T, Nakashima K (2006) Methyl-CpG binding proteins are involved in restricting differentiation plasticity in neurons. J Neurosci Res 84:969–979.

Squillaro T, Alessio N, Cipollaro M, Melone MAB, Hayek G, Renieri A, Giordano A, Galderisi U (2012) Reduced expression of MECP2 affects cell commitment and maintenance in neurons by triggering senescence: new perspective for Rett syndrome. Mol Biol Cell 23:1435–1445.

Stancheva I, Collins AL, Van den Veyver IB, Zoghbi H, Meehan RR (2003) A mutant form of MeCP2 protein associated with human Rett syndrome cannot be displaced from methylated DNA by notch in Xenopus embryos. Mol Cell 12:425–435.

Sztainberg Y, Chen H-M, Swann JW, Hao S, Tang B, Wu Z, Tang J, Wan Y-W, Liu Z, Rigo F, Zoghbi HY (2015) Reversal of phenotypes in MECP2 duplication mice using genetic rescue or antisense oligonucleotides. Nature 528:123–126.

Takizawa T, Nakashima K, Namihira M, Ochiai W, Uemura A, Yanagisawa M, Fujita N,

Nakao M, Taga T (2001) DNA Methylation Is a Critical Cell-Intrinsic Determinant of Astrocyte Differentiation in the Fetal Brain. Dev Cell 1:749–758.

Tropea D, Giacometti E, Wilson NR, Beard C, McCurry C, Fu DD, Flannery R, Jaenisch R, Sur M (2009) Partial reversal of Rett Syndrome-like symptoms in MeCP2 mutant mice. Proc Natl Acad Sci USA 106:2029–2034.

Tsujimura K, Abematsu M, Kohyama J, Namihira M, Nakashima K (2009) Neuronal differentiation of neural precursor cells is promoted by the methyl-CpG-binding protein MeCP2. Experimental Neurology 219:104–111.